Electrons in 5f Systems

Dissertation

zur Erlangung des akademischen Grades
Doctor rerum naturalium (Dr. rer. nat.)

vorgelegt

der Fakultät Mathematik und Naturwissenschaften
der Technischen Universität Dresden

von

M.Sc. Duc-Anh Le
geb. am 26 September, 1980 in HungYen, Vietnam

Dresden, 2010

Max-Planck Institut für Physik Complexer Systeme
Nöthnitzer Str. 38, 01187 Dresden.

Eingereicht am 07.07.2010

Berichterstatter

1. Gutachter: **Prof. Peter Fulde**
   Max-Planck Institut für Physik Complexer Systeme
   Nöthnitzer Str. 38, 01187 Dresden.

2. Gutachter: **Prof. Dr. Klaus Becker**
   Institut für Theoretische Physik
   Technische Universität Dresden, 01062 Dresden.

Contents

List of Figures

List of Tables

Chapter 1

Introduction

In conventional metals, i.e., systems with weakly correlated electrons, valence electrons are assumed to be completely detached from their ions. In the Sommerfeld-Bethe theory [1], as in an ideal gas, electron-electron interactions are completely neglected. The crystal lattice is not explicitly taken into account. A quantum-mechanical justification is given by Bloch's theorem, an unbound electron moves in a constant periodic potential like a free electron in a vacuum with an effective mass. A restriction of available electron states due to Pauli's exclusion principle is taken into account by Fermi-Dirac statistics. This free electron with renormalized mass model has proven to be very successful in explaining experimentally observed properties of simple metals. This success was a surprise for some time since electron-electron repulsions are not weak in any metal and one might therefore expect that they modify strongly the properties of a system of independent electrons. The success of electron with renormalized mass model has been understood since Landau [2, 3] proposed the Fermi-liquid theory, which explains why, at sufficiently low temperature, some of the properties of an interacting fermion system are very similar to those of a free Fermi gas, and why other properties differ. For example, specific heat, compressibility, spin-susceptibility, and other quantities show the same qualitative behavior (e.g., dependence on temperature) as for a free Fermi gas, but the magnitude is (sometimes strongly) changed. The theory assumes that there exists a one-to-one

correspondence between the excitations of the complex interacting electron system and those of independent electrons. However, the energy of a many-particle state is not simply a sum of the single-particle energies of all occupied states. Instead, the change in energy for a given change $\delta n_{\mathbf{k}}$ in occupation of states $\mathbf{k}$ contains terms both linear and quadratic in $\delta n_{\mathbf{k}}$. The linear contribution corresponds to renormalized single-particle energies, which involve, e.g., a change in the particle dispersion. The quadratic terms correspond to a sort of "mean-field" interaction between quasiparticles, which is parameterized by the so-called Landau parameters and determines the behaviour of such quantities as density oscillations (and spin-density oscillations) in the Fermi liquid. In addition to the mean-field interactions, some weak interactions between quasiparticles are also included in the theory, which lead to scattering of quasiparticles off each other.

For metallic phases of compounds with strongly correlated electrons at temperatures below T^*, the quasiparticle concept is still appliable. The characteristic temperature T^* is usually on the order of a few up to a few tens of Kelvin. We speak of a heavy-fermion system when the electron effective mass is hundreds or even thousands of times larger than that of a free electron. Often heavy-fermion compounds contain Ce, Yb, U, or Np as one of their constituents, e.g., $CeCu_2Si_2$, $YbAl_3$, UPt_3, $NpBe_{13}$, implying $4f$ or $5f$ electrons are involved. There are remarkable differences between conventional metals and heavy-fermion systems. First, the reasons for the renormalization of electron mass are different. In conventional metals, the renormalization of electron mass results mainly from the periodic potential of electron-lattice interaction. Whereas in heavy-fermion compounds, the renormalization of electron mass results primarily from electron-electron interactions. Second, the quasiparticle interactions play a more important role in heavy-fermion systems than they do in conventional metals. Note that the quasiparticle interactions can influence strongly not only static thermodynamic quantities such as the compressibility or spin susceptibility, but also dynamic properties like low-energy plasmon excitations or hydrodynamic fluctuations.

The quasiparticle Fermi-liquid theory can be applied for a large number of strongly correlated metallic electron systems. However, there are also a numerous examples where

the Fermi-liquid concept for low-energy excitations is not appliable. Note that the basic assumption of the Landau theory fails if bound states appear when the interaction is turned on. For example, the ground-state of a superconductor is not related in a direct way to any state of the free Fermi gas. Another example is the separation of charge and spin degrees of freedom, which occurs when electron correlations are so strong that electrons are localized. In that case, the coupling of spins on different sites leads to low-energy magnetic excitations, whereas charge excitations, which can be observed by photoelectron spectroscopy, have much higher energy. For such a system, the effects due to electron-electron interactions are more complicated and must be taken into account with care. The physics of the system results from a competition between the Coulomb interaction of electrons and their kinetic energy. In order to minimize the total energy of the system, the terms of the Coulomb energy want to keep the electrons as far apart as possible, to localize them, whereas the terms of the kinetic energy prefer to have as many electrons as possible delocalized. A very well-known example for such an effect due to electron correlations is the Mott-Hubbard transition [4] from a narrow-band metal with delocalized electrons to an insulator with localized electrons. Experimentally, the occurrence of a Mott-Hubbard transition can be observed, e.g., in V_2O_3 [5]. Most studies of systems with strongly correlated electron models were carried out without accounting for orbital degeneracy, such as the single-band Hubbard (SBH) model [6]. However, in real systems, which are more complex, one has to deal with orbital degeneracy.

In order to see the differences between systems with weakly and strongly correlated electrons, one can consider the ground-state of a molecular H_2 in the molecular-orbital (MO) limit and in the Heitler-London (HL) limit. For the sake of clarity, the spin component of the total wavefunction is omitted. In the weak correlation limit, the interaction of the two electrons is treated within a mean-field approximation, the MO form of the ground-state wavefunction is

$$\psi_{MO}\left(\mathbf{r}_1, \mathbf{r}_2\right) = \frac{1}{2}\left[\phi_1(\mathbf{r}_1)\phi_1(\mathbf{r}_2) + \phi_1(\mathbf{r}_1)\phi_2(\mathbf{r}_2) + \phi_2(\mathbf{r}_1)\phi_1(\mathbf{r}_2) + \phi_2(\mathbf{r}_1)\phi_2(\mathbf{r}_2)\right], \qquad (1.1)$$

where the single-electron wavefunctions $\phi_{1,2}(\mathbf{r})$ are centered on atoms 1 and 2 of the

H_2 molecule. In the strong correlation limit, the interaction of the two electrons is so strong such that they avoid being in the same atom, the HL form of the ground-state wavefunction is

$$\psi_{HL}\left(\mathbf{r}_1, \mathbf{r}_2\right) = \frac{1}{\sqrt{2}}\left[\phi_1(\mathbf{r}_1)\phi_2(\mathbf{r}_2) + \phi_2(\mathbf{r}_1)\phi_1(\mathbf{r}_2)\right]. \tag{1.2}$$

It is seen that the HL wavefunction (1.2) does not contain ionic configurations $\phi_1(\mathbf{r}_1)\phi_1(\mathbf{r}_2)$ and $\phi_2(\mathbf{r}_1)\phi_2(\mathbf{r}_2)$, whilst in the MO wavefunction (1.1) they have equal weight - like non-ionic configurations. Note that the ionic configurations introduce an additional Coulomb repulsion energy cost for the electrons. These contributions are completely suppressed in the HL limit. This demonstrates an important feature of electron correlations, namely, the partial suppression of electronic charge fluctuations on an atomic site. The former are called inter-atomic correlations because charge fluctuations at an atomic site are caused by an overlap of wavefunctions of different atoms. The partial suppression of charge fluctuations in an atomic site keeps the Coulomb repulsions small, but it is disadvantageous for the kinetic energy of the system.

In addition to inter-atomic correlations we must also consider intra-atomic correlations. Consider an isolated atom or ion in a configuration with a given number of valence electrons, e.g., a Mn^{3+} ion in configuration $3d^4$ or a Ho^{3+} ion with its configuration $4f^{10}$. In-out correlations optimally fill the electrons into the atomic subshells by a proper radial distribution in order to reduce their on-site Coulomb repulsion energy. Hund's rules achieve the same by optimally distribute the electrons in the open subshell. In our example, the ground-states predicted by Hund's rules for Mn^{3+} and Ho^{3+} are ${}^5D_0$ and ${}^5I_8$, respectively. Note that when considering an ion in a solid we may face a different situation because the ion is subject to the crystal field. The outcome is decided by the competition between the crystal field and the interactions that are responsible for Hund's rules. For Mn^{3+} in, e.g., $LaMnO_3$, the prediction $S = 2$ is absolutely relevant, $L = 2$ might be true, and $J = 0$ is not correct. In contrast, the predicted ground-state ${}^5I_8$ remains valid for Ho^{3+} in, e.g., HoF_3. It is worth remembering that inter-atomic correlations can be strong even when intra-atomic correlations are moderate or weak. For example, let us assume

that one would be able to increase the lattice constant of a Si crystal. The intra-atomic correlations on a Si site are fairly moderate, but the inter-atomic correlations become stronger while the lattice constant is increasing. When the limit of separate atoms is approached, fluctuations in the electron number at a site are reduced to zero by the strong inter-atomic correlations.

The field of strongly correlated electron systems has been constantly growing for about three decades [7, 8]. Many experimental as well as theoretical studies have been undertaken to understand the physics of these systems such as: transition metal oxides ($3d$ electron systems), lanthanides ($4f$ electron systems) and actinides ($5f$ electron systems). The valence electrons that are most strongly correlated are the $4f$ ones because their atomic wavefunction is very close to the nucleus and their tendency to delocalize is very small. In fact, among lanthanide compounds, only $4f$-electrons in Ce or Yb ions show a noticeable degree of itineracy. Electronic correlations in actinides or in transition-metal ions are smaller than those in lanthanides, but they also play an important role in understanding the physics of these systems. Continuing this consideration, the $5f$ electrons are more delocalized than the $4f$ electrons but they are still more strongly correlated than the $3d$ electrons in transition metals. Therefore, the $5f$ electrons may have a dual character: both delocalized and localized features.

The two different behaviors of the $5f$ electrons in the actinide series become clearer when one looks at the Wigner-Seitz radii as a function of atomic number Z for different member of $5d$, $4f$, and $5f$ metal series (see Fig. 1.1). The itinerant behavior of the electrons in $5d$ transition metals shows up in a parabolic shape of the Wigner-Seitz radius, whereas the localized feature of the $4f$ electrons is visible in a mostly constant shape of the radius. It is because the $5d$ electrons participate in bonding whereas the $4f$ electrons do not. Interestingly, the $5f$ series shows both behaviors. First, a parabolic-like decrease in volume is observed with increasing the f-electron count, similar to the $5d$ series, i.e., for light actinide elements the itinerancy of $5f$ electrons is dominant. Then, when the f-electron count is large enough, a similar behavior to the $4f$ series is seen [9], i.e., for heavy actinide elements the localized tendency is dominant. Thus, for those in the middle

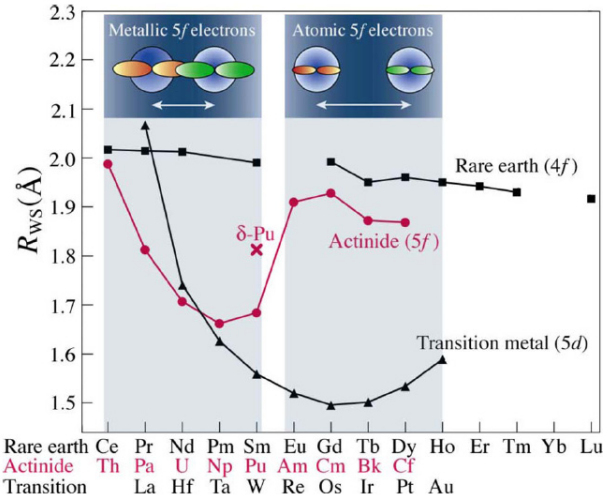

Figure 1.1: Wigner-Seitz radii for different member of 5d, 4f, and 5f metal series as a function of atomic number Z. The upper-left insets schematically illustrate localized and delocalized 5f states between adjacent actinide atoms. Taken from [9].

of actinide series their $5f$ electrons may have both localized and delocalized features. This means that the study of the $5f$ electrons is a very interesting topic.

In the last few years, a number of experimental and theoretical works have been performed in the field of $5f$ electron systems. It turned out that these systems have rich and non-trivial low temperature properties, including heavy-fermion behavior, unconventional superconductivity, and magnetic ordering [8]. Of particular interest is the UPd_2Al_3 compound, which has a two-component electronic character that is quite unique among all U-based heavy-fermion compounds, because it displays both pronounced local-moment and heavy-mass itinerant behavior. Moreover, the itinerant electrons in UPd_2Al_3 are found to be superconducting well below the antiferromagentic magnetic ordering critical temperature, whereas magnetism generally suppresses superconductivity in conventional metals. Using the inelastic neutron scattering experiment, far below the critical temperature $T_C = 1.8K$, Sato *et al.* [10] obtained two peaks in the scattering intensity spectra shown in Fig. 1.2. The lower energy peak corresponds to non-local $5f$ electrons and the higher one corresponds to the local-moment made of localized $5f$ electrons. This is an

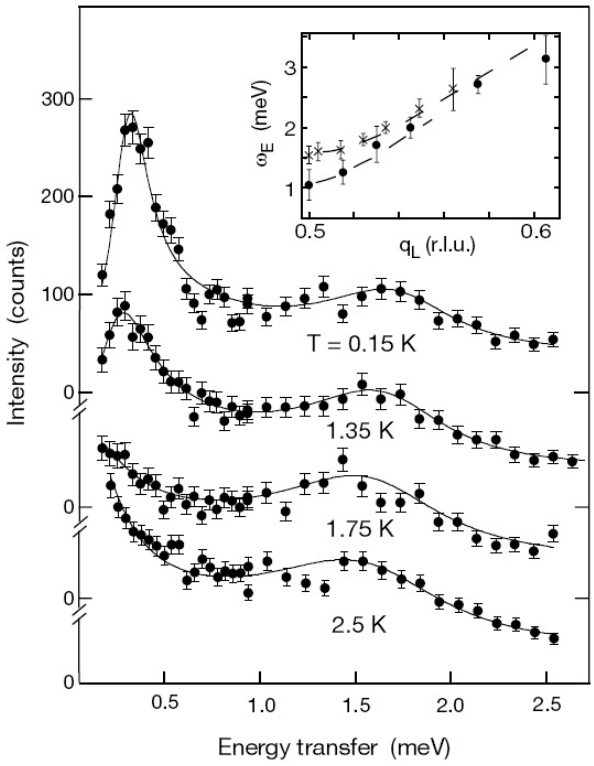

Figure 1.2: Temperature evolution of the inelastic neutron scattering spectrum in UPd_2Al_3. Taken from [10].

evidence for the coexistence of $5f$-derived quasiparticles and the $5f$ localized moments. In addition, Fujimori *et al.* [11] used soft x-ray angle-resolved photoelectron spectroscopy to study the band-structure of UPd_2Al_3. They found that the f-bands, which form the Fermi surfaces at low temperatures, are excluded from the Fermi serfaces at high temperatures. Their results demonstates how the same f eletrons can be both itinerant and localized.

Another interesting U-based heavy-fermion compound is UPt_3. The experiments in UPt_3 show that the Sommerfeld coefficient γ of the linear low-temperature specific heat and the Pauli-like spin susceptibility χ_S are strongly enhanced. Both findings can be explained by attaching to the quasiparticles a large effective mass m^* that is about 20 times bigger than the band mass m_b obtained from the standard local-density approximation (LDA) calculations [14, 15]. Indeed, heavy quasiparticles have been observed in

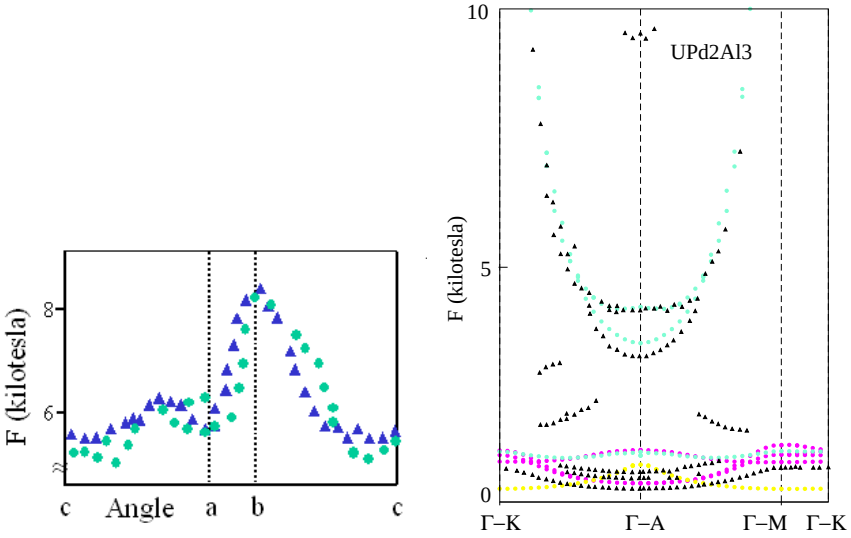

Figure 1.3: De Haas van Alphen cross sections for the heavy quasiparticles in UPt_3 (left panel) and UPd_2Al_3 (right panel). The experimental (theoretical) data is marked by triangles (circle) symbols.) [12, 13].

de Haas van Alphen (dHvA) experiments [16, 17]. These experiments unambiguously confirm that UPt_3 has to be regarded as a strongly correlated Fermi liquid. Although a complete picture of the low-temperature phase of UPt_3 has emerged, a comprehensive theoretical picture of the heavy quasiparticles is still missing. The failure of standard LDA calculations in explaining the large effective mass enhancement in UPt_3 suggests that alternative or complementary approaches have to be developed. In order to explain the large effective mass enhancement, Zwicknagl, Yaresko, and Fulde [12] proposed a microscopic description of heavy fermions in UPt_3. Their theory is based on the assumption that some of the $5f$ electrons are localized and that the itinerant $5f$ electrons are scattering inelastically by the localized ones. Band-structure calculations based on this supposition reproduced the observed dHvA frequencies very well [12, 13] (see Fig. 1.3). Furthermore, the assumption that the $5f$ electrons are simultaneously localized and itinerant gives the correct equilibrium volume for δ-Pu [18]. These studies have proven that the partial localization of $5f$ electrons is an important key for understanding the physics

of $5f$ electron systems.

It is worth recalling that the origin of partial localization in the $3d$ and $5f$ systems is quite different [19]. In the $3d$ systems, the large crystalline electric field (CEF) set up by the surrounding environment of transition metal ions plays a major role. The splitting due to the CEF is often larger than the bandwidth, for example, as in the manganites. In case of a cubic lattice, the CEF splits the five $3d$ orbitals into a t_{2g} triplet and an e_g doublet and the corresponding sub-bands are well separated. When Hund's rule energy is larger than this splitting and when the orbital energy of the t_{2g} is lower than that of the e_g states, the following scenario is applied: if the $3d$ electron number per ion exceeds 3, i.e., $3 < n_d < 4$, the t_{2g} states will be occupied by three $3d$ electrons. The three electrons are localized in a high-spin state with the total spin $S = 3/2$. The remaining $n_d - 3$ electrons occupy e_g states and are delocalized. The situation is different if the CEF splitting is larger than Hund's rule coupling. In that case, the t_{2g} sub-band will accommodate up to six electrons. When the $3d$ electron number per ion n_d is larger than 6, only (n_d-6) electrons will be itinerant and contribute to metallic behavior. In compounds with $5f$ electrons we face a different situation. Since the $5f$ electrons are closer to the nuclei than the $3d$ electrons are, the CEF splitting is smaller and less relevant. But, Hund's rule coupling is larger and more important. Therefore, when we consider a situation where the $5f$ electron number per actinide ion n_f exceeds two, i.e., $3 > n_f > 2$, only those $5f$ electrons that enable the remaining ones to form a Hund's rule state will delocalize. Otherwise, the Coulomb interaction is increased so much that delocalization is disadvantageous as far as energy is concerned. Therefore, Hund's rule correlations may strongly enhance hopping anisotropies (anisotropies in the hopping matrix elements) and eventually lead to the coexistence of band-like itinerant $5f$ states with localized atomic-like ones. It means that a study of the dual nature of the $5f$ electrons in more detail is highly necessary to understand the physics of actinides.

In order to study the dual nature of $5f$ electrons, Efremov, Hasselmann, Runge, Fulde, and Zwicknagl [20] proposed an effective model, which is a multi-orbital Hubbard model, for the $5f$ electrons in U-based compounds. The microscopic Hamiltonian of the effective

model includes both the local interaction and hopping terms (kinetic energy) between nearest neighboring sites. In the effective model, the $5f-$electrons are characterized by effective hoppings, and by a local interaction, which takes into account the Coulomb repulsion and Hund's rule coupling. Assuming that the spin-orbit coupling is strong, the jj-coupling scheme is used and eight unfavorable high energy $5f$ states with total angular momentum $j = \frac{7}{2}$ are neglected. Thus, the number of $5f$ orbitals in the model is reduced to 6 instead of being 14 in the most general case. By considering the fact that intra-atomic correlations are strong, compared to the kinetic energy, one expects that even small cluster models are capable of capturing the main physics described above for large systems. These models, namely, the two-site and three-site models, were first studied by exact diagonalization [21]. It turned out that, in the small hopping regime, depending on anisotropies of hopping parameters, two partially localized phases in which two electrons are localized can be seen: one which has electrons with the quantum number j_z being equal to $\frac{1}{2}$ and $\frac{5}{2}$ localized, the other with $j_z = \frac{3}{2}$ and $\frac{5}{2}$ orbitals that are localized. In these phases, the microscopic mechanism for the partial localization is the Hund's rule mechanism mentioned above: the intra-atomic correlations strongly enhance hopping anisotropies so that the smaller hopping matrix elements are renormalized to zero whereas the dominant hopping matrix element is slightly influenced. In the intermediate hopping regime, one obtains a phase in which only the electron with the quantum number $j_z = \frac{5}{2}$ is localized. It is obvious that the Hund's rule mechanism does not apply for one localized electron phase, so what is the physics of this phase? Furthermore, it is known that clusters of small sizes sometimes display features that disappear in the bulk limit or washed out at finite temperature. Therefore, it is natural to question if the partially localized phases of small cluster models survive in the thermodynamic limit? In addition, the exact diagonalization calculation of a four-site model [22] showed a phase characterized by the localization of the $j_z = 3/2$ orbital. This phase has not been observed in the two-site and the three-site models. Thus, it is legitimate to question if any new partially localized phase shows up in the thermodynamic limit? In order to answer these above challenging questions, investigations of the effective model in a lattice are required. In this thesis we

want to deal with these topics and the main purpose of this work is to resolve questions of that kind.

The effective model in the thermodynamic limit cannot, of course, be solved exactly. Therefore, appropriate approximations that are able to capture the main physics of the effective model on a lattice need to be developed. Runge *et al.* [23] have applied various approximations for the two-site model. Their study pointed out that the Hartree-Fock approximation (HFA) results showed little resemblance with the exact ones. In contrast, the Gutzwiller approximation (GA) to Gutzwiller wavefunction results showed a good agreement with the exact diagonalization calculations. It suggests that one can use the GA approach to study the effective model in the thermodynamic limit. However, it is known that for the SBH model, the results derived from the GA method are identical to those of the paramagnetic saddle-point solution within the slave-boson theory introduced by Kotliar and Ruckenstein (KR) [24]. In fact, KR's approach uncovers the limitations of the GA and it opens up a systematic way of improving the Gutzwiller solution by taking into account the effect of fluctuations around the saddle point [25]. In addition, by using the Green-function method KR's theory can be easily generalized to deal with complicated systems with spin- and/or orbital-ordered states [26].

The first attempt to apply slave-boson technique for the effective model was carried out by Zwicknagl in Ref. [27]. In her work, the free energy was minimized in a restricted Hilbert space spanned by the 2- and 3-electron states and a constant density of states (DOS) was assumed. She obtained three partially localized phases for different values of hopping parameters: electrons with $j_z = \frac{1}{2}$ and $\frac{5}{2}$ localized in the first phase, electrons with $j_z = \frac{3}{2}$ and $\frac{5}{2}$ localized in the second, and electrons with $j_z = \frac{3}{2}$ localized in the last. Her results show that the partial localization feature of the $5f$ electrons obtained in the small cluster models survives in the thermodynamic limit. That is an important observation. However, these results were only mentioned shortly in her work. On the other hand, there are two drawbacks in the theory. Firstly, it does not give exact solution in the non-interacting limit because of the complex form of the local interaction. Secondly, due to the assumption of the restricted Hilbert space, the 5f band-filling cannot deviate from 2.5

so much. Thus, the theory ceases to be a good approximation when electron bandwidths are of the same order of Hund's rule splittings. Consequently, the phase that has only the $j_z = \frac{5}{2}$ localized orbital, which shows up in the intermediate hopping regime, has not been obtained and discussed in her work. Note that the partial localization transition from a delocalized phase to a partiatly localized phase and vice versa is equivalent to the orbital-selective Mott transition. The latter was first proposed by Anisimov *et al.* [28] for $Ca_{2-x}Sr_xRuO_4$. However, the term partial localization will be used throughout this work.

In this thesis, we use the rotationally invariant slave-boson mean-field (RISBMF) method [29] and the infinite time evolving block decimation (iTEBD) method [30] to study the effective model on a lattice. The former is a generalization of KR's theory for a multi-band model with arbitrary local interactions. It is worth mentioning that the RISBMF theory is exact in the non-interacting and in the atomic limits. Thus, it does not suffer from the problem in the non-interacting limit as Zwicknagl's theory does. Moreover, we introduce slave bosons for not only the 2- and 3-electron states but also for all other states. The mapping of the full local Hilbert space enables us to consider an arbitrary band-filling. However, we will restrict ourselves to a band-filling of 2.5 to make a comparison with the previous results [21, 22, 27]. With the purpose of assessing the validity the RISBMF method we use the iTEBD method to study the effective model on an infinite linear chain. The iTEBD algorithm is a numerical scheme used to simulate infinite 1D quantum many-body systems, characterized by nearest-neighboring hoppings and interactions. It is dubbed infinite time evolving block decimation because it dynamically identifies the relevant low-dimensional Hilbert subspaces of an exponentially larger original Hilbert space. The algorithm, based on the matrix product states (MPS) formalism [31], is highly efficient when the amount of entanglement in the system is limited, a requirement which is fulfilled by a large class of quantum many-body systems in one dimension.

This thesis is organized as follows. In the next chapter we briefly describe the microscopic Hamiltonian of the effective model and reproduce the results of the two-site cluster case in detail. The slave-boson formalism for the effective model is described in chapter 3. We start this chapter with a brief introduction of the auxiliary particle technique. Then,

we recall some slave-boson approaches for the Hubbard model in order to discuss the main physics ideas of slave-boson theory. Afterward, we derive RISBMF equations for the effective model in detail. A classification of partially localized phases is addressed at the end of chapter 3. In chapter 4 we then present numeric solutions for the RISBMF equations for the effective model on a lattice characterized by a constant density of states. The phase diagram and the physics of the partially localized phases will be discussed through this chapter. In chapter 5, we present results for the effective model on an infinite linear chain by using the iTEBD method. Finally, chapter 6 contains our conclusions.

Chapter 2

Effective Model

In this chapter we rederive the microscopic Hamiltonian for the effective model [20]. The Hamiltonian, which is a multi-orbital Hubbard model, is obtained form a more realistic model, namely, a generalization of the well-known periodic multi-orbital Anderson model [32]. The effective model for small cluster systems has been analysed in Ref. [20, 21, 22, 23]. We reproduce here some important results of the two-site cluster case to compare later with our results in a lattice.

2.1 Effective Hamiltonian

In actinide-based heavy-fermion compounds the direct overlap between $5f$ wavefunctions at neighboring sites is rather small because of the large distances between actinide ions. However, itineracy of the strongly correlated $5f$ electrons can be enhanced by hybridization with weakly correlated conduction electrons. In order to describe these electron systems in actinide-based heavy fermion compounds, the following generalization of the well-known Anderson model is used [32]

$$H = H_f + H_c + H_{cf}, \tag{2.1}$$

where H_f, H_c and H_{cf} describe the $5f$ electrons, the conduction electrons and the hybridization between the two subsystems, respectively. A $5f$ electron has the orbital an-

gular momentum $l = 3$ and the spin $s = \frac{1}{2}$, thus, in the noninteracting case, $5f$ states are 14-fold degenerate. This degeneracy can be partially lifted by either electron-electron interactions or spin-orbit coupling. The latter is large for $5f$ systems. One thus adopts the $jj-$coupling scheme which yields two one-electron multiplet states with angular momenta $j = \frac{7}{2}$ and $j = \frac{5}{2}$. Considering the fact that the spin-orbit splitting, which is approximately $1eV$, is large one also neglects the contributions from excited multiplet $j = \frac{7}{2}$ states and classify $5f$ electrons by their angular momentum $j = \frac{5}{2}$ and their z-projection j_z.
H_f is given by

$$H_f = -\mu \sum_a f^\dagger_{aj_z} f_{aj_z} + \sum_a \hat{U}(a), \tag{2.2}$$

where μ is the chemical potential. Throughout this work we concentrate on the intermediate valence regime by taking the $5f$ band-filling $n_f = 2.5$, which is appropriate for U-based compounds. Here $f^\dagger_{aj_z}(f_{aj_z})$ creates (annihilates) an electron at site a in a $5f$ state with angular momentum $j = \frac{5}{2}$ and z-projection j_z. The local interaction at site a is then given by

$$\hat{U}(a) \equiv \frac{1}{2} \sum_{j_{z1},...,j_{z4}} U_{j_{z1},j_{z2},j_{z3},j_{z4}} f^\dagger_{aj_{z1}} f^\dagger_{aj_{z2}} f_{aj_{z4}} f_{aj_{z3}} \ , \tag{2.3}$$

where the Coulomb matrix elements $U_{j_{z1},j_{z2},j_{z3},j_{z4}}$ for $j_{zi} = -\frac{5}{2}, .., \frac{5}{2}$,

$$U_{j_{z1},j_{z2},j_{z3},j_{z4}} \equiv \delta_{j_{z1}+j_{z2},j_{z3}+j_{z4}} \sum_J U_J C^{JJ_z}_{\frac{5}{2}j_{z1};\frac{5}{2}j_{z2}} C^{JJ_z}_{\frac{5}{2}j_{z3};\frac{5}{2}j_{z4}} \tag{2.4}$$

are expressed in terms of the usual Clebsch-Gordan coefficients $C^{JJ_z}_{\frac{5}{2}j_z;\frac{5}{2}j_{z'}}$ and the Coulomb parameters U_J. Here J denotes the total angular momentum of two $5f$ electrons and $J_z \equiv j_{z1}+j_{z2} = j_{z3}+j_{z4}$. The sum is restricted by the antisymmetry of the Clebsch-Gordan coefficients $C^{JJ_z}_{\frac{5}{2}j_z;\frac{5}{2}j_{z'}}$ to even values $J = 0, 2, 4$. In our calculations, we fix the values of the coefficients U_J, which are determined from local density approximation (LDA) wave functions for UPt_3, i.e., $U_4 = 17.21\ eV$, $U_2 = 18.28\ eV$, and $U_0 = 21.00\ eV$ [20]. The weakly correlated conduction electrons are described by

$$H_c = \sum_{n\mathbf{k}\sigma} \varepsilon_{n\mathbf{k}} c^\dagger_{n\mathbf{k}\sigma} c_{n\mathbf{k}\sigma} \tag{2.5}$$

where $c^{\dagger}_{n\mathbf{k}\sigma}(c_{n\mathbf{k}\sigma})$ creates (annihilates) a conduction electron in a state with band index n, wave vector $\mathbf{k}$ and spin projection σ whose energy is denoted by $\varepsilon_{n\mathbf{k}}$.
The coupling between the two subsystems is given by

$$H_{cf} = \sum_{aj_z n\mathbf{k}\sigma} V_{j_z\sigma n\mathbf{k}} c^{\dagger}_{n\mathbf{k}\sigma} f_{aj_z} e^{-i\mathbf{k}.\mathbf{R}_a} + \text{H.c.}, \tag{2.6}$$

where $V_{j_z\sigma n\mathbf{k}}$ are hybridization matrix elements.

In order to study high-energy effects one has to consider with the multi-orbital Anderson model (2.1) which explicitly accounts for the dynamics of the conduction electrons. However, in the low-energy regime, one replaces it by a simpler effective Hamiltonian which is a multi-orbital Hubbard model

$$H = H_f + H_c + H_{cf} \Longrightarrow H_f + K_f^{eff}, \tag{2.7}$$

where the couplings of the $5f$- states at different sites via the conduction electrons are taken into account by effective hoppings

$$K_f^{eff} = -\sum_{\langle ab\rangle j_z j_{z'}} t_{abj_z j_{z'}} \left(f^{\dagger}_{aj_z} f_{bj_{z'}} + \text{H.c.} \right). \tag{2.8}$$

Here $t_{abj_z j_{z'}}$ are effective hopping integrals and a, b are nearest neighboring sites. The effective model (2.7) is justified for systems where LDA band-structure calculations yield (almost) pure $5f$ states [19] . This is the case of the well-known heavy fermion superconductor UPt_3 and U dipnictides where the effective hopping is mediated by the p states of Pt and the pnictogen ions, respectively. It is clear that the effective hopping integrals sensitively depend on the chemical composition and on the structure of the system under consideration. In fact they can be varied by applying an external pressure. For that reason, we treat them as variable parameters throughout this work. We also assume that the effective hopping matrices between nearest neighboring sites are diagonal in the orbital indices and do not depend on site index, i.e.,

$$t_{abj_z j_{z'}} = \delta_{j_z j_{z'}} t_{j_z}. \tag{2.9}$$

Of course, this is an idealization of the true physical situation. This simplification not only enables us to decrease the number of system parameters but also helps us to save

the computational effort. For example, when this simplification is made in a two-site problem with 5 electrons one only has to diagonalize 98-by-98 matrices instead of 792-by-792 matrices. Furthermore, we also set $t_{jz} = t_{-jz}$ in order to conserve up and down symmetry in the bulk materials. With the assumption (2.9), the effective kinetic term (2.8) becomes

$$K_f^{eff} = -\sum_{\langle ab\rangle j_z} t_{j_z} \left(f^\dagger{}_{aj_z} f_{bj_{z'}} + \text{H.c.} \right), \tag{2.10}$$

and finally the effective model Hamiltonian reads

$$H = -\sum_{\langle a,b\rangle, j_z} t_{j_z} \left(f^\dagger{}_{aj_z} f_{bj_z} + \text{H.c.} \right) - \mu \sum_a f^\dagger{}_{aj_z} f_{aj_z} + \sum_a \hat{U}(a). \tag{2.11}$$

This is the microscopic Hamiltonian for the effective model which was first proposed in Ref. [20]. Note that the on-site interactions $\hat{U}(a)$ is defined by Eq. (2.3). The effective model has been widely applied to investigate the physical properties of $5f$ electrons in U-based compounds [19, 21, 23, 27, 33, 32].

2.2 Two-site cluster case

In order to compare the finite cluster model results with the ones in the thermodynamic limit, we reproduce and analyze in this section in detail some of the results of Ref. [21]. Since the results for the two-site and the three-site models are qualitatively similar we will only concentrate on the former.

For the two-site system equation (2.11) becomes

$$H = -\sum_{j_z} t_{j_z} \left(f^\dagger{}_{1j_z} f_{2j_z} + \text{H.c.} \right) + \sum_{a=1}^{2} \hat{U}(a) - \sum_{a=1,jz}^{2} h j_z f^\dagger{}_{aj_z} f_{aj_z}. \tag{2.12}$$

Note that the term having the chemical potential disappears because one deals with the canonical ensemble. The newly added last term in Eq. (2.12) describes an applied magnetic field. The latter is included in the Zeeman energy h. In order to mimic the intermediate valence situation in U-based heavy-fermion compounds, the number of electrons in the two sites is chosen to be five.

The Hamiltonian (2.12) conserves the z-component of the total angular momentum of the electrons at the two sites $\mathcal{J}_z = J_{1z} + J_{2z}$, where J_{1z} (J_{2z}) is the angular momentum projection on site 1 (2), respectively. For this system, the total angular momentum projection $\mathcal{J}_z$ can only take half-integer values in the interval from $-\frac{17}{2}$ to $\frac{17}{2}$. One thus characterizes the eigenstates by their $\mathcal{J}_z$ value.

Similar to Ref. [21], here we consider $t_{\frac{1}{2}} = t_{\frac{5}{2}}$ and $t_{\frac{3}{2}}$ as independent parameters. The choice of parameters is motivated by the LDA calculations for UPt_3 compound [12], where $t_{\frac{3}{2}} > t_{\frac{1}{2}}, t_{\frac{5}{2}}$. However, for later comparison with the results for a lattice we use in the following plots the label "bandwidth" W_{jz} instead of hopping parameter t_{j_z}. The relation between the two quantities is assumed to be the same as the one in a 1D system, i.e., $W_{jz} = 4|t_{jz}|$. Lastly to reduce the notations we will set $W \equiv W_{\frac{3}{2}}$ and $W' \equiv W_{\frac{1}{2}} = W_{\frac{5}{2}}$. Note that the phase diagrams of the two-site model shown below are calculated by exact diagonalization of the Hamiltonian (2.12).

Fig. 2.1 presents the phase diagram in $W-W'$ plane when a vanishingly small magnetic field is applied. In this case, five different phases are visible: three "low-spin" ($\mathcal{J}_z = \frac{1}{2}, \frac{3}{2}, \frac{5}{2}$) and two "high-spin" ($\mathcal{J}_z = \frac{11}{2}, \frac{15}{2}$). The characteristics of the two species are very different. In these "low-spin" phases, each orbital-dependent occupation is either close to zero or to one-half, i.e., all orbitals are either unoccupied or itinerant. On the other hand, in these "high-spin" phases, the occupations for some particular orbitals are close to unity, i.e., those orbitals are nearly fully occupied, i.e., partial localization takes place. In more detail, in the $\mathcal{J}_z = \frac{11}{2}$ phase the $j_z = \frac{5}{2}$ orbital is localized while in the $\mathcal{J}_z = \frac{15}{2}$ phase the $j_z = \frac{1}{2}, \frac{5}{2}$ orbitals are localized. These phases are named "$j_z = \frac{5}{2}$ localized phase" and "$j_z = \frac{1}{2}, \frac{5}{2}$ localized phase", respectively. The demonstration for localization of the orbitals is shown in Fig. 2.2. It should be kept in mind that one orbital is called localized if the corresponding occupancy is close to 1.

Fig. 2.3 presents the evolution of the phase diagram shown in Fig. 2.1 with increasing applied magnetic field. Note that even a small value of h can change noticeably the phase diagram because the interactions are of order $\frac{t_{j_z}^2}{U_0 - U_4}$ and therefore relatively small. One notices three new phases show up. They are two "high-spin" phases with $\mathcal{J}_z = \frac{13}{2}, \frac{17}{2}$

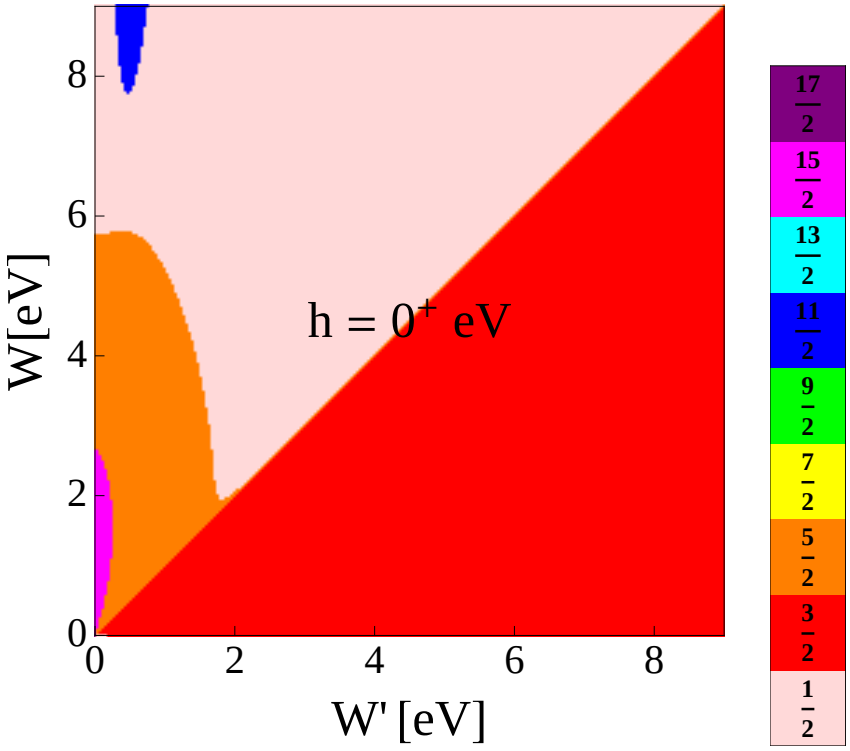

Figure 2.1: Phase diagram of two-site cluster model in a vanishingly small magnetic field.

and one new "intermediate-spin" phase with $\mathcal{J}_z = \frac{7}{2}$. Now the "low-spin" phases require larger hopping integrals in order to be stabilized. The regions of "high-spin" phases grow with increasing magnetic field. It is understandable since the magnetic term in the Hamiltonian (2.12) favors states with high $\mathcal{J}_z$.

Now let us analyze these three new phases. In the $\mathcal{J}_z = \frac{7}{2}$ phase, the $j_z = \frac{1}{2}$ orbital is highly occupied with a corresponding occupancy of about 0.9. When the magnetic field is large enough, this phase disappears. Thus, one guesses that it will also disappear in the thermodynamic limit because the surrounding (magnetic) environment acts as an (internal) effective magnetic field on the two sites. Similar to the $\mathcal{J}_z = \frac{11}{2}$ and $\mathcal{J}_z = \frac{15}{2}$ phases, the $\mathcal{J}_z = \frac{13}{2}$ and $\mathcal{J}_z = \frac{17}{2}$ phases are characterized by the localization of some orbitals. In the $\mathcal{J}_z = \frac{13}{2}$ phase, the $j_z = \frac{5}{2}$ orbital is localized; in the $\mathcal{J}_z = \frac{17}{2}$ phase, the $j_z = \frac{3}{2}, \frac{5}{2}$ orbitals are localized. The latter phase is named "$j_z = \frac{3}{2}, \frac{5}{2}$ localized phase".

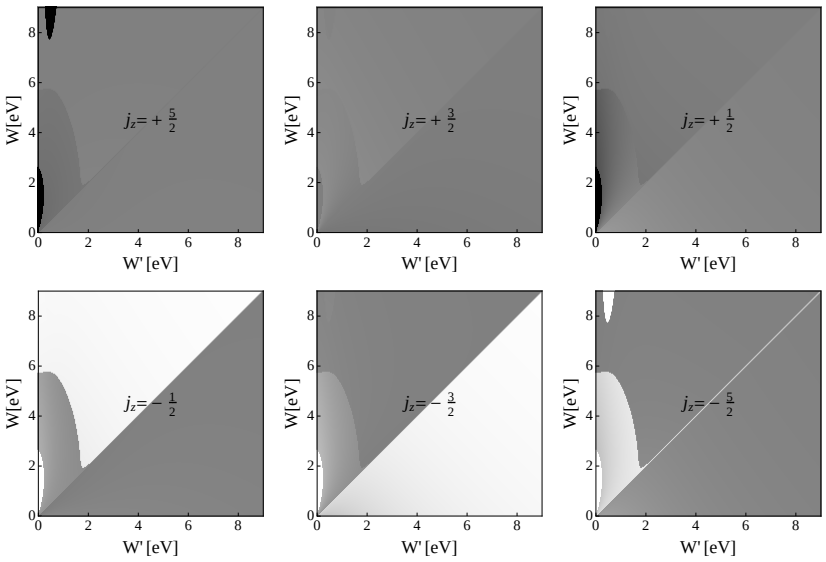

Figure 2.2: Gray-scale plot of occupation n_{j_z} for j_z orbital which is indicated in the center of each graph when $h = 0^+ eV$. Black areas correspond to fully occupied states while white areas present empty state.

Note that all possible phases with different $\mathcal{J}_z$ have appeared except the $\mathcal{J}_z = \frac{9}{2}$ phase. If one continues to increase the magnetic field no new phase shows up. However, it is interesting to notice that when $h > 0.025eV$ there is a new region in which an "old phase" with $\mathcal{J}_z = \frac{11}{2}$ appears. That is where W' is about $0.6eV$ and W is small enough. The old $\mathcal{J}_z = \frac{11}{2}$ phase is different from the new $\mathcal{J}_z = \frac{11}{2}$ one as soon as the orbital localization is concerned. In the latter, depending on the magnitude of the magnetic field and the values of W', the occupation of $j_z = \frac{3}{2}$ orbital varies from 0.9 to 1.0 therefore this orbital can be considered as a localized one. Thus, we name this phase "$j_z = \frac{3}{2}$ localized phase".

In conclusion all "high-spin" phases are characterized by the localizations of some orbitals: they are the $j_z = \frac{3}{2}$ localized phase, $j_z = \frac{5}{2}$ localized phase, $j_z = \frac{1}{2}$, $\frac{5}{2}$ localized phase and $j_z = \frac{3}{2}$, $\frac{5}{2}$ localized phase. A summary of phases in the two-site model is given in Table 2.1. Note that, since the local interaction mixes various j_z orbitals the concept of "occupying" j_z state in "small spin" phases is only approximate. Futhermore the "paramagnetic" interpretation in "small spin" phases is appropriate only if the corresponding

hopping is much larger than the energy differences $|\Delta U_J|$ resulting in the Hund's rule.

It is known that clusters of small sizes sometimes display features that disappear in the bulk limit or washed out at finite temperature. Therefore, it is natural to question if the partially localized phases discussed above survive in a lattice case? In addition, the exact diagonalization calculation for the four-site model [22] showed a phase characterized by the localization of the $j_z = 3/2$ orbital. This phase has not been observed in the two-site case. Thus, it is legitimate to question if any new partially localized phase shows up in a lattice case? These questions will be answered in the following chapters.

$\mathcal{J}_z$	Properties	Notice
$\frac{1}{2}$	$j_z = -\frac{1}{2}$ is almost unoccupied, $j_z = \pm\frac{3}{2}$, $\pm\frac{5}{2}$ are approximately paramagnetic	"Small spin"
$\frac{3}{2}$	$j_z = -\frac{3}{2}$ is almost unoccupied, $j_z = \pm\frac{1}{2}$, $\pm\frac{5}{2}$ are approximately paramagnetic	"Small spin"
$\frac{5}{2}$	$j_z = -\frac{5}{2}$ is almost unoccupied, $j_z = \pm\frac{1}{2} \pm \frac{3}{2}$ are approximately paramagnetic	"Small spin"
$\frac{7}{2}$	$j_z = \frac{1}{2}$ is highly occupied	"Intermediate spin"
$\frac{9}{2}$	$j_z = \frac{1}{2}$, $\frac{3}{2}$ are highly occupied	"Intermediate spin"
$\frac{11}{2}$	$j_z = \frac{5}{2}$ or $j_z = \frac{3}{2}$ is highly occupied	"High spin"
$\frac{13}{2}$	$\frac{5}{2}$ is highly occupied	"High spin"
$\frac{15}{2}$	$j_z = \frac{1}{2}$, $\frac{5}{2}$ are localized	"High spin"
$\frac{17}{2}$	$j_z = \frac{3}{2}$, $\frac{5}{2}$ are localized	"High spin"

Table 2.1: A summary of phases in the two-site model.

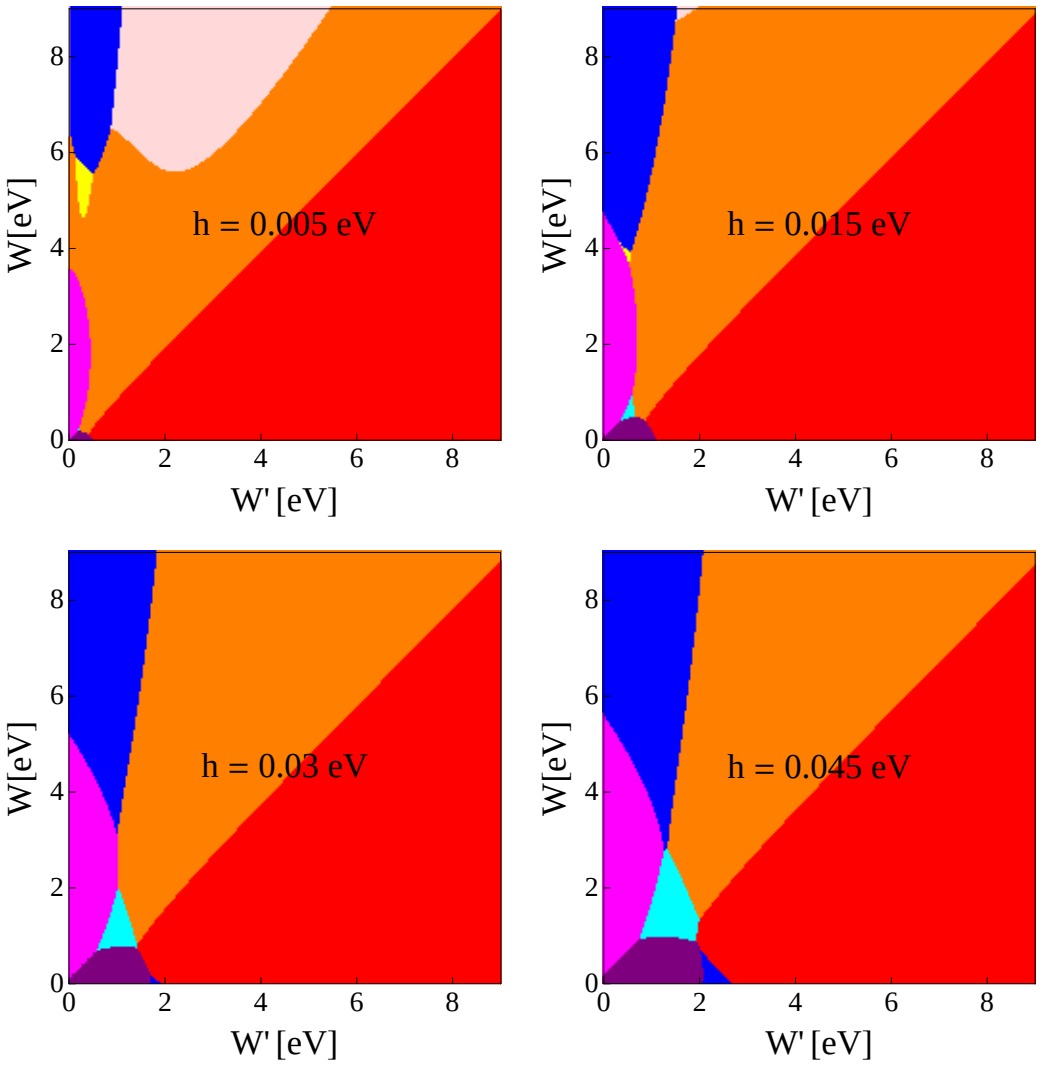

Figure 2.3: The evolution of the phase diagram shown in Fig. 2.1 in a magnetic field.

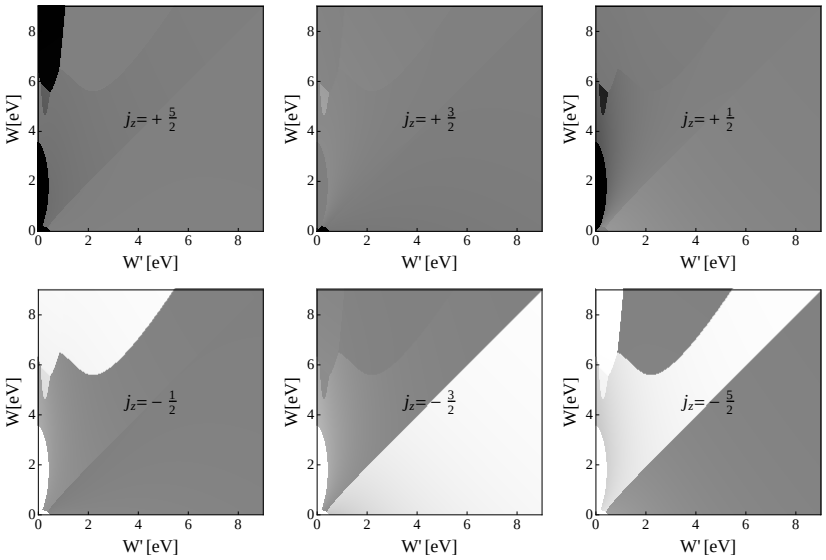

Figure 2.4: Gray-scale plot of occupation n_{j_z} for j_z orbital which is indicated in the center of each graph for $h = 0.005\ eV$. Black areas correspond to fully occupied states while white areas present empty state.

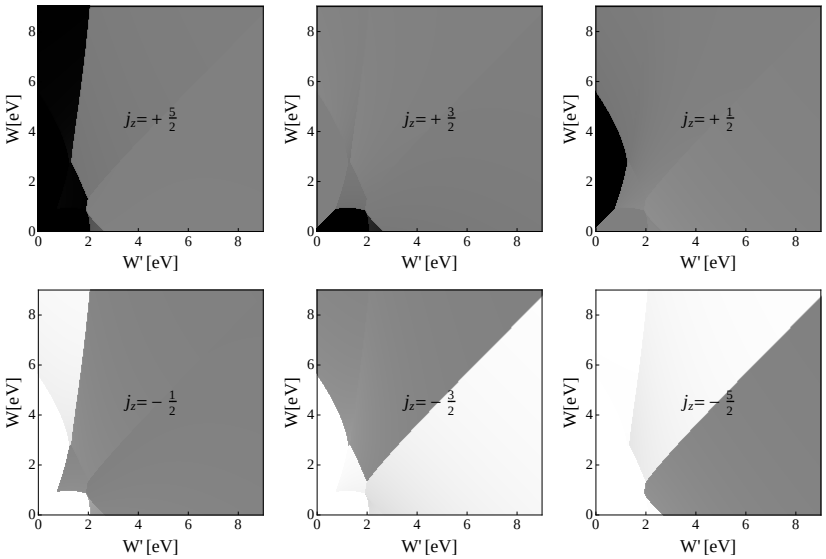

Figure 2.5: Gray-scale plot of occupation n_{j_z} for j_z orbital which is indicated in the center of each graph for $h = 0.030\ eV$. Black areas correspond to fully occupied states while white areas present empty state.

Chapter 3

Slave-boson formalism

3.1 Introduction

Originally, auxiliary particle formulation was first proposed by Barnes [34, 35] and then it was recovered and extended by Read and Newns [36] and Coleman [37] in their work on the mixed valence problem using the Anderson model with two-fold (i.e., spin) degeneracy. Kotliar and Ruckenstein (KR) [24] improved and adapted this method to the single band Hubbard (SBH) model. Qualitatively, the basic idea of KR is that, in a strongly correlated system, the electron is accompanied in the hopping process by a "backflow" of spin and charge excitations of the medium. In a quasiparticle (QP) picture this shows up as a renormalization of the hopping amplitude and as a result leading to a change of the electron effective mass [24]. The qualitative idea is realized by rewriting the original Hamiltonian in terms of two auxiliary fermions and a set of four slave bosons, which keep track of the environment by measuring the occupation number in each of the four possible local states available for hopping. These four states are an empty state, two singly occupied states, and a doubly occupied state. The local interaction is simply taken into account by rescaling the hopping parameter $t \to \tilde{t} = Zt$, where Z is the QP weight.

For the SBH model, KR's approach provides a good description of the low temperature and the low energy Fermi-liquid properties of the system: the excitations are described

as effective excitations of non-interacting QP system. The paramagnetic saddle-point solution within KR's approach at zero temperature is identical to that derived from the Gutzwiller approximation to Gutzwiller's wavefunction. In fact, KR's approach uncovers the limitations of the Gutzwiller approximation and it opens up a systematic way of improving the Gutzwiller solution by taking into account the effect of fluctuations around the saddle point [25]. Moreover, KR's approach leads to a novel strong-coupling mean-field theory which allows for a unified treatment of antiferromagnetism and ferromagnetism, metal-to-insulator transition, and Kondo compensation effects.

However, there is a problem that KR's approach is not manifestly spin-rotational invariant. That is because of the assumption of a distinct spin quantization axis. This problem is generated by embedding the physical Hilbert space of fermion states, which possesses the full spin-rotational invariance, into a much larger Hilbert space of auxiliary boson states, which does not possess this symetry [38]. As a result, it leads to two restrictions in KR's approach: (i) Local interactions are restricted to density-density ones; (ii) when an approximation is made, it is very difficult to project the enlarged Hilbert space of auxiliary particle states onto the original physical Hilbert space.

The above restrictions of KR's approach were cured by Li, Wölfle and Hirschfeld (LWH) in the "Spin-rotation invariant slave-boson approach" for the SBH model [38]. The main advantage of LWH's approach is that for a two-fold degenerate model with density-density interactions, e.g., the SBH model, LWH's saddle-point approximation recovers that of KR's approach. When going beyond a mean-field level by taking into account the effect of fluctuations around the saddle-point, LWH's approach gives some results that have found to be missing in KR's approach. For example, contributions from transverse spin fluctuations are not found within KR's theory [39]. However, they are obtained within LWH's approach whose results are consistent with the results derived within Fermi-liquid theory [40]. Another advantage of LWH's approach is that, for a two-fold degenerate model with generic interactions, e.g., the SBH model in a transverse magnetic field, it takes into account all terms of the local Hamiltonian whereas KR's approach neglects those terms which do not commute with the occupation operator, $n = n_\uparrow + n_\downarrow$.

After LWH's theory, slave-boson theory was further extended by Fresard and Wölfle [41]. Fresard's and Wölfle's approach is manifestly not only spin-rotation but also charge-rotation (particle-hole transformation) invariant. In addition to normal states, superconducting states were also analyzed within slave-boson theories [42, 43, 44, 45].

Several later works have attempted to construct a slave-boson theory for models with arbitrary degeneracy $N > 2$. If the local interactions of the multi-band model under consideration are restricted to density-density interactions and a mean-field solution is desired one can start to build a new slave-boson representation from KR's formulation [46, 47, 48]. However, if one would like to go beyond a mean-field level or if one would like to consider a generic model, e.g., the local Hamiltonian includes exchange interactions, they should start from LWH's formulation to develop a rotationally invariant slave-boson (RISB) representation. This method has been developped by Lechermann, Georges, Kotliar, and Olivier [29]. In this thesis we apply the RISB formulation at a mean-field level to the effective model described by the Hamiltonian (2.11). Before we are going to present the application of the RISB method to the effective model, in the following section let us recall some slave-boson approaches for the SBH model to discuss some essential physical ideas of auxiliary particle theories.

3.2 Slave-boson formalism for the Hubbard model

The Hubbard model has been used as a model for a study of strongly correlated electron systems such as transition metal, valence-mixing and high-T_C materials. The SBH model has been extensively investigated by using various methods such as the Gutzwiller approximation to Gutzwiller's wavefunction, Hubbard I and Hubbard III approximations, auxiliary particle techniques, dynamical mean-field theory, etc. In this section we discuss the main ideas of auxiliary particle theories by briefly recalling three slave-boson approaches to the SBH model.

We start from the finite-U Hubbard model whose Hamiltonian reads

$$H = -t \sum_{\langle ij \rangle \sigma} (c^{\dagger}_{i\sigma} c_{j\sigma} + \text{H.c.}) + U \sum_{i} n_{i\uparrow} n_{i\downarrow} - \mu \sum_{i\sigma} n_{i\sigma}. \tag{3.1}$$

Here t and U are respectively, the nearest-neighbor hopping and the on-site Coulomb repulsion between electrons of different spins, $c^{\dagger}_{i\sigma}$ ($c_{i\sigma}$) are creation (annihilation) operators for an electron of spin σ at site i, and μ is the chemical potential.

There are four possible states at a site i: $|0i\rangle$, $|\uparrow i\rangle$, $|\downarrow i\rangle$, and $|\uparrow\downarrow i\rangle$. They correspond to an empty site, one up (down) spin state and a doubly occupied site, respectively. Using Hubbard projection operators [49], we have the completeness relation for each site i:

$$|0i\rangle\langle 0i| + |\uparrow i\rangle\langle\uparrow i| + |\downarrow i\rangle\langle\downarrow i| + |\uparrow\downarrow i\rangle\langle\uparrow\downarrow i| = 1. \tag{3.2}$$

Since $|0i\rangle$, $|\uparrow i\rangle$, $|\downarrow i\rangle$, and $|\uparrow\downarrow i\rangle$ form a complete basis for site i, any local operator, i.e., affecting only the electron of site i can be written in terms of the projection operators. For example, the annihilation electron operators are expressed by

$$c_{i\uparrow} = |0i\rangle\langle\uparrow i| + |\downarrow i\rangle\langle\uparrow\downarrow i|, \tag{3.3}$$

$$c_{i\downarrow} = |0i\rangle\langle\downarrow i| - |\uparrow i\rangle\langle\uparrow\downarrow i|. \tag{3.4}$$

Note that the appearance of the minus sign in the expression of $c_{i\downarrow}$ is to preserve the canonical anticommutation relations of fermions. As it was shown by Hubbard [49], some of the projection operators are fermion-like, some boson-like. Their commutators or anticommutators form an algebra. These algebraic properties of the projection operators are exactly reproduced by a combined fermion-boson field theory [50], i.e., the projection operators are represented in terms of auxiliary fermions and auxiliary bosons.

However, the representation of the projection operators in terms of auxiliary particles is not unique. Basically, for normal phases of the SBH model, there are two different ways of introducing auxiliary particles. Barnes [34, 35], Read and Newns [36], Coleman [37], and Zou and Anderson [50] introduced two fermions and two bosons. Kotliar and Ruckenstein [24], and Lavagna [25] introduced two fermions and four bosons. In the former case, the charge and spin degrees of freedom are not treated on the same footing as they are treated

in the latter. Although Li, Wölfle and Hirschfeld [38] used two fermions and six bosons, their slave-boson theory belongs to the latter for this reason.

3.2.1 Barnes' approach

Initially, Barnes's approach [34, 35] was proposed for the Anderson model. The approach has been widely used for the Anderson model, especially in the strong correlation limit $U \to \infty$. Later, Zou and Anderson [50] showed, how one applied the method to the SBH model. The mapping is as follows:

$$|0i\rangle \mapsto e_i^\dagger |vac\rangle, \tag{3.5}$$

$$|\uparrow i\rangle \mapsto S_{i\uparrow}^\dagger |vac\rangle, \tag{3.6}$$

$$|\downarrow i\rangle \mapsto S_{i\downarrow}^\dagger |vac\rangle, \tag{3.7}$$

$$|\uparrow\downarrow i\rangle \mapsto d_i^\dagger |vac\rangle. \tag{3.8}$$

Here e_i and d_i are Bose fields and $S_{i\sigma}$ are Fermi fields, $|vac\rangle$ is the vacuum. Due to the completeness condition (3.2) the auxiliary fields have to fulfill the following constraint:

$$e_i^\dagger e_i + d_i^\dagger d_i + \sum_\sigma S_{i\sigma}^\dagger S_{i\sigma} = 1. \tag{3.9}$$

Using Eqs. (3.3)–(3.4) the electron operators $c_{i\sigma}$ are expressed in terms of auxiliary fields as

$$c_{i\uparrow} = e_i^\dagger S_{i\uparrow} + d_i S_{i\downarrow}^\dagger, \tag{3.10}$$

$$c_{i\downarrow} = e_i^\dagger S_{i\downarrow} - d_i S_{i\uparrow}^\dagger. \tag{3.11}$$

Substituting Eqs. (3.10)–(3.11) into Eq. (3.1), one finds

$$H = H_0 + tH', \tag{3.12}$$

where

$$H_0 = -t \sum_{\langle ij\rangle\sigma} (e_i e_j^\dagger - d_i d_j^\dagger) S_{i\sigma}^\dagger S_{j\sigma} + \text{H.c.} + \mu \sum_i (e_i^\dagger e_i - d_i^\dagger d_i) - \mu \mathcal{N}, \tag{3.13}$$

$$H' = -\sum_{\langle ij\rangle} \left[(e_i d_j + e_j d_i) S_{i\uparrow}^\dagger S_{i\downarrow}^\dagger + \text{H.c.} \right]. \tag{3.14}$$

Here $\mathcal{N}$ is the number of the lattice sites. Zou and Anderson [50] pointed out the nature of the transformation (3.10)–(3.11): physically $e_i^\dagger$ corresponds to creating an empty site and $d_i^\dagger$ a doubly occupied site. Therefore, $e_i^\dagger$ and $d_i^\dagger$ have opposite charges (e and -e, respectively). It is clear that from Eqs. (3.10)–(3.11) one can treat $S_{i\sigma}^\dagger$ as a neutral particle. However, the fact that only states $|0i\rangle$ and $|\uparrow\downarrow i\rangle$ are represented by Bose operators while $|i\sigma\rangle$ are represented by pseudofermion operators leads to a problem when a mean-field approximation is made. The reason is that the charge excitations are well represented by the slave-bosons e and d, whereas the spin excitations are not. This fact shows up in $1/N$ expansion of N-orbital degeneracy generation of the $N = 2$ single band model: while charge fluctuations appear in order $1/N$, spin excitations only show up in order $1/N^2$. This means spin correlations appear only as a second-order process. For this reason the Barnes approach is good for system whose spin fluctuations are small and not relevant. One is tempted to do a mean-field theory on the Hamiltonian (3.12), namely replace e_i and d_i by their classical values. However, this is incorrect because the representation of $c_{i\uparrow}$ and $c_{i\downarrow}$ by Eqs. (3.10)–(3.11) has the peculiarity of mixing fermion particles and holes. As a result, the Hamiltonian (3.12) contains many virtual processes which ought to be eliminated before one lets bosons condense, i.e, performing the mean-field approximation. Using a canonical transformation $\tilde{S}$ one can eliminate the H' term in H to order t/U, i.e., $tH' + [H_0, \tilde{S}] = 0$. For sufficiently large U, one neglects terms of order of $(t/U)^2$ and restricts oneself within the subspace determined by Eq. (3.9), yielding

$$\tilde{S} = \frac{t}{U}\sum_{\langle ij\rangle}(e_i^\dagger d_j^\dagger + e_j^\dagger d_i^\dagger)S_{j\downarrow}S_{i\uparrow} - \text{H.c.}, \tag{3.15}$$

$$H_{eff} = H_0 - \frac{4t^2}{U}\sum_{\langle ij\rangle}\left(S_{i\uparrow}^\dagger S_{j\downarrow}^\dagger S_{j\downarrow}S_{i\uparrow} + S_{i\uparrow}^\dagger S_{j\uparrow}S_{j\downarrow}^\dagger S_{i\downarrow}\right), \tag{3.16}$$

where H_0 is defined by Eq. (3.13). Now one can replace e_i and d_i in Eq. (3.16) by their classical values to carry out a mean-field approximation. However, when solving the problem a supplementary approximation still needs to be made in the neutral fermion fields $S_{i\sigma}$. That is because Eq. (3.16) contains terms of four fermion operators, e.g., $S_{i\uparrow}^\dagger S_{j\downarrow}^\dagger S_{j\downarrow}S_{i\uparrow}$. Furthermore, one has to keep in mind that the effective Hamiltonian (3.16) is good only

for the large-U limit. Due to these reasons Barnes approach has not been widely used for the Hubbard model. It is therefore desirable to explore alternative slave-boson representations. One obvious possibility is a representation in terms of two Schwinger bosons and two spinless fermions. The detail mapping reads

$$|0i\rangle \mapsto f_i^\dagger|vac\rangle, \tag{3.17}$$

$$|\uparrow i\rangle \mapsto a_{i\uparrow}^\dagger|vac\rangle, \tag{3.18}$$

$$|\downarrow i\rangle \mapsto a_{i\downarrow}^\dagger|vac\rangle, \tag{3.19}$$

$$|\uparrow\downarrow i\rangle \mapsto h_i^\dagger|vac\rangle. \tag{3.20}$$

Here $a_{i\uparrow}^\dagger$ and $a_{i\downarrow}^\dagger$ are Bose operators, assumed to transform as a two-component spinor under a rotation in spin space, and $f_i^\dagger$ and $h_i^\dagger$ are spinless Fermi operators [51]. The electron operators are expressed as

$$c_{i\uparrow} = f_i^\dagger a_{i\uparrow} + h_i a_{i\downarrow}^\dagger, \tag{3.21}$$

$$c_{i\downarrow} = f_i^\dagger a_{i\downarrow} - h a_{i\uparrow}^\dagger. \tag{3.22}$$

The anticommunication relations of the operators $c_{i\sigma}$ are preserved if the $a_{i\sigma}$ (f_i, h_i) operators obey canonical commutation (anticommutation) relations and the following constraint

$$\sum_\sigma a_{i\sigma}^\dagger a_{i\sigma} + f_i^\dagger f_i + h_i^\dagger h_i = 1, \tag{3.23}$$

is satisfied. However, the fact that only states $|i\sigma\rangle$ are represented by Bose operators while $|0i\rangle$ and $|\uparrow\downarrow i\rangle$ are represented by pseudofermion operators leads to a similar problem mentioned earlier in Barnes' approach. Here the roles of fermions and bosons are interchanged. Spin and charge excitations are still treated unequally. In contrast to Barnes' approach the above representation using Schwinger bosons is good for investigating the effect of spin fluctuations.

3.2.2 Kotliar and Ruckenstein's approach

In Barnes' approach, only two of the four local states are mapped onto slave-bosons. Because of this reason, Barnes' representation suffers from a problem that charge and spin excitations are treated unequally as mentioned above. In order to cure this problem, a complete mapping of the four local states onto slave bosons needs to be made. This idea was first introduced by KR [24], who proposed a representation in terms of two auxiliary fermions $f_{i\uparrow}$, $f_{i\downarrow}$ and of slave bosons e_i and d_i for the empty and doubly occupied states and two bosons $p_{i\uparrow}$, $p_{i\downarrow}$ for singly occupied states at site i. The introduction of auxiliary particles is to help characterize these states which enlarge the original Hilbert space to the one of fermion and boson states. The mapping detail is the following:

$$|0i\rangle \mapsto e_i^\dagger|vac\rangle, \tag{3.24}$$

$$|\uparrow i\rangle \mapsto p_{i\uparrow}^\dagger f_\uparrow^\dagger|vac\rangle, \tag{3.25}$$

$$|\downarrow i\rangle \mapsto p_{i\downarrow}^\dagger f_\downarrow^\dagger|vac\rangle, \tag{3.26}$$

$$|\uparrow\downarrow i\rangle \mapsto d_i^\dagger f_{i\uparrow}^\dagger f_{i\downarrow}^\dagger|vac\rangle. \tag{3.27}$$

Here e_i, $p_{i\sigma}$ and d_i are Bose fields and $f_{i\sigma}$ are fermions. The squares of expectation values of Bose fields are supposed to give the occupation probabilities of the four states. In terms of auxiliary particles the electron operators are represented as

$$c_{i\sigma} = R_{i\sigma} f_{i\sigma}, \tag{3.28}$$

$$R_{i\sigma} = e_i^\dagger p_{i\sigma} + p_{i\bar{\sigma}}^\dagger d_i, \tag{3.29}$$

where $\bar{\sigma}$ is the complement of σ. Note that the peculiarity of mixing fermion particles and holes as seen in Eqs. (3.10)–(3.11) no longer occurs. To make this representation physically meaningful, it must be accompanied by three constraints. They ensure that only the physically relevant subspace of the enlarged Hilbert space is considered. One constraint is

$$P_i \equiv e_i^\dagger e_i + \sum_\sigma p_{i\sigma}^\dagger p_{i\sigma} + d_i^\dagger d_i - 1 = 0, \tag{3.30}$$

which states that a site is either empty, singly occupied, or doubly occupied. The two remaining constraints are

$$Q_{i\sigma} \equiv f^\dagger_{i\sigma} f_{i\sigma} - p^\dagger_{i\sigma} p_{i\sigma} - d^\dagger_i d_i = 0, \tag{3.31}$$

they ensure that when an electron with spin σ is at site i, this site is either singly occupied with spin σ or doubly occupied. Introduction of the Bose fields allows us to linearize the local interaction and to make the Hamiltonian being quadratic in term of fermions. The SBH model is rewritten in terms of the auxiliary fields as

$$H = -t \sum_{\langle ij\rangle\sigma} (R^\dagger_{i\sigma} f^\dagger_{i\sigma} f_{j\sigma} R_{j\sigma} + \text{H.c.}) + U \sum_i d^\dagger_i d_i + \mu \sum_{i\sigma} f^\dagger_{i\sigma} f_{i\sigma}. \tag{3.32}$$

The effect of the operators $R^\dagger_{i\sigma}$, $R_{j\sigma}$ is the following: when an electron with spin σ is annihilated at site j, either a doubly occupied site goes over into a singly occupied site with spin $\bar{\sigma}$ or a singly occupied site with spin σ goes over into an empty site. This is described by the operator $R_{j\sigma}$. Similarly, when an electron hops onto site i, a singly occupied state is created if the site was empty before, or a doubly occupied state is created when before the site was singly occupied with spin $\bar{\sigma}$. This is ensured by the operator $R^\dagger_{i\sigma}$. The Coulomb term is bilinear in the boson operators and acts only on doubly occupied sites.

One checks that the operators P_i and $Q_{i\sigma}$ commute with the Hamiltonian (3.32), i.e., once in the physical subspace of the enlarged Hilbert space, we remain in it. Therefore the constraints (3.30) and (3.31) are enforced at each site by time-independent Lagrange multipliers, which we symbolize by $\lambda^{(1)}_i$ and $\lambda^{(2)}_{i\sigma}$, respectively. One finds

$$\begin{aligned} H &= -t \sum_{\langle ij\rangle\sigma} (R^\dagger_{i\sigma} f^\dagger_{i\sigma} f_{j\sigma} R_{j\sigma} + \text{H.c.}) + U \sum_i d^\dagger_i d_i + \mu \sum_{i\sigma} f^\dagger_{i\sigma} f_{i\sigma} \\ &\quad + \sum_i \lambda^{(1)}_i (e^\dagger_i e_i + \sum_\sigma p^\dagger_{i\sigma} p_{i\sigma} + d^\dagger_i d_i - 1) \\ &\quad + \sum_{i\sigma} \lambda^{(2)}_{i\sigma} (f^\dagger_{i\sigma} f_{i\sigma} - p^\dagger_{i\sigma} p_{i\sigma} - d^\dagger_i d_i). \end{aligned} \tag{3.33}$$

The mean-field approximation replaces the Bose fields by their classical values, which we assume to be real. The operators $e^\dagger_i$, e_i, $p^\dagger_{i\sigma}$, $p_{i\sigma}$, and $d^\dagger_i$, d_i are replaced by their

expectation values e, p_σ, d. In the noninteracting limit $U = 0$, one can easily find a paramagnetic state, i.e., $p_\uparrow = p_\downarrow$. Consequently, the constraints (3.30)–(3.31) reduce to

$$e^2 + 2p^2 + d^2 = 1, \tag{3.34}$$

$$p^2 + d^2 = < f^\dagger_\sigma f_\sigma >= n/2, \tag{3.35}$$

where n denotes the total band filling. At the half-filling, i.e., $n = 1$, one easily finds $e^2 = p^2 = d^2 = \frac{1}{4}$ and thus $\langle R^\dagger_{i\sigma} R_{j\sigma}\rangle = e^2 p^2_\sigma + d^2 p^2_{\bar\sigma} + 2edp_\sigma p_{\bar\sigma} = \frac{1}{4}$, rather than unity as it should be for the noninteracting system. In order to resolve this problem one notes the fact that the procedure described above is not unique; there are many different Hamiltonians, $\tilde H$ with different properties in the enlarged Hilbert space which lead to the same spectrum as the Hamiltonian (3.1) when restricted to the physical Hilbert space defined by the constraints (3.30) and (3.31). This arbitrariness poses no problem as long as the constraints are handled exactly. However, any approximation which relaxes the constraints is sensitive to the precise choice of $\tilde H$. KR exploited this fact by taking that form of $\tilde H$ that gives exact results in the non-interacting limit within mean-field approximation. $\tilde H$ is obtained from H in Eq. (3.33) by replacing the operator $R_{i\sigma}$ by another operator, $\tilde R_{i\sigma}$

$$\tilde R_{i\sigma} = (1 - d^\dagger_i d_i - p^\dagger_{i\sigma} p_{i\sigma})^{-1/2} R_{i\sigma} (1 - e^\dagger_i e_i - p^\dagger_{i\bar\sigma} p_{i\bar\sigma})^{-1/2}, \tag{3.36}$$

which has the same eigenvalues as $R_{i\sigma}$ in the physical Hilbert space. Finally KR's representation of the SBH model reads

$$\begin{aligned} H = & -t \sum_{\langle ij\rangle\sigma} (\tilde R^\dagger_{i\sigma} f^\dagger_{i\sigma} f_{j\sigma} \tilde R_{j\sigma} + \text{H.c.}) + U \sum_i d^\dagger_i d_i + \mu \sum_{i\sigma} f^\dagger_{i\sigma} f_{i\sigma} \\ & + \sum_i \lambda^{(1)}_i (e^\dagger_i e_i + \sum_\sigma p^\dagger_{i\sigma} p_{i\sigma} + d^\dagger_i d_i - 1) \\ & + \sum_{i\sigma} \lambda^{(2)}_{i\sigma} (f^\dagger_{i\sigma} f_{i\sigma} - p^\dagger_{i\sigma} p_{i\sigma} - d^\dagger_i d_i). \end{aligned} \tag{3.37}$$

Within the mean-field approximation one finds

$$\begin{aligned} H &= -t\sum_{\langle ij\rangle\sigma} Z_\sigma (f^\dagger_{i\sigma} f_{j\sigma} + \text{H.c.}) + \sum_{i\sigma} (\mu - \lambda^{(2)}_\sigma) f^\dagger_{i\sigma} f_{i\sigma} \\ &\quad + \mathcal{N}\left(Ud^2 + \lambda^{(1)}(e^2 + \sum_\sigma p^2_\sigma + d^2 - 1) - \sum_\sigma \lambda^{(2)}_\sigma (p^2_\sigma + d^2) \right), \end{aligned} \tag{3.38}$$

where $\mathcal{N}$ is the number of the lattice sites and Z_σ is the QP weight that is evaluated at the saddle point as $Z_\sigma = \langle \tilde{R}^\dagger_{i\sigma} \tilde{R}_{j\sigma} \rangle$. As pointed previously, the above formulation of the slave-boson theory is not rotationally invariant in spin space because we have assumed a distinct spin quantization axis. An improvement of the theory will be discussed in the next section.

3.2.3 Li, Wölfle and Hirschfeld's approach

As we mentioned earlier in the introduction part of this chapter, there are two restrictions within KR's approach due to the assumption of a distinct spin quantization axis. In this section let us recall the slave-boson representation of LWH [38] to discuss how these restrictions were resolved.

The idea of LWH is that KR's representation of $|\sigma i\rangle$ is not spin-rotation invariant, but depends on the choice of a quantization axis in spin space. In order to retrieve the two degrees of freedom associated with the quantization axis, it is the best to interpret the operator product $p^\dagger_{i\sigma} f^\dagger_{i\sigma}$ in Eqs. (3.25)–(3.26) as creating a composite particle, whose spin should be 1/2. Since the spin of the auxiliary fermion $f_{i\sigma}$ should be 1/2 as well, possible spin values for the p-bosons are $S = 0$ and $S = 1$. From this consideration one realizes that to construct a spin-rotation invariant representation one needs four p-bosons instead of just two as in KR's approach. Similarly to KR's representation, LWH introduce two auxiliary fermions $f_{i\sigma}$ to account for the quasiparticle degrees of freedom. But the way they introduce slave bosons is different from that of KR. In order to understand LWH's representation, let us consider the one-particle Hilbert space at site i. There are two physical states, namely $|\uparrow i\rangle$ and $|\downarrow i\rangle$, and there are two auxiliary fermion states,

namely $f^{\dagger}_{i\uparrow}|vac\rangle$ and $f^{\dagger}_{i\downarrow}|vac\rangle$. For each pair of physical state $|\sigma i\rangle$ and auxiliary fermion state $f^{\dagger}_{i\sigma'}|vac\rangle$ they introduce a slave boson $p^{\dagger}_{i\sigma\sigma'}$, where the first and second spin index represent the physical state and auxiliary fermion state, respectively. Note that the slave bosons $p^{\dagger}_{i\sigma\sigma'}$ can be written in a matrix form

$$\underline{p}^{\dagger}_{i} = \begin{pmatrix} p^{\dagger}_{i\uparrow\uparrow} & p^{\dagger}_{i\uparrow\downarrow} \\ p^{\dagger}_{i\downarrow\uparrow} & p^{\dagger}_{i\downarrow\downarrow} \end{pmatrix}, \tag{3.39}$$

which leads to a concept of *diagonal bosons* ($p^{\dagger}_{i\uparrow\uparrow}$ and $p^{\dagger}_{i\downarrow\downarrow}$) , i.e., $\sigma = \sigma'$, and *off-diagonal bosons* ($p^{\dagger}_{i\uparrow\downarrow}$ and $p^{\dagger}_{i\downarrow\uparrow}$), i.e., $\sigma \neq \sigma'$. From here on we use underlined symbols to represent matrices. The KR mapping is recovered by neglecting all off-diagonal bosons $p^{\dagger}_{i\uparrow\downarrow}$ and $p^{\dagger}_{i\downarrow\uparrow}$ and by setting the diagonal bosons: $p^{\dagger}_{i\sigma\sigma} \mapsto p^{\dagger}_{i\sigma}$. The mapping detail is as follows:

$$|0i\rangle \mapsto e^{\dagger}_{i}|vac\rangle, \tag{3.40}$$

$$|\uparrow i\rangle \mapsto \frac{1}{\sqrt{2}}\left(p^{\dagger}_{i\uparrow\uparrow}f^{\dagger}_{\uparrow} + p^{\dagger}_{i\uparrow\downarrow}f^{\dagger}_{\downarrow}\right)|vac\rangle, \tag{3.41}$$

$$|\downarrow i\rangle \mapsto \frac{1}{\sqrt{2}}\left(p^{\dagger}_{i\downarrow\uparrow}f^{\dagger}_{\uparrow} + p^{\dagger}_{i\downarrow\downarrow}f^{\dagger}_{\downarrow}\right)|vac\rangle, \tag{3.42}$$

$$|\uparrow\downarrow i\rangle \mapsto d^{\dagger}_{i}f^{\dagger}_{i\uparrow}f^{\dagger}_{i\downarrow}|vac\rangle. \tag{3.43}$$

Here all e_i, $p_{i\sigma,\sigma'}$ and d_i are Bose fields. It is useful to represent $p^{\dagger}_{i\sigma\sigma'}$ in terms of its projections onto the usual Pauli matrices $\underline{\tau}_1$, $\underline{\tau}_2$, $\underline{\tau}_3$ and the unit matrix $\underline{\tau}_0$

$$p^{\dagger}_{i\nu} = \frac{1}{\sqrt{2}} tr\left(\underline{\tau}_{\nu}\underline{p}^{\dagger}_{i}\right). \tag{3.44}$$

As it is expected, the boson fields $p^{\dagger}_{i\sigma\sigma'}$ form a spin singlet $p^{\dagger}_{i0}$ and a spin triplet $\mathbf{p}^{\dagger}_{i} = \left(p^{\dagger}_{i1}, p^{\dagger}_{i2}, p^{\dagger}_{i3}\right)$. The set of triplet components $\mathbf{p}^{\dagger}_{i}$ transforms as a vector under spin rotations, while $p^{\dagger}_{i0}$ transforms as a scalar. The spin-zero boson $p^{\dagger}_{i0}$ represents the charge degrees of freedom of the spinor states, whereas the spin-one boson $\mathbf{p}^{\dagger}_{i}$ describes the spin degrees of freedom. However, one should note that these fields do not automatically represent the electron charge and spin operators, because the density operators involve the square of the matrix $\underline{p}_i$. In terms of auxiliary particles the electron operators are

represented as

$$c^\dagger_{i\sigma} = \sum_{\sigma'} R^\dagger_{i\sigma\sigma'} f^\dagger_{i\sigma'}, \tag{3.45}$$

$$c_{i\sigma} = \sum_{\sigma'} f_{i\sigma'} R_{i\sigma'\sigma}, \tag{3.46}$$

$$R_{i\sigma'\sigma} = e^\dagger_i p_{i\sigma'\sigma} + \sigma\sigma' p^\dagger_{i\bar{\sigma}\bar{\sigma}'} d_i. \tag{3.47}$$

The operator $R_{i\sigma'\sigma}$ describes the sum of processes: from a singly occupied site to an empty site and from a doubly occupied site to a singly occupied site with time-reversed spin. The term evolving the operator d_i may be expressed in a more transparent way by using the transformation properties of $p_{i\sigma\sigma'}$ under the time-reversal operator $\hat{T}$: $\tilde{p}_{i0} = \hat{T} p_{i0} \hat{T}^{-1} = p_{i0}$, $\tilde{\mathbf{p}}_i = \hat{T}\mathbf{p}_i\hat{T}^{-1} = -\mathbf{p}_i$, implying

$$\tilde{p}_{i\sigma\sigma'} = \left(\hat{T}\underline{p}_i\hat{T}^{-1}\right)_{\sigma\sigma'} = \sigma\sigma' p_{i\bar{\sigma}'\bar{\sigma}}. \tag{3.48}$$

It follows that

$$\underline{R}_i = e^\dagger_i \underline{p}_i + \underline{\tilde{p}}^\dagger_i d_i, \tag{3.49}$$

which is a generalization of Eq. (3.29). It is important to note that in KR's formalism the spin index σ carried by the physical operator $c_{i\sigma}$ is identical to that of the QP operator $f_{i\sigma}$. But in LWH's method it is different: the physical operator $c_{i\sigma}$ is connected with not only the QP operator $f_{i\sigma}$ but also with the QP operator $f_{i\bar{\sigma}}$ of the complementary spin. Similarly to KR's approach the form of the rotation matrix $\underline{R}_i$ is not unique. One can construct a new one by multiplying it with an arbitrary operator whose eigenvalues are unity in the physical subspace. As we mentioned in the previous section, one exploits this arbitrariness such that the mean-field approximation gives exact results in the noninteracting limit by taking the following form of $\underline{R}_i$:

$$\underline{\tilde{R}}_i = \left[(1 - d^\dagger_i d_i)\underline{\tau}_0 - \underline{p}^\dagger_i \underline{p}_i\right]^{-1/2} \underline{\mathrm{R}}_i \left[(1 - e^\dagger_i e_i)\underline{\tau}_0 - \underline{\tilde{p}}^\dagger_i \underline{\tilde{p}}_i\right]^{-1/2}. \tag{3.50}$$

In terms of auxiliary particles the SBH Hamiltonian reads

$$H = -t \sum_{\langle ij\rangle\sigma\sigma_1\sigma_2} (\tilde{R}^\dagger_{i\sigma\sigma_1} f^\dagger_{i\sigma_1} f_{j\sigma_2} \tilde{R}_{j\sigma_2\sigma} + \mathrm{H.c.}) + U\sum_i d^\dagger_i d_i + \mu \sum_{i\sigma} f^\dagger_{i\sigma} f_{i\sigma}. \tag{3.51}$$

To make this representation physically meaningful, it must be accompanied by five constraints. They ensure that only the physically relevant part of the enlarged Hilbert space is considered. One constraint is

$$P_i = e^\dagger_i e_i + \sum_{\sigma\sigma'} p^\dagger_{i\sigma\sigma'} p_{i\sigma'\sigma} + d^\dagger_i d_i - 1 = 0, \tag{3.52}$$

which states that a site is either empty, singly occupied, or doubly occupied. The four remaining constraints are

$$Q_{i\sigma\sigma'} = f^\dagger_{i\sigma} f_{i\sigma'} - \sum_{\sigma_1} p^\dagger_{i\sigma_1\sigma'} p_{i\sigma\sigma_1} - \delta_{\sigma\sigma'} d^\dagger_i d_i = 0. \tag{3.53}$$

They ensure that the number of electrons must match the number of p bosons and d bosons. One can write the constraints (3.53) explicitly as

$$\begin{aligned}
Q_{i\uparrow\uparrow} &= f^\dagger_{i\uparrow} f_{i\uparrow} - p^\dagger_{i\uparrow\uparrow} p_{i\uparrow\uparrow} - p^\dagger_{i\downarrow\uparrow} p_{i\uparrow\downarrow} - d^\dagger_i d_i = 0, && (3.54)\\
Q_{i\downarrow\downarrow} &= f^\dagger_{i\downarrow} f_{i\downarrow} - p^\dagger_{i\downarrow\downarrow} p_{i\downarrow\downarrow} - p^\dagger_{i\uparrow\downarrow} p_{i\downarrow\uparrow} - d^\dagger_i d_i = 0, && (3.55)\\
Q_{i\uparrow\downarrow} &= f^\dagger_{i\uparrow} f_{i\downarrow} - p^\dagger_{i\uparrow\downarrow} p_{i\uparrow\uparrow} - p^\dagger_{i\downarrow\downarrow} p_{i\uparrow\downarrow} = 0, && (3.56)\\
Q_{i\downarrow\uparrow} &= f^\dagger_{i\downarrow} f_{i\uparrow} - p^\dagger_{i\downarrow\uparrow} p_{i\downarrow\downarrow} - p^\dagger_{i\uparrow\uparrow} p_{i\downarrow\uparrow} = 0. && (3.57)
\end{aligned}$$

There are thus two additional constrains (3.56)–(3.57) compared to KR's formulation. Note that Barnes' approach was also generalized to be spin-and charge-rotational invariant by Alvarez, Balseiro, and Ceccatto [52]. The idea is that bosons and fermions are exactly integrated out by help of a Hubbard-Stratonovich transformation. Afterward a saddle point approximation is made by replacing the Hubbard-Stratonovich fields and Lagrange multipliers by c-numbers which are determined by minimizing the effective action.

3.3 Slave-boson formalism for the effective model

In the previous section we have discussed an application of LWH's approach for the single-band Hubbard model. Here, we apply a generalization of LWH's approach for a multi-orbital model, namely, the RISB method [29] for the effective model defined by the Hamiltonian (2.11).

We first describe the auxiliary particles introduced on each site within the RISB formalism. For the sake of clarity, we skip here the site index. We introduce six auxiliary fermions d_{j_z} to account for the QP degrees of freedom. Slave bosons are introduced to connect the physical Hilbert space (of original $f^\dagger_{j_z}$ operators) and the auxiliary Hilbert space (of auxiliary $d^\dagger_{j_z}$ operators). In order to define the slave bosons one needs to choose two basis sets: one for the Hilbert space of $f^\dagger_{j_z}$ operators, the other for that of $d^\dagger_{j_z}$ operators. In the RISB formalism, the two basis sets can be arbitrarily chosen. However, for convenience, a multiplet-Fock basis is used, namely, we choose the multiplet basis Γ for the physical Hilbert space and the Fock basis $n \equiv |n\rangle$ for the auxiliary Hilbert space. We speak of Fock-Fock (multiplet-multiplet) basis when the Fock (multiplet) basis is chosen for both physical states and auxiliary states, respectively. The choice of the multiplet-Fock basis is to make the local interaction being diagonalized in the multiplet basis and to simplify some equations, e.g., the constraints. The label $\Gamma \equiv |M; \mathcal{J}, \mathcal{J}_z\rangle$ refers to an eigenstate of the local interaction $\hat{U}(a)$ defined by Eq. (2.3), which is a multiplet state of M electrons forming a total angular momentum $\mathcal{J}$ with a component $\mathcal{J}_z$ in the $z-$direction. Whereas $n \equiv |n\rangle$ denotes a Fock state of auxiliary fermion particles, which is an eigenstate of the occupation number operator $\sum_{j_z} d^\dagger_{j_z} d_{j_z}$.

For each pair of a physical state Γ and an auxiliary state $|n\rangle$, we introduce a slave-boson creation operator $\phi^\dagger_{\Gamma n}$. As a result, within the RISB approach, a density matrix is constructed instead of just a probability amplitude for each state. This approach might lead to an enormous amount of auxiliary bosons, but, as we will see in the following, symmetries allow to cancel most of these bosons without loosing any generality. Both slave-boson methods, i.e., the ones developped by KR and by Hasegawa, can be obtained as approximations from the RISB formalism: first one has to choose, respectively, the Fock-Fock or the multiplet-multiplet basis, and then to neglect, as an approximation, all *off diagonal* bosons $\phi_{nn'}$ (with $n \neq n'$) or $\phi_{\Gamma\Gamma'}$ (with $\Gamma \neq \Gamma'$). In order not to be misleading, we would like to emphasis that the first index of a slave boson, e.g., $\phi_{nn'}$, refers to a state in the original Hilbert state whereas the second refers to a state in the auxiliary space. So that whenever comparing the two indices, e.g., $n \neq n'$ or $n = n'$

as mentioned above, one understands that the physical state $|n\rangle$ is compared with the counterpart of the auxiliary state $|n'\rangle$ in the physical Hilbert space. The counter part of an auxiliary $|n'\rangle$ state is obtained by simply replacing its $d^\dagger_{j_z}$ with $f^\dagger_{j_z}$. The auxiliary bosons $\phi^\dagger_{\Gamma n}$ which are relevant here are the ones for which the overlap between the multiplet state $|\Gamma\rangle$ and the Fock state $|n\rangle$ is non-zero. Intuitively, this results from the fact that each inter-site hopping term in the Hamiltonian (2.11) transforms local Fock states into other local Fock sates, while the interaction $\hat{U}$ is diagonal in the multiplet basis. We thus omit all the bosons $\phi^\dagger_{\Gamma n}$ that have $\langle n|\Gamma\rangle = 0$. Thus, there are 116 bosons in our current problem (see Appendix A). It follows that the QP weight matrix as we will see below is diagonal and the number of constraints is $N + 1 = 7$. Note that, since $\mathcal{J}_z$ is a good quantum number, $\mathcal{J}_z(\Gamma) \neq \mathcal{J}_z(n)$ follows that $\langle n|\Gamma\rangle = 0$. As a consequence, bosons which have $\mathcal{J}_z(\Gamma) \neq \mathcal{J}_z(n)$ are cancelled.

The local $f-$electron operators are expressed in term of auxiliary bosons and fermions as follows:

$$f_{j_z} = R^\dagger_{j_z}[\Phi]\; d_{j_z}, \tag{3.58}$$

where the operator $R^\dagger_{j_z}[\Phi]$ is defined as

$$R^\dagger_{j_z}[\Phi] \equiv \frac{\hat{\gamma}_{j_z}[\Phi]}{\sqrt{\hat{n}_{j_z}[\Phi]\,(1-\hat{n}_{j_z}[\Phi])}}, \tag{3.59}$$

with

$$\hat{\gamma}_{j_z}[\Phi] \equiv \sum_{\Gamma\Gamma',nn'} \langle\Gamma|f^\dagger_{j_z}|\Gamma'\rangle\langle n|f^\dagger_{j_z}|n'\rangle\; \phi^\dagger{}_{\Gamma n}\phi_{\Gamma' n'}, \tag{3.60}$$

$$\hat{n}_{j_z}[\Phi] \equiv \sum_{\Gamma n} \phi^\dagger{}_{\Gamma n}\phi_{\Gamma n}\langle n|f^\dagger_{j_z}f_{j_z}|n\rangle. \tag{3.61}$$

Reintroducing the site index, the Hamiltonian (2.11) is written in terms of the auxiliary operators as

$$H = -\sum_{\langle a,b\rangle,\, j_z} t_{j_z}\left[R_{j_z}[\Phi_a]R^\dagger_{j_z}[\Phi_b]d^\dagger_{aj_z}d_{bj_z} + H.c.\right] + \sum_{a,\,\Gamma n} E_\Gamma \phi^\dagger_{a,\Gamma n}\phi_{a,\Gamma n}, \tag{3.62}$$

where E_Γ are the eigenvalues of the local Hamiltonian $\hat{U}$ (see Appendix A). We will see later that within the mean-field approximation the operators $R^\dagger_{j_z}[\Phi]$ are connected to

the QP weights by the relations $Z_{j_z} = |R_{j_z}|^2$. The unphysical states introduced by the slave-boson mapping are projected out by imposing the local constraints:

$$1 = \sum_{\Gamma n} \phi^\dagger_{a,\Gamma n}\phi_{a,\Gamma n}, \tag{3.63}$$

$$d^\dagger_{aj_z}d_{aj_z} = \sum_{\Gamma n}\langle n|f^\dagger_{j_z}f_{j_z}|n\rangle\phi^\dagger_{a,\Gamma n}\phi_{a,\Gamma n}. \tag{3.64}$$

It is clear that the basis for the physical Hilbert space can be chosen arbitrarily in the RISB formalism due to its rotational invariance. One can change a basis from the multiple-basis $|\Gamma\rangle$ to the Fock-basis $|n\rangle$ and consider Fock-Fock bosons $\phi_{n'n}$ by using the following linear transformation

$$\phi^\dagger_{n'n} = \sum_{\Gamma}\langle\Gamma|n'\rangle\phi^\dagger_{\Gamma n}. \tag{3.65}$$

But as mentioned above here we use the eigenstates $|\Gamma\rangle$ of the local Hamiltonian as a basis set for convenience. The diagonal Fock-Fock bosons ϕ_{nn} are the ones introduced in the Kotliar-Ruckenstein formalism.

In particular, our local Hamiltonian is a real and symmetric matrix. Therefore in the numerical calculations we use the same linear combinations of the Fock states which define the atomic multiplet $|\Gamma\rangle$ as a basis set $|\Gamma'\rangle$ for quasiparticles and corresponding bosons $\phi_{\Gamma\Gamma'}$ are considered. This is useful for interpreting the results at the saddle-point (see the next Chapters). The relation between the multiplet-multiplet bosons $\phi_{\Gamma\Gamma'}$ and the multiplet-Fock bosons $\phi_{\Gamma n}$is the following

$$\phi^\dagger_{\Gamma\Gamma'} = \sum_{n}\langle n|\Gamma'\rangle\phi^\dagger_{\Gamma n}. \tag{3.66}$$

Nevertheless, one can combine the above two linear transformations (3.65) and (3.66) to find the relation between the Fock-Fock bosons and the multiplet-multiplet bosons:

$$\phi^\dagger_{\Gamma\Gamma'} = \sum_{nn'}\langle\Gamma|n'\rangle\langle n|\Gamma'\rangle\phi^\dagger_{n'n}. \tag{3.67}$$

3.3.1 Mean-field approximation

In this section we derive mean-field equations for paramagnetic and ferromagnetic phases by assuming that the groundstate is invariant under shifts by one lattice site. The gen-

eralization to antiferromagnetic phases on a bipartite lattice can be easily derived in an analogous way as developed by Hasegawa [26]. Following the standard slave-boson mean-field approaches, we make the following approximations:
(i) The bosonic operators are replaced by their expectation values: $\phi^{\dagger}_{a,\Gamma n}, \phi_{a,\Gamma n} \longrightarrow \varphi_{\Gamma n}$.
(ii) The constraints (3.63-3.64) are taken into account by introducing seven homogeneous Lagrange multipliers λ and λ_{j_z}. Invoking the momentum space representation, $d_{\mathbf{k}j_z} \equiv 1/\sqrt{\mathcal{N}} \sum_a e^{i\mathbf{k}\mathbf{r}_a} d_{aj_z}$, the Hamiltonian (3.62) is thus approximated by

$$\begin{aligned} H^{MF} &= \sum_{\mathbf{k},j_z} \varepsilon_{\mathbf{k}j_z} Z_{j_z}[\Phi] d^{\dagger}_{\mathbf{k}j_z} d_{\mathbf{k}j_z} - \sum_{\mathbf{k},j_z} \lambda_{j_z} d^{\dagger}_{\mathbf{k}j_z} d_{\mathbf{k}j_z} + \mathcal{N} \sum_{\Gamma n} E_{\Gamma}\, \varphi^2_{\Gamma n} \\ &\quad + \lambda \mathcal{N} \left(\sum_{\Gamma n} \varphi^2_{\Gamma n} - 1 \right) + \mathcal{N} \sum_{j_z} \lambda_{j_z} n_{j_z}[\Phi] + \mu \mathcal{N} \left(\sum_{j_z} n_{j_z}[\Phi] - n_f \right), \end{aligned} \tag{3.68}$$

where $\varepsilon_{\mathbf{k}j_z}$ are the energy levels associated with the nearest neighbor hopping integrals t_{j_z}, $\mathcal{N}$ is the total number of sites, and μ is the chemical potential, introduced to adjust the electronic filling n_f. The QP weight is

$$Z_{j_z}[\Phi] \equiv R^2_{j_z}[\Phi] = \frac{\gamma^2_{j_z}[\Phi]}{n_{j_z}[\Phi]\,(1 - n_{j_z}[\Phi])}, \tag{3.69}$$

where γ_{j_z} and n_{j_z} are explicit functions of $\varphi_{\Gamma n}$, which are defined in a similar way as the operators $\hat{\gamma}_{j_z}$ and $\hat{n}_{j_z}$ in Eqs. (3.60)–(3.61)

$$\gamma_{j_z}[\Phi] \equiv \sum_{\Gamma\Gamma', nn'} \langle \Gamma | f^{\dagger}_{j_z} | \Gamma' \rangle \langle n | f^{\dagger}_{j_z} | n' \rangle\, \varphi^*_{\Gamma n} \varphi_{\Gamma' n'}, \tag{3.70}$$

$$n_{j_z}[\Phi] \equiv \sum_{\Gamma n} \varphi^*_{\Gamma n} \varphi_{\Gamma n} \langle n | f^{\dagger}_{j_z} f_{j_z} | n \rangle. \tag{3.71}$$

The mean-field parameters λ, λ_{j_z}, μ, and $\varphi_{\Gamma n}$ are determined self-consistently by minimizing the free energy $\mathcal{F} \equiv -\frac{1}{\beta} \ln Tr[e^{-\beta H^{MF}}]$. Here $\beta = \frac{1}{k_B T}$, k_B is the Boltzmann constant and T is the temperature of the system. Assuming that this minimum is obtained at a

saddle-point, one has

$$\sum_{\Gamma n} \varphi^2_{\Gamma n} = 1, \tag{3.72}$$

$$n_{j_z}[\Phi] = \frac{1}{\mathcal{N}} \sum_{\mathbf{k}} \langle d^\dagger_{\mathbf{k}j_z} d_{\mathbf{k}j_z} \rangle, \tag{3.73}$$

$$\sum_{j_z} n_{j_z}[\Phi] = n_f, \tag{3.74}$$

$$\begin{aligned} 2(E_\Gamma + \lambda)\varphi_{\Gamma n} &= -\sum_{j_z} (\lambda_{j_z} + \mu) \frac{\partial n_{j_z}[\Phi]}{\partial \varphi_{\Gamma n}} \\ &\quad -\frac{1}{\mathcal{N}} \sum_{j_z} \frac{\partial Z_{j_z}[\Phi]}{\partial \varphi_{\Gamma n}} \sum_{\mathbf{k}} \varepsilon_{\mathbf{k}j_z} \langle d^\dagger_{\mathbf{k}j_z} d_{\mathbf{k}j_z} \rangle, \end{aligned} \tag{3.75}$$

with

$$\langle d^\dagger_{\mathbf{k}j_z} d_{\mathbf{k}j_z} \rangle = n_F \left(\varepsilon_{\mathbf{k}j_z} \, Z_{j_z}[\Phi] - \lambda_{j_z} \right), \tag{3.76}$$

where $n_F(\varepsilon) \equiv 1/\left(1 + e^{\beta\varepsilon}\right)$ is the Fermi distribution function. The partial derivatives in Eq. (3.75) can be easily expressed analytically from the explicit expressions given by Eqs. (3.60)–(3.61). One obtains

$$\frac{\partial Z_{j_z}[\Phi]}{\partial \varphi_{\Gamma n}} = Z_{j_z}[\Phi] \frac{2n_{j_z}[\Phi] - 1}{n_{j_z}[\Phi](1 - n_{j_z}[\Phi])} \frac{\partial n_{j_z}[\Phi]}{\partial \varphi_{\Gamma n}} + 2 \frac{\gamma_{j_z}[\Phi]}{n_{j_z}[\Phi](1 - n_{j_z}[\Phi])} \frac{\partial \gamma_{j_z}[\Phi]}{\partial \varphi_{\Gamma n}}, \tag{3.77}$$

with

$$\frac{\partial \gamma_{j_z}[\Phi]}{\partial \varphi_{\Gamma n}} = \sum_{\Gamma' n'} \langle \Gamma | f^\dagger_{j_z} | \Gamma' \rangle \langle n | f^\dagger_{j_z} | n' \rangle \varphi_{\Gamma' n'}, \tag{3.78}$$

$$\frac{\partial n_{j_z}[\Phi]}{\partial \varphi_{\Gamma n}} = 2\varphi_{\Gamma n} \langle n | f^\dagger_{j_z} f_{j_z} | n \rangle. \tag{3.79}$$

3.3.2 Bare density of states

We introduce the orbital-dependent bare density of states (DOS)

$$\rho_0^{j_z}(\omega) \equiv \frac{1}{\mathcal{N}} \sum_{\mathbf{k}} \delta \left(\omega - \varepsilon_{\mathbf{k}j_z} \right), \tag{3.80}$$

the mean-field equations (3.72)–(3.75) are rewritten as

$$\sum_{\Gamma n} \varphi_{\Gamma n}^2 = 1, \tag{3.81}$$

$$n_{j_z}[\Phi] = \int d\omega\ \rho_0^{j_z}(\omega)\ n_F(\omega Z_{j_z}[\Phi] - \lambda_{j_z}), \tag{3.82}$$

$$\sum_{j_z} n_{j_z}[\Phi] = n_f, \tag{3.83}$$

$$\begin{aligned} 2(E_\Gamma + \lambda)\varphi_{\Gamma n} &= -\sum_{j_z}(\lambda_{j_z} + \mu)\frac{\partial n_{j_z}[\Phi]}{\partial \varphi_{\Gamma n}} \\ &\quad - \sum_{j_z} \frac{\partial Z_{j_z}[\Phi]}{\partial \varphi_{\Gamma n}} \int d\omega\ \omega\ \rho_0^{j_z}(\omega)\ n_F(\omega Z_{j_z}[\Phi] - \lambda_{j_z}). \end{aligned} \tag{3.84}$$

Eqs. (3.81)–(3.84) are RISBMF equations for the effective model defined by the Hamiltonian (2.11) within the RISB method. In this work we will consider only the ground state properties of the systems, i.e., at temperature $T = 0$. In this limit the Fermi distribution function $n_F(\varepsilon)$ becomes the Heaviside function $\theta(-\varepsilon)$. After taking this limit one can even go further in simplifying Eq. (3.82) and Eq. (3.84) if a specific analytical form of the bare density of states is chosen. We manage to solve the RISBMF equations (3.81)–(3.84) for two different cases of the bare density of states, namely, a constant density of states and a density of states of an infinite linear chain. Results for the constant density of states are discussed in the next chapter and those for an infinite linear chain are briefly mentioned in appendix D. We focus mainly on results of the constant density of states case because the RISBMF equations can be simplified further considerably. The simplification not only helps us to reduce numerical efforts significantly but also enable us to understand better the physics of the system.

3.3.3 Classification of partially localized phases

This section is devoted to classify partially localized phases which are discussed in the next chapters. In the effective model we have obtained a number of different PM and FM phases which are characterized by a localization of some $5f$ orbitals. We use magnetic order (PM or FM) and j_z quantum numbers of localized orbitals to classify the obtained

phases.

An j_z orbital is called a localized one if the corresponding effective hopping, or alternatively the QP weight is renormalized to zero

$$Z_{|jz|} = 0, \tag{3.85}$$

and the orbital occupation

$$n_{jz} + n_{-jz} = 1. \tag{3.86}$$

More precisely, in a PM case $n_{jz} = n_{-jz} = 0.5$ while $n_{jz} = 1$, $n_{-jz} = 0$ in FM one.

As it is known, for any j_z-orbital in a PM phase one has "up" ($j_z > 0$) and "down" ($j_z < 0$) symmetry. Thus, in discussion of PM phases, it is enough to discuss only "up" orbitals. In contrast to a PM phase, the "up" and "down" symmetry is broken in a FM phase. Hence, one has to discuss both "up" and "down" orbitals when discussing FM phase.

In more detail we also distinguish between fully polarized ferromagnetic state and partially polarized ferromagnetic state. For the sake of simplification they will be addressed as SFM (saturated FM) and FM, respectively.

Chapter 4

Numerical results for a constant density of states

In this chapter, we present numerical results of the RISBMF Eqs. (3.81)–(3.84) for the effective model described by the microscopic Hamiltonian (2.11). Here we consider the effective model on a lattice characterized by an orbital-dependent constant density of states (DOS)

$$\rho_{0j_z}(\omega) = \frac{1}{W_{jz}}\theta\left(\frac{W_{jz}}{2} - |\omega|\right), \tag{4.1}$$

where W_{j_z} is the bare bandwidth of the j_z orbital. Using Eq. (4.1) the RISBMF Eqs. (3.81)–(3.84) are rewritten as follows

$$\sum_{\Gamma n} \varphi^2_{\Gamma n} = 1, \tag{4.2}$$

$$\lambda_{j_z} = \left(n_{j_z}[\Phi] - \frac{1}{2}\right) W_{j_z} Z_{j_z}[\Phi] \ , \tag{4.3}$$

$$\sum_{j_z} n_{j_z}[\Phi] = n_f, \tag{4.4}$$

$$\left[E_\Gamma + \lambda + \mu \sum_{j_z} \langle n|{f^\dagger}_{j_z} f_{j_z}|n\rangle\right] \varphi_{\Gamma n} = \sum_{j_z} \frac{W_{j_z}}{2} \gamma_{j_z}[\Phi] \frac{\partial \gamma_{j_z}[\Phi]}{\partial \varphi_{\Gamma n}} \ . \tag{4.5}$$

Note that $\gamma_{j_z}[\Phi]$ and $\frac{\partial \gamma_{j_z}[\Phi]}{\partial \varphi_{\Gamma n}}$ are explicit functions of Φ, given by Eqs. (3.70) and (3.78), respectively. Solving the mean-field equations (4.2)–(4.5) one obtains several solutions

with differences in energy and symmetry. The coexistence of two (or even more) solutions can occur in the vicinity of the transitions where one or two orbitals are localized. In all situations, the physical solution is determined from the ground-state energy. The latter is obtained from H^{MF} (3.68) as follows

$$E[\Phi] = \langle H^{MF} \rangle = -\sum_{j_z} \frac{W_{j_z}}{2} \gamma_{j_z}^2 + \sum_{\Gamma n} E_\Gamma \varphi_{\Gamma n}^2 \ . \tag{4.6}$$

In calculations, we consider $W \equiv W_{\frac{3}{2}}$ and $W' \equiv W_{\frac{1}{2}} = W_{\frac{5}{2}}$ as independent parameters while the on-site Coulomb integrals U_J are fixed to their atomic values. The latter are determined from local density approximation (LDA) wavefunctions for UPt_3, i. e., $U_4 = 17.21\ eV$, $U_2 = 18.28\ eV$, and $U_0 = 21.00\ eV$ [20]. This consideration can be applied for U-based compounds in which the Coulomb interaction weakly depends on the chemical environment, whereas the electron bandwidths vary strongly from compound to compound. We concentrate on the intermediate valence regime by taking the $5f$ band filling $n_f = 2.5$. For a given set of W and W', using the Powell hybrid method [53], the non-linear mean-field equations (4.2)–(4.5) are solved numerically to determine the mean-field parameters $\varphi_{\Gamma n}$, λ_{j_z}, λ, and μ. The electronic occupations n_{j_z} and the QP weights Z_{j_z} are computed by using Eqs. (3.61) and (3.69), respectively.

4.1 Non-interacting and atomic limits

One of the many advantages of the RISBMF method is the possibility of giving exact solutions in the non-interacting and in the atomic limits [29]. The exact solutions for the non-interacting and the atomic limits are used to test the numerical coding program. Moreover, for intermediate interactions, these results can be used as initial values for the minimizing procedures.

In the non-interacting limit, the ground-state is a paramagnetic (PM) state in which all orbitals are fully itinerant. Technically, it is most advantageous to use the Fock-basis for both physical and auxiliary states to consider Fock-Fock bosons $\varphi_{nn'}$. Especially, in the highest symmetry case, i.e., for the isotropic ($W = W'$) model at half-filling $n_f = 3$,

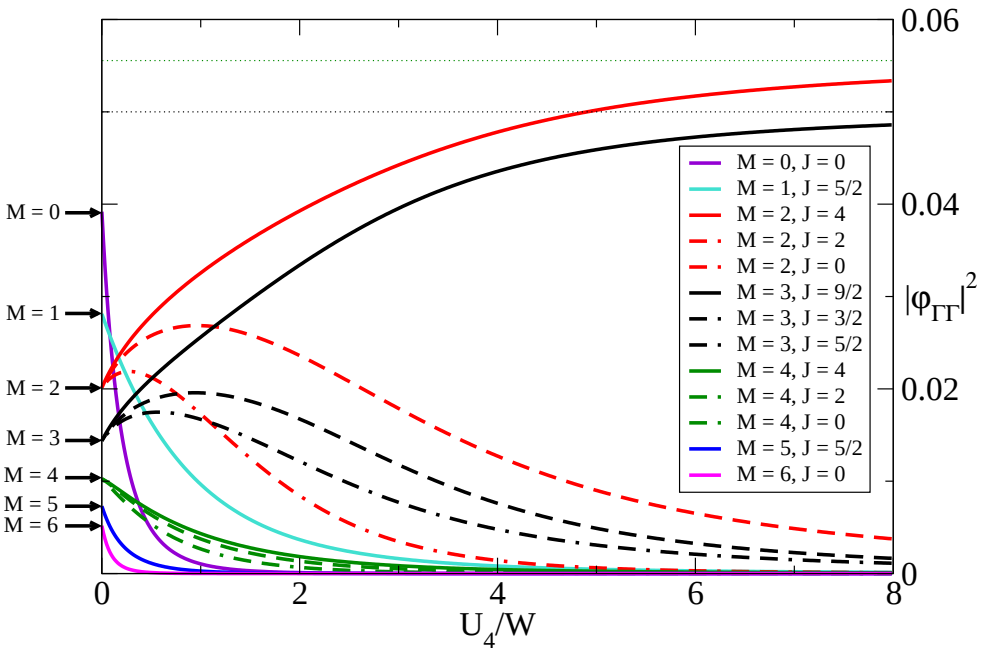

Figure 4.1: Diagonal boson occupations $|\varphi_{\Gamma\Gamma}|^2$ as a function of U_4/W in PM phase for isotropic case. The thin dotted lines are the values of diagonal Bose occupations in the atomic limit for $M = 2$ (upper line) and $M = 3$ (lower line).

all 64 possible local states are equivalent. Using Eqs. (3.65) and (4.2) one obtains the slave boson mean-field values associated to the M-electron Fock state $|n\rangle$

$$\varphi_{nn'} = \frac{\delta_{n,n'}}{\sqrt{64}}. \tag{4.7}$$

In the case of $n_f = 2.5$, the solution is obtained by smoothly decreasing the band-filling n_f from 3 to 2.5 step by step. Instead of the fully symmetric solution (4.7) one finds

$$\varphi_{nn'} = \delta_{n,n'}\varphi_{nn}. \tag{4.8}$$

While the global symmetry between all charge sectors is broken, one still has the local symmetry, i.e., all φ_{nn} in a given M-electron Hilbert subspace are identical (see Fig. 4.1). As mentioned in the previous chapter, the choice of the two basis sets to define slave bosons

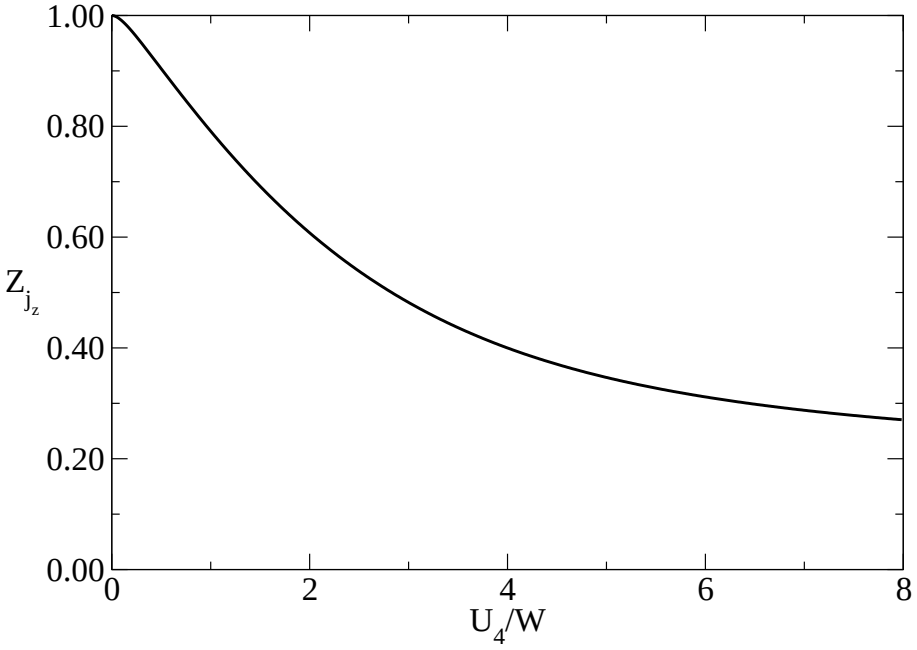

Figure 4.2: QP weights as a function of U_4/W in PM phase for isotropic case.

are flexible. Instead of using these Fock-Fock bosons $\varphi_{nn'}$, one can choose the multiplet-basis to represent both physical and auxiliary states to consider multiplet-multiplet bosons $\varphi_{\Gamma\Gamma'}$. The latter are obtained by performing the linear transformation (3.67)

$$\varphi_{\Gamma\Gamma'} = \sum_{nn'} \langle\Gamma|n'\rangle\langle n|\Gamma'\rangle\varphi_{n'n}. \tag{4.9}$$

It follows from Eqs. (4.8) and (4.9) that

$$\varphi_{\Gamma\Gamma'} = \delta_{\Gamma,\Gamma'}\varphi_{\Gamma\Gamma}, \tag{4.10}$$

$$\varphi_{\Gamma\Gamma} = \delta_{M(\Gamma),M'(n)}\varphi_{nn}. \tag{4.11}$$

Here $M(\Gamma)$ and $M'(n)$ are the number of particles contained in states Γ and n respectively. The values of diagonal bosons $\varphi_{\Gamma\Gamma}$, which are non-zero, depend on values of hopping parameters and are determined numerically. The results of $|\varphi_{\Gamma\Gamma}|^2$ in the isotropic case, i.e., $W = W'$, is shown in Fig. 4.1 (see where $U_4/W \to 0$).

In contrast to the non-interacting case, there is no hopping in the atomic limit and the number of electrons on a given site is conserved. It is natural to use the multiplet-basis to represent both physical and auxiliary states to consider multiplet-multiplet bosons $\varphi_{\Gamma\Gamma'}$. We find that all off-diagonal boson values $\varphi_{\Gamma\Gamma'}$ ($\Gamma \neq \Gamma'$) are zero, similar to the non-interacting case. The diagonal ones $\varphi_{\Gamma\Gamma}$ are also zero in all M-particle Hilbert subspaces, except when $M = 2$, 3. In addition, $\varphi_{\Gamma\Gamma}$ are non-zero only if the states Γ satisfy Hund's rule, i.e., $J(\Gamma) = 4$ for $M(\Gamma) = 2$ and $J(\Gamma) = \frac{9}{2}$ for $M(\Gamma) = 3$. Formally we can write

$$\varphi_{\Gamma\Gamma'} = \delta_{\Gamma\Gamma'} \left(\delta_{M(\Gamma),2} + \delta_{M(\Gamma),3}\right) \left(\delta_{J(\Gamma),4} + \delta_{J(\Gamma),\frac{9}{2}}\right) \varphi_{\Gamma\Gamma}, \tag{4.12}$$

where $J(\Gamma)$ denotes the total angular momentum of the state Γ. The values of $\varphi_{\Gamma\Gamma}$ are not unique, any set of $\varphi_{\Gamma\Gamma}$ satisfying the following conditions is a solution of the mean-field equations with the same energy per site $E_0 = \frac{U_4+U_{9/2}}{2}$

$$\sum_{J_z=-4}^{4} |\varphi_{|M=2;J=4,J_z\rangle,|M=2;J=4,J_z\rangle}|^2 = \frac{1}{2}, \tag{4.13}$$

$$\sum_{J_z=-\frac{9}{2}}^{\frac{9}{2}} |\varphi_{|M=3;J=\frac{9}{2},J_z\rangle,|M=3;J=\frac{9}{2},J_z\rangle}|^2 = \frac{1}{2}. \tag{4.14}$$

The ground-state is thus highly degenerate. Note that in Eqs. (4.13) and (4.14) we have written explicitly $|M; J, J_z$ instead of Γ as usual. The actual values of $\varphi_{\Gamma\Gamma}$ depend on the way bandwidths are decreased to approach the atomic limit. For example, if $W = W' \to 0$, one obtains a symmetric solution, from Eqs. (4.13)-(4.14) it follows

$$|\varphi_{|M=2;J=4,J_z\rangle,|M=2;J=4,J_z\rangle}|^2 = \frac{1}{18} \qquad \forall J_z = -4, ..., 4, \tag{4.15}$$

$$|\varphi_{|M=3;J=\frac{9}{2},J_z\rangle,|M=3;J=\frac{9}{2},J_z\rangle}|^2 = \frac{1}{20} \qquad \forall J_z = -\frac{9}{2}, ..., \frac{9}{2}. \tag{4.16}$$

These values are represented by thin dotted lines in Fig. 4.1.

In principle, both exact solutions in the non-interacting and atomic limits can be used as an initial guess for the minimizing procedures for intermediate interactions. However, since the ground-state in the atomic limit is highly degenerate, the minimizing procedures are easily affected by a small change in values of model parameters. Indeed, a small

change in the bandwidths leads to a big jump of the mean-field parameters, i.e., $\varphi_{\Gamma n}$, λ_{j_z}, λ, and μ. Consequently, the minimizing procedures usually lead to diverging results if one starts from the atomic limit. In actual calculations, we use the non-interacting solution as the initial step and then the local interaction is tuned gradually to the wanted values. Furthermore, we also try to find the physical solution by choosing the initial values randomly. It turns out that the solutions in two cases are in good agreement with each other. However, in the latter case, one has to try a lot of random initial configurations to obtain the ground-state. Anyhow, far away from the transition point, the mean-field equations are easily solved. On the other hand, the physical solution becomes more difficult to be found in the regime close to the transition point, particularly, in the case when more than two solutions coexist.

4.2 Hopping anisotropy and Hund's rule splitting effects

From calculations for small cluster systems [21], it turned out that the partially localized phase results from the influence of intra-atomic correlations on anisotropies of hopping matrix elements. Thus, one expects a similar situation for a lattice. In order to demonstrate this, we will first discuss the effect of the local interaction whereas the hopping anisotropies are neglected. Afterwards the effect of hopping anisotropies will be discussed by omitting Hund's rule splittings.

We start from the non-interacting limit ($U_4/W \ll 1$) to go to the atomic limit ($U_4/W \gg 1$) along the isotropic line $W = W'$ on the phase diagram. We choose the multiplet-basis to represent both physical and auxiliary states to consider multiplet-multiplet bosons $\varphi_{\Gamma\Gamma'}$. In the isotropic case, the ground-state is in a PM phase in which all orbitals are delocalized. The off-diagonal boson occupations vanish whereas those of diagonal bosons have non-zero values. The latter are plotted as functions of U_4/W in Fig. 4.1. It shows that in the strong interaction regime, only diagonal bosons in sectors

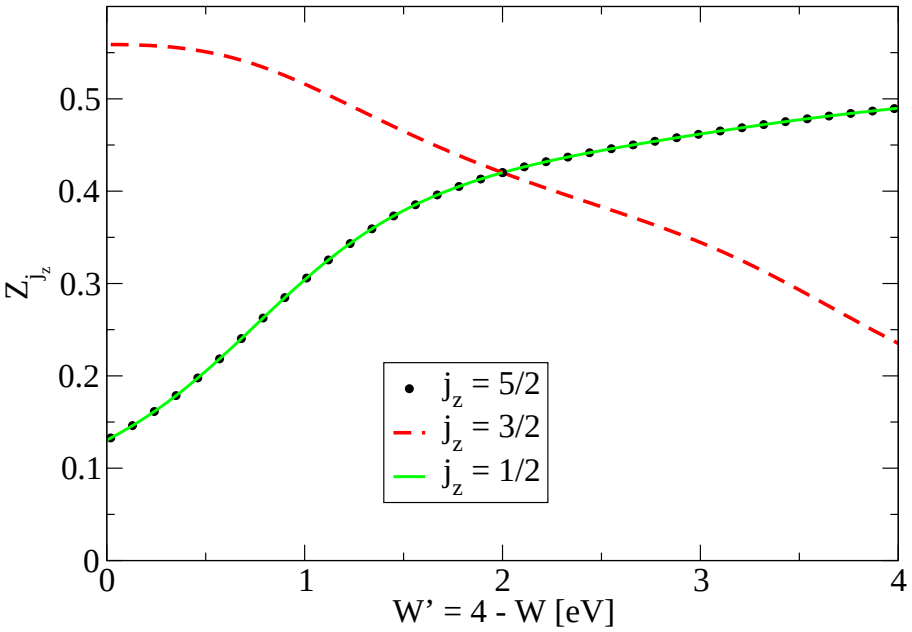

Figure 4.3: QP weights for different orbitals when the local energy splitting between the sectors of total angular momentum are cancelled ($U_0 = U_2 = U_4$).

of charge $M = 2$ and $M = 3$ are important, i.e., their occupations are not close to zero. More precisely, only the diagonal bosons associated with Hund's rule states in sectors of charge $M = 2$ and $M = 3$ are important. The occupations of these important bosons asymptotically approach their values in the atomic limit (thin dotted lines in Fig. 4.1) when the interaction gets stronger as expected. Fig. 4.2 shows the QP weights as a function of U_4/W. It is clear that the local interaction equally renormalizes all j_z orbitals so that the effective bandwidths $W_{j_z} Z_{j_z}$ remain isotropic. Furthermore, we demonstrate that the QP weights $Z_{j_z} \to 1$ when $U_4/W \to 0$ as it is expected for the non-interacting limit. As long as we are in the isotropic line, the QP weights are finite even when the interaction is very strong. All orbitals are equally filled with an occupation of $\frac{2.5}{6}$. This means that a partial localization transition does not take place in the isotropic case.

Now we neglect the local energy splittings between sectors of total angular momentum by setting $U_0 = U_2 = U_4$. The QP weights as functions of W' when $W = 4 - W'$ are shown in Fig. 4.3. It is shown that the hopping anisotropies are enhanced by the local interaction. However, none of effective bandwidths $W_{j_z} Z_{j_z}$ is renormalized to zero, i.e., a partially localized phase does not take place.

In conclusion, one needs not only hopping anisotropies but also local energy splittings between the different sectors of total angular momentum in order to obtain a partially localized state.

4.3 Quasiparticle weights and occupancies

The QP weights and occupancies of the $5f$ orbitals are used to classify partially localized phases as shown in Sect. 3.3.3. In this section, we describe and label different numerical solutions of the mean-field equations (4.2)–(4.5). Before going to discuss the phase diagrams in the whole $W - W'$ plane, we choose two different lines on the plane to show the variation of the QP weights and occupancies for different values of bandwidths. Respectively, they are plotted in Fig. 4.4 and Fig. 4.5, where the left panel is for $W + W' = 2eV$ line, the right panel is for $W + W' = 4eV$ line. Note that in the upper panel only PM solutions are considered whereas in the lower panel we consider both PM and FM solutions. It is worth mentioning that in each $W + W' = const$ line on the phase diagram, besides a weakly anisotropic regime $W \approx W'$ there are two highly anisotropic regimes corresponding to $W \ll W'$ and $W \gg W'$.

Let us first discuss the $W + W' = 2eV$ case. In the weakly anisotropic regime, we obtain a PM solution with all orbitals that are delocalized. In contrast, for the highly anisotropic regime where $W' \ll W$, we obtain one PM and one FM solutions. In the former, the QP weights for the $j_z = \pm\frac{1}{2}$ and the $j_z = \pm\frac{5}{2}$ orbitals are renormalized to zero whereas those for the $j_z = \pm\frac{3}{2}$ orbitals remain finite. In the latter, the QP weights for all orbitals are renormalized to zero except for the $j_z = \frac{3}{2}$ orbital. Note that when the QP weight for a given orbital vanishes, this orbital can be either localized or empty depending

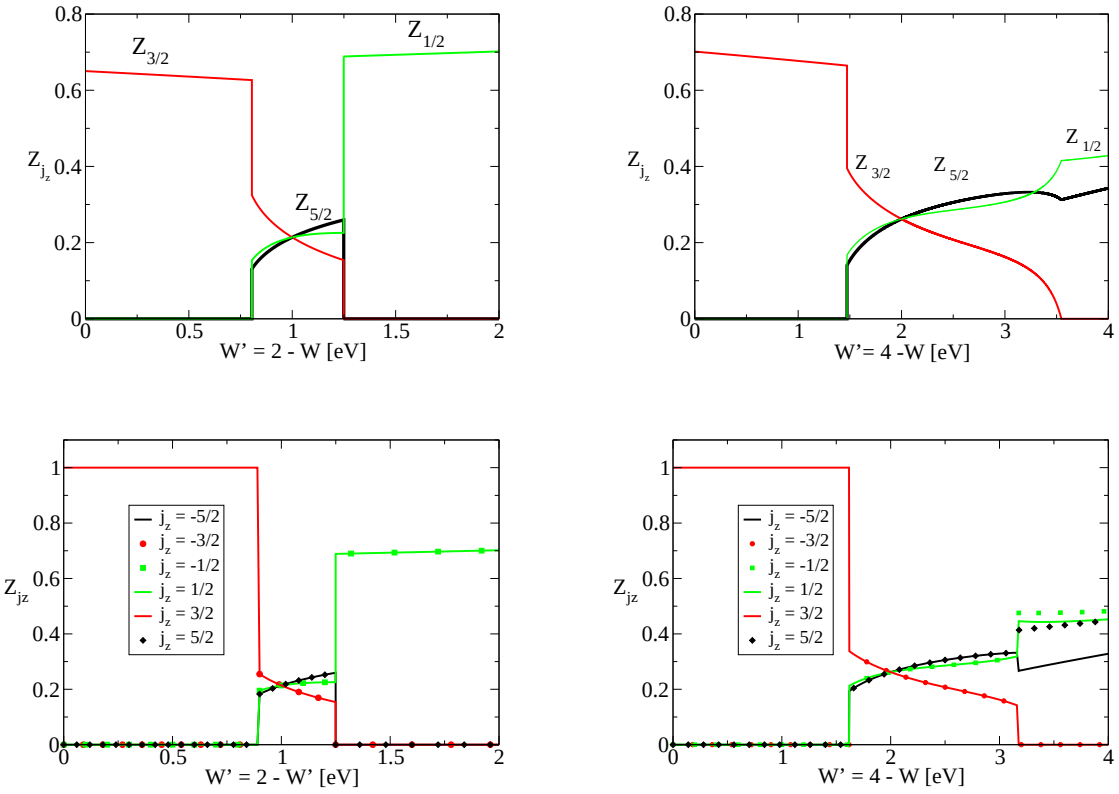

Figure 4.4: The upper (lower) panel describes the QP weights for different orbitals in the PM (FM) phase diagram.

on the corresponding occupancy (showed in Fig. 4.5). We find that in the PM phase the $j_z = \pm\frac{1}{2}$ and $j_z = \pm\frac{5}{2}$ orbitals are localized whereas the $\pm\frac{3}{2}$ orbitals are delocalized. In the FM phase, the $\frac{1}{2}$ and $\frac{5}{2}$ orbitals are localized, the $\frac{3}{2}$ orbital is delocalized while the remaining orbitals with $j_z = -\frac{1}{2}, -\frac{3}{2}, -\frac{5}{2}$ are unoccupied. These two phases are named *"PM $j_z = \frac{1}{2}, \frac{5}{2}$ localized phase"* and *"SFM $j_z = \frac{1}{2}, \frac{5}{2}$ localized phase"*, respectively. The latter is labeled SFM because all orbitals with negative j_z are empty, i.e., it is a fully polarized (saturated) state. For the other highly anisotropic regime where $W \ll W'$, we obtain three solutions: one PM and two FM. In the PM phase, the $\pm\frac{3}{2}$ and $\pm\frac{5}{2}$ orbitals are localized while the $\pm\frac{1}{2}$ orbitals are delocalized. This phase is named *"PM $j_z = \frac{3}{2}, \frac{5}{2}$ localized phase"*. One of these two FM phases is fully polarized, in which the

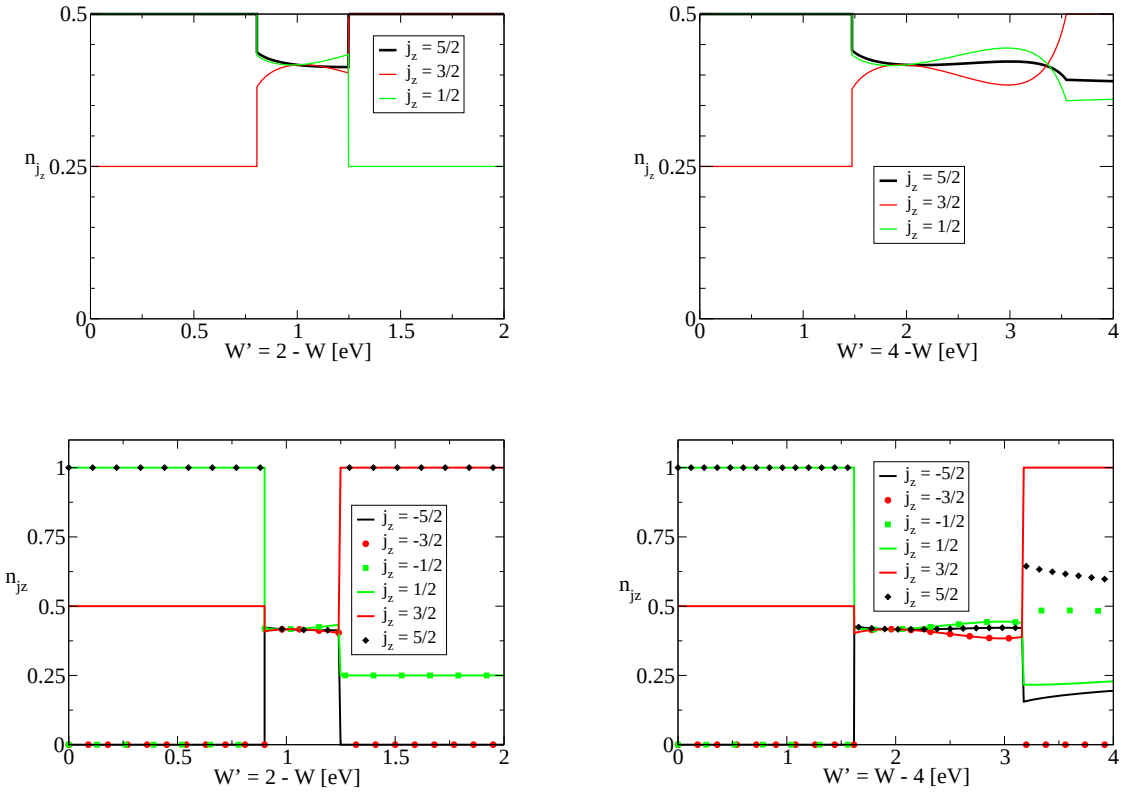

Figure 4.5: The upper (lower) panel describes occupation numbers for the different orbitals in PM (FM) phase diagram.

$\frac{3}{2}$, $\frac{5}{2}$ orbitals are localized, and the $\frac{1}{2}$ orbital is delocalized whereas the remaining orbitals with $j_z = -\frac{1}{2}, -\frac{3}{2}, -\frac{5}{2}$ are empty. It is named *"SFM $j_z = \frac{3}{2}, \frac{5}{2}$ localized phase"*. In the other FM phase, the delocalized $\pm\frac{1}{2}$ orbitals form a PM state whereas the $\frac{3}{2}$ and $\frac{5}{2}$ orbitals are localized and those orbitals with $j_z = -\frac{3}{2}, -\frac{5}{2}$ are empty. It is named *"FM $j_z = \frac{3}{2}, \frac{5}{2}$ localized phase"*.

Now we discuss results along the $W + W' = 4eV$ line. Similar to the previous case, in the weakly anisotropic regime, we obtain a PM non-localized phase; in the highly anisotropic regime where $W' \ll W$, we obtain a PM and a SFM $j_z = \frac{1}{2}, \frac{5}{2}$ localized phases. On the other hand, in the highly anisotropic regime where $W \ll W'$, we face a different situation. We obtain two solutions, one PM and one FM. In the PM phase the

$\pm\frac{3}{2}$ orbitals are localized and in the FM phase the $\frac{3}{2}$ orbital is localized and the $-\frac{3}{2}$ orbital is empty. They are denoted by *"PM $j_z = \frac{3}{2}$ localized phase"* and *"FM $j_z = \frac{3}{2}$ localized phase"*, respectively.

By changing the total values of W and W', one visits all possible $W + W' = const$ lines on the phase diagrams in the $W - W'$ plan. For W' small and W large enough, in addition to the PM and SFM $j_z = \frac{1}{2}, \frac{5}{2}$ localized phases, we obtain a new partly polarized FM solution, which is similar to the SFM $j_z = \frac{1}{2}, \frac{5}{2}$ localized phase except that the $-\frac{3}{2}$ orbital is no longer empty. This phase is named *"FM $j_z = \frac{1}{2}, \frac{5}{2}$ localized phase"*. For $W' \sim 2.5eV$ and W large enough, we obtain two new partially localized solutions, one PM and one FM. In the former the $\pm\frac{5}{2}$ orbitals are localized whereas in the latter the $\frac{5}{2}$ orbital is localized and the $-\frac{5}{2}$ orbital is empty. They are named *"PM $j_z = \frac{5}{2}$ localized phase"* and *"FM $j_z = \frac{5}{2}$ localized phase"*, respectively.

In summary, we have obtained and labeled ten partially localized solutions whose characteristics are summarized in Table 4.1. It is remarkable that in a SFM/FM partially localized phase if a j_z orbital is localized then its counterpart, i.e., the $-j_z$ orbital is empty.

4.4 Ground-state energy

As mentioned earlier, for highly anisotropic regimes depending on the choice of the electron bandwidths, we obtained ten partially localized solutions. In the left (right) panel of Fig. 4.6, we plot energies for different phases as a function of W' when the value of $W + W'$ is fixed to $2eV$ ($4eV$). It turns out that in most cases, the PM localized phase is unstable toward the FM one. One exception is the case where W is small and $W' < 2.5eV$ the ground-state is degenerate (the energies of the PM and the FM solutions are equal). Anyhow, the importance is that the ground-state in this highly anisotropic regime is in a partially localized phase.

For the weakly anisotropic regime, the ground-state is in a PM non-localized phase. By adjusting the electron bandwidths one can see the transition from a non-localized

	$Z_{\frac{5}{2}}$	$Z_{\frac{3}{2}}$	$Z_{\frac{1}{2}}$	$Z_{-\frac{1}{2}}$	$Z_{-\frac{3}{2}}$	$Z_{-\frac{5}{2}}$	$n_{\frac{5}{2}}$	$n_{\frac{3}{2}}$	$n_{\frac{1}{2}}$	$n_{-\frac{1}{2}}$	$n_{-\frac{3}{2}}$	$n_{-\frac{5}{2}}$
PM $j_z = \frac{1}{2}, \frac{5}{2}$	0	x	0	0	x	0	0.5	0.25	0.5	0.5	0.25	0.5
FM $j_z = \frac{1}{2}, \frac{5}{2}$	0	x	0	0	x	0	1	x	1	0	x	0
SFM $j_z = \frac{1}{2}, \frac{5}{2}$	0	1	0	0	0	0	1	0.5	1	0	0	0
PM $j_z = \frac{3}{2}, \frac{5}{2}$	0	0	x	x	0	0	0.5	0.5	0.25	0.25	0.5	0.5
FM $j_z = \frac{3}{2}, \frac{5}{2}$	0	0	x	x	0	0	1	1	0.25	0.25	0	0
SFM $j_z = \frac{3}{2}, \frac{5}{2}$	0	0	1	0	0	0	1	1	0.5	0	0	0
PM $j_z = \frac{5}{2}$	0	x	x	x	x	0	0.5	x	x	x	x	0.5
FM $j_z = \frac{5}{2}$	0	x	x	x	x	0	1	x	x	x	x	0
PM $j_z = \frac{3}{2}$	x	0	x	x	0	x	x	0.5	x	x	0.5	x
FM $j_z = \frac{3}{2}$	x	0	x	x	0	x	x	1	x	x	0	x

Table 4.1: Characteristic of the ten partially localized phases. Notation 'x' means this quantity depends on the actual values of electron bandwidths, $0 < x < 1$.

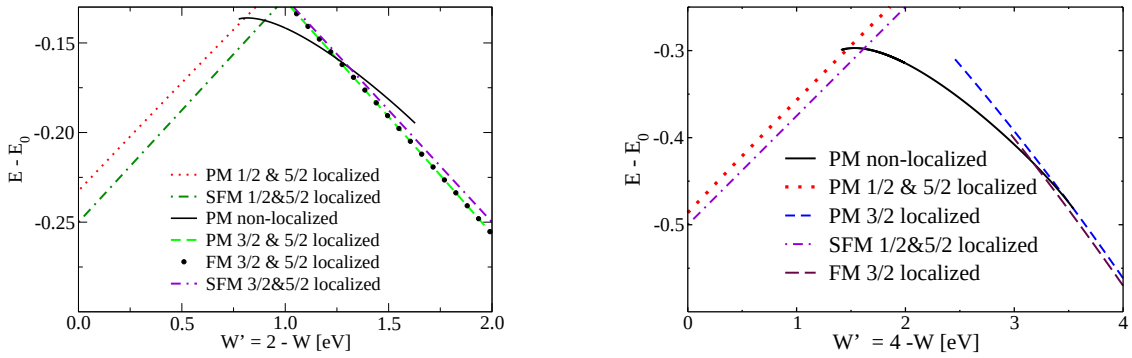

Figure 4.6: Energy of different solutions when moving from the $j_z = \frac{1}{2}, \frac{5}{2}$ localized phase, through the non-localized phase, to the $j_z = \frac{3}{2}, \frac{5}{2}$ localized phase along $W + W' = 2eV$ and $W + W' = 4eV$ lines. The magnetic order of each solution is also indicated. The characteristic of each phase is listed in the Table 4.1. Here $E_0 = \frac{U_4 + U_{\frac{9}{2}}}{2}$ is the ground-state energy per site in the atomic limit.

phase to a partially localized one and vice versa. In most cases, the transition is first-order except for the second-order phase transition between a non-localized phase and a single orbital localized phase when they have the same magnetic order, i. e., they are both PM or both FM.

Let us point out the correction of the critical value for partial localization transition due to magnetic ordering. Generally the critical value will shift toward the isotropic line ($W = W'$). For example, along the line $W + W' = 2eV$, the transition takes place at $W' = 0.8eV$ in the PM diagram but this value is shift to $W' = 0.9eV$ (about 11 percents) in the FM phase diagram. It is clear that the influence of magnetic order on partial localization transition is important for a quantitative discussion of the partial localization transition.

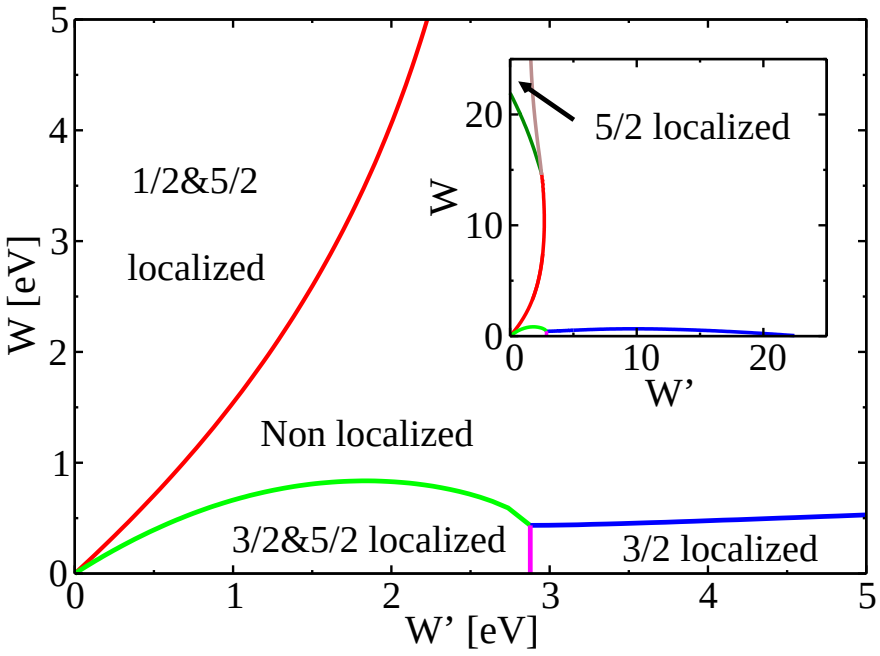

Figure 4.7: PM phase diagram. The inset shows the phase diagram for larger values of electron bandwidths.

4.5 Phase diagrams

Fig. 4.7 is the PM phase diagram in which we restricted ourselves to PM solutions. Due to the 'up' and 'down' symmetry of a PM state the number of mean-field equations is reduced by a factor of 2, thus the mean-field parameters are easily determined. When this restriction is left out, i.e., considering the FM instabilities in addition to PM phases, we obtain the FM phase diagram as shown in Fig. 4.8. The magnetic order of the ground-state and the j_z quantum number of localized orbitals are indicated inside the phase diagrams. The characteristic of each phase is given in the Table 4.1. It is worth knowing that in a FM partially localized phase, if a j_z orbital is localized then its counterpart, the $-j_z$ orbital, will be empty. The latter helps to reduce the interaction between these j_z and $-j_z$ electrons. As a result, the energy of a FM partially localized phase is lower

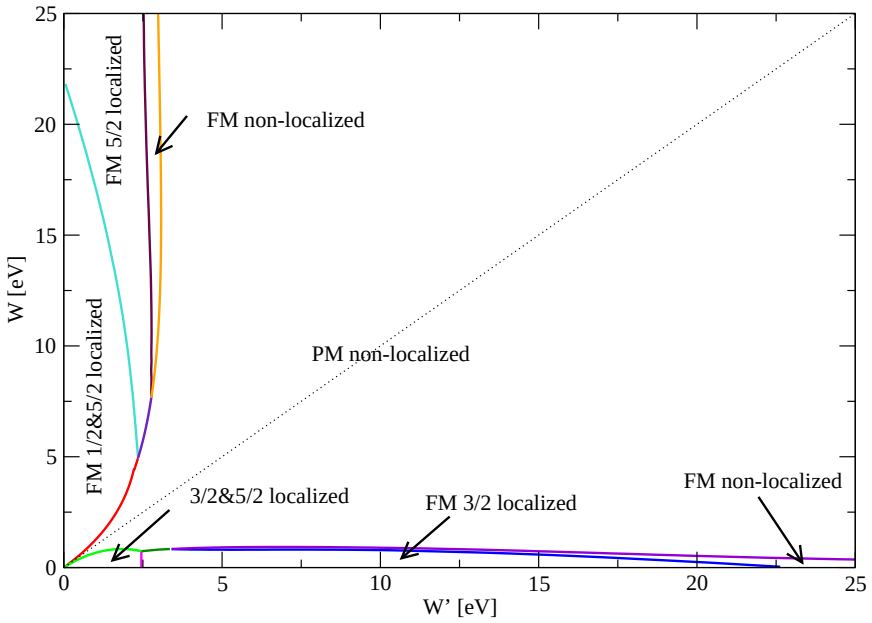

Figure 4.8: FM phase diagram. The dotted line is a guide for the eye, corresponding to $W = W'$.

than that of a PM one. This explains why the regions of the partially localized phases in the FM phase diagram are larger than those in the PM phase diagram. However, by concentrating only on the orbital localization one sees that the shape of the PM and FM phase diagrams are qualitatively similar. It means one can deal with only PM solutions to get a sketchy view of the problem before going deeply into details with more complicated solutions.

For a large region extended around the isotropic line ($W = W'$), the ground-state is in a non-localized state whose magnetic order can be either PM or FM depending on the values of electron bandwidths. Besides the non-localized state, we have found ten different partially localized solutions, which are labeled in Sect. 4.3(see also table 4.1). Regardlessly to their magnetic order, they fall into four categories according to their

localized orbitals, namely, $j_z = \frac{1}{2}, \frac{5}{2}$ localized phases, $j_z = \frac{3}{2}, \frac{5}{2}$ localized phases, $j_z = \frac{5}{2}$ localized phases, and $j_z = \frac{3}{2}$ localized phases. In the first two categories two orbitals are localized whereas in the last two categories only a single orbital is localized. Our results are in good agreement with the finite cluster results [21] and with the results in Ref. [27]. However, the magnetic order of the non-localized phase is different. Indeed, depending on electron bandwidths, the non-localized phase here can be either FM or PM state whereas in Ref. [27] it is FM state.

Note that besides the partial localization transition one also has the PM/FM magnetic transition. We find that for small values of electron bandwidths the two transitions occur simultaneously. On the other hand, for intermediate values they take place in turn. Furthermore, regarding to the partial localization transition, two electrons can be localized in turn or simultaneously depending on the values of electron bandwidths.

In the following we discuss in more detail the characteristic of each partially localized phase, partial localization and magnetic phase transitions in the FM phase diagram. The average Coulomb repulsion of about U_J is irrelevant for the low energy physics of the model. It simply restricts the relevant local configurations to the states containing either two or three electrons. However, the energy differences of the U_J values, which are of the order of 1eV and thus slightly larger than the typical bandwidth of f-electrons, play the crucial role. This consideration clearly not only has the advantage of conceptual simplicity for the interpretation but also can be used as an approximation, i.e., one neglects contributions of all local states containing less than two electrons or containing more than three electrons [27]. Note that this approximation is equivalent to let all $U_J \to \infty$ while their differences are kept to be constant. Thus this approximation is good for the small hopping regime, i.e., where electron bandwidths are much smaller than each U_J. However, one keeps in mind that these values of U_J are computed without accounting for the screening effect. Note that the isotropically averaged Coulomb repulsion (U_0) in a metal is reduced as compared to its value in an atom. On the other hand, the anisotropic parts (U_2, U_4) of the Coulomb interaction are (usually) not screened and hence retain their atomic values. Thus, the quantity $\triangle U = U_2 - U_4 = 1.07eV$ is not renormalized by

the screening effect. Nevertheless, we do not attempt at an ab initio calculation of these parameters but we fixed them to their atomic values as mentioned earlier in Sect. 2.1. The reduction of U_J, to some extent, can be seen in a model calculation by looking at electron bandwidths that are larger than the typical bandwidth of f-electrons. Thus, it is desirable to study not only the small hopping regime but also the intermediate hopping regime.

4.5.1 Two-localized-electron phase

Let us first discuss the regime where $W' \ll W \ll \triangle U$, i.e., strong interactions and large anisotropies. In this regime, we obtain two solutions. They are the PM and SFM $j_z = \frac{1}{2}, \frac{5}{2}$ localized phases. It turns out that the latter is the ground-state. The SFM $j_z = \frac{1}{2}, \frac{5}{2}$ localized phase can be understood as follows: because the electron bandwidths are much smaller than Hund's rule splitting $\triangle U$ so the ground-state is obtained if the local interactions are optimized, i.e., by arranging some of the $5f$ electrons to form Hund's rule multiplets. For example, the Hund's rule multiplets are $|M = 2; J = 4, J_z\rangle$ for two electrons and $|M = 3; J = \frac{9}{2}, J_z\rangle$ for three electrons. Only these electrons whose hopping processes enable both initial and final states satisfying Hund's rule will be delocalized. Otherwise, the Coulomb energy is increased so much that delocalization is disadvantageous as far as energy is concerned. As pointed out earlier, the partial suppression of charge fluctuations due to the large on-site Coulomb interaction leads to the fact that every site is occupied by either two or three electrons. That means electrons can only hop from a site with three electrons to the neighboring site with two electrons. Whereas the hopping processes from a site with two electrons to a site with three electrons are energetically unfavorable because they will generate local four-electron states with very high energy. Note that in order to form a Hund's rule state on a site containing two electrons, one can ferromagnetically combine either $j_z = \frac{1}{2}$ or $j_z = \frac{3}{2}$ with $j_z = \frac{5}{2}$ electrons. But in the present case, the hopping integral of the $\frac{3}{2}$ orbital is the largest one. Thus, $j_z = \frac{3}{2}$-electron should not be present in the site with two electrons. Consequently,

the itinerant electron has $j_z = \frac{3}{2}$ and two localized electrons have $j_z = \frac{1}{2}$ and $j_z = \frac{5}{2}$. Note that the SFM $j_z = \frac{1}{2}, \frac{5}{2}$ localized phase is the thermodynamic generalization of the $J_z = \frac{15}{2}$ phase obtained from the two-site calculation [21]. Furthermore, for $W' = 0$, we found that the macroscopic states made of local configurations $|M = 2; J = 4, J_z = 3\rangle$ and $|M = 3; J = \frac{9}{2}, J_z = \frac{9}{2}\rangle$ are (FM) eigenstates of the Hamiltonian (2.11). This property had been already obtained for the two-site model [21]. We find that it is a more general property which holds also for the lattice case (see Appendix C). From our mean-field result, one can conclude that this family of eigenstates contains the true ground-state for $W' = 0$ and sufficiently small W. Although in above explanation we assumed $W' \ll W \ll \Delta U$, the calculations show that the SFM $j_z = \frac{1}{2}, \frac{5}{2}$ localized phase is still the ground-state of the system even when W is comparable to ΔU and W'. That is because the local interactions renormalize the electron bandwidths to smaller values, i.e., $W_{j_z} \to W_{j_z} Z_{j_z}$. For W large enough the $-\frac{3}{2}$ orbital starts to be occupied, the ground-state is in the FM $j_z = \frac{1}{2}, \frac{5}{2}$ localized phase. This is because the four-electron state $|M = 4; J = 4, J_z = 3\rangle$ (corresponding to the Fock state $|M = 4; -\frac{3}{2}, \frac{1}{2}, \frac{3}{2}, \frac{5}{2}\rangle$), which fulfills Hund's rule, is good for both hopping processes of $j_z = -\frac{3}{2}, \frac{3}{2}$ electrons.

Now we go to the regime where $W \ll W' \ll \triangle U$. In this regime, we obtain three solutions. They are the PM, FM, and SFM $j_z = \frac{3}{2}, \frac{5}{2}$ localized phases. Their energies are the same, i.e, the ground-state is degenerate. In the SFM, it is quite similar to the SFM $j_z = \frac{1}{2}, \frac{5}{2}$ localized phase in the previous section, but here, the $\frac{1}{2}$ orbital takes over the role of the $\frac{3}{2}$ orbital: the $\frac{1}{2}$ orbital is delocalized while the $j_z = \frac{3}{2}$ and $j_z = \frac{5}{2}$ electrons are localized to form a Hund's rule state. Note that in the previous case the localization of the $j_z = \frac{1}{2}, \frac{5}{2}$ electrons prevents the presence of $j_z = -\frac{3}{2}$-electron. However, in the present case we face a different situation, that is the localization of the $j_z = \frac{3}{2}, \frac{5}{2}$ electrons doesn't prevent the presence of $j_z = -\frac{1}{2}$-electron. Thus, both $j_z = \frac{1}{2}$ and $j_z = -\frac{1}{2}$ electrons are able to show up. It is understandable since one can either add $j_z = \frac{1}{2}$-electron or $j_z = -\frac{1}{2}$-electron to the local Hund's rule state containing $j_z = \frac{3}{2}, \frac{5}{2}$ electrons $|M = 2; J = 4, J_z = 4\rangle$ to form a Hund's rule state with three electrons.

As mentioned earlier, for small W and W', we can restrict ourselves to the sectors

of charge $M = 2$ and $M = 3$. In these $j_z = \frac{3}{2}, \frac{5}{2}$ partially localized phases, the original Hamiltonian (2.11) can be approximated to a simpler model that is a single band Hubbard model at quarter filling of $j_z = \pm\frac{1}{2}-$electrons with infinite on-site Coulomb repulsion, which is decoupled from the ferromagnetically ordered $j_z = \frac{3}{2}, \frac{5}{2}$ localized electrons. This simpler model explains why the SFM and FM states are degenerate when a constant density of state (4.1) is assumed. This also explains why the FM and PM states are degenerate because the latter can be interpreted as a linear combination of the FM state with its counterpart obtained by flipping the quantization axis. When W' becomes comparable with ΔU the four-electron states resulting from charge fluctuations are no longer prohibited. The local multiplet state $|M = 4; J = 4, J_z = 4\rangle$ (corresponding to the Fock state $|M = 4; -\frac{1}{2}, \frac{1}{2}, \frac{3}{2}, \frac{5}{2}\rangle$) helps the system lower its energy. However, the energy of the SFM phase cannot be lowered by the state $|M = 4; J = 4, J_z = 4\rangle$ because the $-\frac{1}{2}$ orbital is empty in this phase. As a result, the degeneracy between these three solutions is partially lifted. The degeneracy between the FM and PM solutions still remains because the state $|M = 4; J = 4, J_z = 4\rangle$ preserves the symmetry between $j_z = -\frac{1}{2}$ and $j_z = \frac{1}{2}$ electrons. Considering the four-electron state $|M = 4; J = 4, J_z = 4\rangle$ is equivalent to characterizing the simpler model discussed above with a finite on-site repulsion. Our ground-state is in good agreement with the one in Ref. [27] where the authors found that $j_z = \frac{3}{2}$ and $j_z = \frac{5}{2}$ electrons are localized in a degenerate ground-state. However, the two-site model calculations [21] showed a non-localized state. It raises some questions: where does this difference come from? Does this come from the finite-size effect of small cluster models or does this come from the mean-field approximation? We will come back to answer these questions in the following chapter when we discuss the numerical results for the iTEBD method.

4.5.2 One-localized-electron phase

Now we turn to the intermediate hopping regime where $\frac{W}{U_4} > 0.3$, $\frac{W'}{U_4} \approx 0.15$. In this regime we obtain two solutions. They are the PM and FM $j_z = \frac{5}{2}$ localized phases.

The ground-state is the FM $j_z = \frac{5}{2}$ localized phase. In fact the presence of this phase was a surprise for a while since in the FM phase there is only one localized electron. Therefore Hund's rule mechanism, which is used earlier to explain these two-localized-electron phases, does not apply here anymore. Thus, it raises two questions: Is this one-localized-electron phase an artifact of the mean-field approximation? If not, what is its physics?

As discussed in the section 2.2, in the $J_z = \frac{11}{2}$ phase of the two-site model the $\frac{5}{2}$ orbital can be considered as a localized one because the corresponding occupation number $n_{\frac{5}{2}}$ is very close to 1. This is consistent with our results since the FM $j_z = \frac{5}{2}$ localized phase is the thermodynamic generalization of the $J_z = \frac{11}{2}$ phase. Therefore, one believes that the FM $j_z = \frac{5}{2}$ localized phase obtained here is not an artifact of the mean-field approach.

Now we analyze how the FM $j_z = \frac{1}{2}, \frac{5}{2}$ localized phase can be transformed into the FM $j_z = \frac{5}{2}$ localized phase when increasing W' and keeping W large enough. When increasing W' the tendency to hop of $j_z = \frac{1}{2}$ and $j_z = \frac{5}{2}$ electrons increases. Above a critical value of W', either $j_z = \frac{1}{2}$ or $j_z = \frac{5}{2}$ electron will be delocalized. Let us look at a site containing three electrons in the SFM $j_z = \frac{1}{2}, \frac{5}{2}$ localized phase to see which electron between $j_z = \frac{1}{2}$ and $j_z = \frac{5}{2}$ ones will be delocalized first. It turns out that the delocalization of the $\frac{1}{2}$ orbital is energetically favorable because the Coulomb interaction between $j_z = \frac{1}{2}$-electron with $j_z = \frac{3}{2}$-electron is larger than that between $j_z = \frac{5}{2}$-electron with $j_z = \frac{3}{2}$-electron. The difference of the energies is $0.68eV$ while $\triangle U = 1.07eV$.

We then analyze how the non-localized phase can be transformed into the FM $j_z = \frac{5}{2}$ localized phase. Starting from a point in the phase diagram with $W = W' > 0.3U_4$ and move to the left by decreasing W' and keeping W constant. Since W and W' are big compared to the Hund's splitting $\triangle U$, the off-diagonal (or the exchange) parts of the local interactions are not important. In contrary, the diagonal elements $U_{j_z,-j_z} \equiv U_{j_z,-j_z,j_z,-j_z}$ (or the direct 'Hubbard type' parts), namely, the Coulomb interaction between j_z and $-j_z$ electrons, play the key role for understanding the partial localization transition. Similar to the Mott transition in the SBH model, the Mott transition in a given j_z orbital is taken

place if the ratio $\frac{U_{j_z,-j_z}}{W_{j_z}}$ gets larger than a critical value. Here we decrease bandwidths of $j_z = \frac{1}{2}$ and $j_z = \frac{5}{2}$ electrons, so the ratios $\frac{U_{\frac{1}{2},-\frac{1}{2}}}{W_{\frac{1}{2}}}$ and $\frac{U_{\frac{5}{2},-\frac{5}{2}}}{W_{\frac{5}{2}}}$ will increase. Note that the electron bandwidths of the $\frac{1}{2}$ and $\frac{5}{2}$ orbitals are chosen to be equal. Therefore, the corresponding ratios will depend on $U_{j_z,-j_z}$ only. Nevertheless, $U_{j_z,-j_z}$ for the $\frac{5}{2}$ orbital is $0.23eV$ larger the value for the $\frac{1}{2}$ orbital. As a result, the criteria of Mott transition in the $\frac{5}{2}$ orbital is fulfilled first. This explains why for intermediate W the localization/delocalization of the $\frac{1}{2}$ orbital and the $\frac{5}{2}$ orbital does not happen at the same time. One notices that the explanation above is naive and qualitative. In fact the problem is more complicated since the orbitals are coupled by local interaction. Thus, starting from a point in the phase diagram with $W = W' > 0.3U_4$ and move to the left by decreasing W' and keeping W constant, the occupations in the $j_z = \pm\frac{1}{2}$ and $j_z = \pm\frac{5}{2}$ orbitals also depend on W. As a results, the criteria for the Mott transition in the $j_z = \pm\frac{1}{2}$ and $j_z = \pm\frac{5}{2}$ orbitals are implicitly dependent on W as seen in the FM phase diagram. For small W, of course, the situation is different because $j_z = \frac{1}{2}$ and $j_z = \frac{5}{2}$ electrons must localize simultaneously in order to form a Hund's rule ground-state as we discussed in the previous sections.

For sufficiently small W (typically less than $1eV$) and intermediate W' (greater than $2.5eV$), we obtain two solutions. They are the PM and FM $j_z = \frac{3}{2}$ localized phases. The ground-state is the latter which is in good agreement with the work of G. Zwicknagl [27]. In a vanishingly small magnetic field, the FM $j_z = \frac{3}{2}$ localized phase was not found in the two-site and three-site models [21]. However, this phase was seen in the four-site model [22]. In addition, for the two-site model under a small magnetic field, as discussed in the section 2.2, there exists a phase in which the $\frac{3}{2}$ orbital is highly occupied ($n_{\frac{3}{2}}$ varies from 0.9 to 1.0 depending on W'). That means our result is consistent with not only the four-site model but also with the two-site model under a small magnetic field. The presence of the small magnetic field in the two-site system can be understood as a result of the surrounding ferromagnetic environment.

Similar to the FM $j_z = \frac{5}{2}$ localized phase discussed above, the mechanism based on

Hund's rule for the partial localization does not apply here. We analyze how the FM $j_z = \frac{3}{2}, \frac{5}{2}$ localized phase can be transformed into the FM $j_z = \frac{3}{2}$ localized phase by increasing W' and keeping W small enough. Note that here the bandwidths for the two localized electrons, i.e., $j_z = \frac{3}{2}$ and $j_z = \frac{5}{2}$ electrons, are different. Because $W \ll W'$ the $\frac{5}{2}$ electron is energetically favorable to be delocalized.

We now discuss how the non-localized phase can be transformed into the FM $j_z = \frac{3}{2}$ localized phase. Starting from one point in the isotropic line of the phase diagram in which $W = W' \gg \triangle U$ we move down vertically by keeping W' constant and decreasing W. Since we keep W' to be large enough, the ratios $\frac{U_{j_z,-j_z}}{W_{j_z}}$ for the $j_z = \frac{1}{2}$ and $\frac{5}{2}$ orbitals are small enough for these orbitals to remain delocalized. But the ratio $\frac{U_{j_z,-j_z}}{W_{j_z}}$ for the $\frac{3}{2}$ orbital gets larger while decreasing W. Below a certain critical value of W, the ratio reaches the critical value for the Mott transition, i.e., the $\frac{3}{2}$ orbital is localized.

4.6 Conclusions

In this chapter, we discussed numerical results of the RISBMF Eqs. (3.81)–(3.84) for the effective model described by the microscopic Hamiltonian (2.11). For simplicity, we considered a lattice characterized by an orbital-dependent constant density of states (4.1). We calculated QP weights, orbital-dependent occupancies and ground-state energy to obtain the PM and FM phase diagrams of the systems (see Fig. 4.7 and Fig. 4.8). We discussed extensively the FM phase diagram. Of particular interest is that in addition to two-localized-electron phases, we obtained one-localized-electron phases. These partially localized phases were analyzed in detail in Sect. 4.5. We proposed a possible mechanism for one-electron-localized phases. This mechanism is similar to that of a single-band Mott-Hubbard transition. The direct on-site Coulomb interaction between j_z and $-j_z$ electrons plays the key role for understanding the partial localization transition. The j_z orbital is localized if the ratio $\frac{U_{jz,-j_z}}{W_{j_z}}$ is above a critical value. Note that mean-field methods can sometimes give artificial results. Thus we will assess the validity of the RISBMF method in the next chapter by using the infinite time-evolving block decimation method [30].

Chapter 5

Infinite time-evolving block decimation method

In this chapter, using infinite time-evolving block decimation (iTEBD) [30] we calculate the ground-state properties of the effective model described by the microscopic Hamiltonian (2.11) for an infinite linear chain. The main purpose of this chapter is to assess the validity of the RISBMF results obtained in chapter 4 and in appendix D. However, we are not going to compute the full phase diagram as we did in the previous chapter, here we only study some particularly interesting points of the phase diagram where the partially localized phases take place in the small hopping regime.

5.1 Introduction

The numerical renormalization group (NRG) was first introduced by Wilson for the Kondo problem in 1971 [54]. Although it was a dramatic breakthrough, this approach has had very little success for anything but impurity problems. When applied to quantum lattice-problems, the approach is flawed due to boundary errors. Within the NRG approach one first divides the infinite linear chain into a set of identical block A. Then, one diagonalizes the Hamiltonian H_{AA} of two neighboring blocks AA joined together to find its eigenvalues

and eigenvectors. Afterward, one keeps only m of the lowest-lying eigenstates to form a new effective, simpler Hamiltonian $H_{A'}$ of a larger block A' representing two neighboring blocks AA. Next, A is replaced by A' and the above steps are performed repeatedly. This procedure can be written formally as

$$H_{A'} = \mathcal{O} H_{AA} \mathcal{O}^{\dagger}, \tag{5.1}$$

where $\mathcal{O}$ is an $m \times l$ matrix, and l is the dimension of H_{AA}. The rows of $\mathcal{O}$ are the m lowest-lying eigenstates of H_{AA}. In this scheme, one assumes that only $m < l$ lowest-lying block eigenstates are important in forming states of larger blocks at later iterations. However, this assumption is not valid for most problems because the true wavefunction and the selected block's eigenstates behave differently at the boundary of the two neighboring blocks joined together. This can be understood in detail by considering a toy model, namely, a 1D tight-binding chain. In this example, the lowest-lying eigenstates of H_A all have nodes at the ends of the block A, such that all product states of AA have nodes at the center AA. In contrast, at the center of AA the amplitude of the true ground-state of AA is maximal. Thus, for such a case, the NRG approach gives poor results.

In 1992, White proposed the so-called density matrix renormalization group (DMRG) formulation [55] to eliminate these flaws of Wilson's NRG approach. Instead of keeping m lowest-lying eigenstates of the Hamiltonian H_{AA}, White chose to keep m other states in such a way that those kept states optimally minimize the error between the true wavefunction and the approximative one in the considering blocks AA. White pointed out that the optimal states need to be kept are m eigenstates of the reduced density matrix ρ_{AA} which have the largest absolute values. In actual calculation, the block A' is not chosen to be two neighboring joined blocks A, i.e., $A' = A + A$. Usually, A' is obtained by adding a single site to the block A, i.e., $A' = A + 1$. The true wavefunction of the entire lattice is replaced by the one of the superblock that is normally chosen as two blocks A plus two sites in between. In fact, the two blocks in the superblock need not have equal sizes. The ground-state for the superblock is obtained using the Lanczos algorithm of matrix diagonalization. Another choice is the Arnoldi method, especially

when dealing with non-hermitian matrices. In systems with symmetries, we may have conserved quantum numbers, e.g., total spin in a Heisenberg model. For such a situation, one can speed up the simulation by searching for the ground-state within each of the sectors into which the Hilbert space is divided. Details of DMRG algorithm are found in Ref. [56].

Recently, Vidal has developed a novel time-dependent simulation method, namely an infinite time-evolving block decimation (iTEBD) method, which applies for infinite one-dimensional systems [30]. The iTEBD method is a descendant of the DMRG method. The crucial new idea of iTEBD is to exploit two facts, namely, invariance under translations of the system and parallelizability of the time-evolving block decimation (TEBD) method [57, 58], to obtain a noticeably simple and fast algorithm. Since the iTEBD method always constructs wavefunctions for the infinite system, its errors do not result from finite size effects but from an assumption that the entanglement of the system is finite. In addition to offering a very competitive alternative to the DMRG method for infinite 1D systems, the iTEBD method plays a key role in entanglement renormalization techniques and in the extention of projected entangled-pair states (PEPS) of $2D$ lattices [59].

The iTEBD method is very efficient to simulate infinite 1D systems. However, the effective model (2.11) has a big number of local states on a given lattice site. In actual calculations, thus, one needs to introduce a supplementary approximation to make the method applicable. Here, only 35 local states of the two- and three-electron Hilbert subspaces are taken into account. This approximation is reasonable in the small hopping regime as we discussed in previous chapters.

5.2 Infinite time-evolving block decimation method

In this section we recall some important equations of the iTEBD method from Ref. [30]. We consider an infinite array of sites, for each site r there are d possible local states. For example, for the effective model (2.11) it is $d = 64$ in general, while $d = 35$ if we

restrict ourselves to the subspace of two and three particles. Let vector $|\Psi\rangle$ denote a pure state of the system and operator $H = \sum_r h^{[r,r+1]}$ be a Hamiltonian with nearest-neighbor hoppings and interactions. We also assume that $|\Psi\rangle$ and H are invariant under shifts by one lattice site. Given an initial state $|\Psi_0\rangle$, our purpose is to simulate an evolution according to H, both in real time

$$|\Psi_t\rangle = \exp(-iHt)|\Psi_0\rangle, \tag{5.2}$$

and in imaginary time

$$|\Psi_\tau\rangle = \frac{\exp(-H\tau)|\Psi_0\rangle}{\|\exp(-H\tau)|\Psi_0\rangle\|}. \tag{5.3}$$

Here $\|...\|$ is the notation for the norm of a state in the Hilbert space.

The iTEBD method represents $|\Psi\rangle$ through matrix product states (MPS) [31]. Let $[\lhd r]$ and $[r+1\rhd]$ denote the semi-infinite sublattices made of sites $\{-\infty, \cdots, r\}$ and $\{r+1, \cdots, \infty\}$. The Schmidt decomposition of $|\Psi\rangle$ [60] according to this bipartition reads

$$|\Psi\rangle = \sum_{\alpha=1}^{\chi} \lambda_\alpha^{[r]} |\Phi_\alpha^{[\lhd r]}\rangle \otimes |\Phi_\alpha^{[r+1\rhd]}\rangle, \tag{5.4}$$

where we assume the Schmidt rank χ, i.e., the number of Schmidt coefficients $\lambda_\alpha^{[r]}$, to be finite [30, 57, 58]. Here, $|\Phi_\alpha^{[\lhd r]}\rangle$ ($|\Phi_\alpha^{[r+1\rhd]}\rangle$) is an eigenvector of the reduced density matrix $\rho^{[\lhd r]}$ ($\rho^{[r+1\rhd]}$) with eigenvalue $|\lambda_\alpha^{[r]}|^2 > 0$. The Schmidt coefficient $\lambda_\alpha^{[r]}$ follows from the relation $\langle\Phi_\alpha^{[\lhd r]}|\Psi\rangle = \lambda_\alpha^{[r]}|\Phi_\alpha^{[r+1\rhd]}\rangle$. In the following, we use a vector $\lambda^{[r]}$ to represent the set of $\lambda_1^{[r]}$, $\lambda_2^{[r]}$..., $\lambda_\chi^{[r]}$.

The spectral decompositions of the reduced density matrices for $[\lhd r]$ and $[r+1\rhd]$ are

$$\rho^{[\lhd r]} = \sum_{\alpha=1}^{\chi} |\lambda_\alpha^{[r]}|^2 \; |\Phi_\alpha^{[\lhd r]}\rangle\langle\Phi_\alpha^{[\lhd r]}|, \tag{5.5}$$

$$\rho^{[r+1\rhd]} = \sum_{\alpha=1}^{\chi} |\lambda_\alpha^{[r]}|^2 \; |\Phi_\alpha^{[r+1\rhd]}\rangle\langle\Phi_\alpha^{[r+1\rhd]}|. \tag{5.6}$$

We use a three-index tensor $\Gamma^{[r]}$ at site r to relate the Schmidt bases for two left halves

$$|\Phi_\alpha^{[\lhd r+1]}\rangle = \sum_{\beta=1}^{\chi}\sum_{i=1}^{d} \lambda_\beta^{[r]} \Gamma_{i\beta\alpha}^{[r+1]} \; |\Phi_\beta^{[\lhd r]}\rangle |i^{[r+1]}\rangle, \tag{5.7}$$

and for two right halves

$$|\Phi_\alpha^{[r\triangleright]}\rangle \;=\; \sum_{\beta=1}^{\chi}\sum_{i=1}^{d}\Gamma_{i\alpha\beta}^{[r]}\lambda_\beta^{[r]}\;|i^{[r]}\rangle|\Phi_\beta^{[r+1\triangleright]}\rangle, \tag{5.8}$$

where $|i^{[r]}\rangle$ are local states at site r.

In particular, $|\Psi\rangle$ can be expanded in the local basis $|i^{[r+1]}\rangle$ for site $r+1$ and in terms of $\lambda^{[r]}\Gamma^{[r+1]}\lambda^{[r+1]}$ as

$$|\Psi\rangle = \sum_{\alpha,\beta=1}^{\chi}\sum_{i=1}^{d}\lambda_\alpha^{[r]}\Gamma_{i\alpha\beta}^{[r+1]}\lambda_\beta^{[r+1]}|\Phi_\alpha^{[\triangleleft r]}\rangle|i^{[r+1]}\rangle|\Phi_\alpha^{[r+2\triangleright]}\rangle, \tag{5.9}$$

or for sites $\{r+1, r+2\}$ in terms of $\lambda^{[r]}\Gamma^{[r+1]}\lambda^{[r+1]}\Gamma^{[r+2]}\lambda^{[r+2]}$, and so on.

The evolution operator $\exp(-iHt)$ in Eq. (5.2) is expanded through a Suzuki-Trotter decomposition [61] as a sequence of operators that act on two neighboring sites. These operators are normally called two-site gates, they read

$$U^{[r,r+1]} \equiv \exp(-ih^{[r,r+1]}\delta t), \qquad \delta t \ll 1, \tag{5.10}$$

which we arrange into gates U^{AB} and U^{BA},

$$U^{AB} \equiv \bigotimes_{r\in\mathbb{Z}} U^{[2r,2r+1]}, \qquad U^{BA} \equiv \bigotimes_{r\in\mathbb{Z}} U^{[2r-1,2r]}. \tag{5.11}$$

Because state $|\Psi\rangle$ is shift invariant, it can be represented with a MPS where $\Gamma^{[r]}$ and $\lambda^{[r]}$ are independent of r. However, we will partially break translational symmetry to simulate the action of gates (5.11) on $|\Psi\rangle$ [30]. Accordingly, we choose a MPS of the form

$$\begin{aligned} \Gamma^{[2r]} &= \Gamma^A, \qquad \lambda^{[2r]} = \lambda^A, \\ \Gamma^{[2r+1]} &= \Gamma^B, \quad \lambda^{[2r+1]} = \lambda^B, \quad r \in \mathbb{Z}. \end{aligned} \tag{5.12}$$

The action of the gates preserves the invariance of the evolved state under shifts by *two* sites, and only tensors $\Gamma^A, \Gamma^B, \lambda^A$ and λ^B need to be updated – a task that is achieved through simple matrix manipulations [30]. Finally, the imaginary time evolution in Eq. (5.3), is simulated by simply replacing the two-site unitary gates $\exp(-ih\;\delta t)$ in Eq. (5.10) with non-unitary gates $\exp(-h\;\delta\tau)$, $\delta\tau \ll 1$. More details of how to update $\Gamma^A, \Gamma^B, \lambda^A$

and λ^B when the two-site gates are applied can be found in any one of Refs. [30, 57, 58]. Note that here A is an arbitrary site and B is its nearest neighbor, i.e., they belong to different sublattices of a bipartite lattice.

5.3 Partial localization

In this section we present results for the effective model described by the microscopic Hamiltonian (2.11) for an infinite linear chain. We consider $W \equiv W_{\frac{3}{2}}$ and $W' \equiv W_{\frac{1}{2}} = W_{\frac{5}{2}}$ as independent variable parameters while the other model parameters are fixed. The values of the Coulomb integrals U_J and the band-filling n_f were chosen in chapter 4. In order to quantify the degree of localization or, alternatively, of the reduction of hopping for a given j_z orbital due to intra-atomic correlations, we use the ratio of the $|j_z|$-projected kinetic energy per site and the bare bandwidth W_{j_z}, i.e.,

$$\frac{T_{j_z}}{W_{j_z}} = \frac{1}{4\mathcal{N}} \sum_{i,\pm} \langle f^\dagger_{i,\pm j_z} f_{i+1,\pm j_z} \rangle, \tag{5.13}$$

where $\mathcal{N}$ is the total number of sites. A small ratio of $\frac{T_{j_z}}{W_{j_z}}$ indicates partial suppression of hopping for electrons in the $\pm j_z$ orbitals.

Let us first analyze the case with $W = 2eV$, $W' \ll 1eV$. The iTEBD ground-state energy E_G as a function of χ is shown in Fig. 5.1. It is seen that $E_G(\chi)$ converges quickly as χ increases. The error $|E_G(\chi) - E_G(\infty)|$ is smaller for bigger χ, where $E_G(\infty)$ is the exact ground-state energy obtained when $\chi \to \infty$. The error is less than $10^{-4}eV$ for $\chi = 10$ meaning that the iTEBD results are very good even for relatively small χ. Fig. 5.2 presents the ratios $\frac{T_{j_z}}{W_{j_z}}$ as a function of χ for different j_z orbitals. The ratios $\frac{T_{j_z}}{W_{j_z}}$ for the $|j_z| = \frac{1}{2}$ and $|j_z| = \frac{5}{2}$ orbitals are normalized to zero whereas the one for the $|j_z| = \frac{3}{2}$ orbitals is still finite. The occupations of different j_z-orbitals when $\chi = 10$ are shown in table 5.1. We find that the ground-state is in the SFM $j_z = \frac{1}{2}, \frac{5}{2}$ localized phase as predicted by the RISBMF method in chapter 4 and appendix D. We would like to mention that, with an increase in the value of χ, expectation values of local operators, e.g., $\hat{n}_{j_z}$,

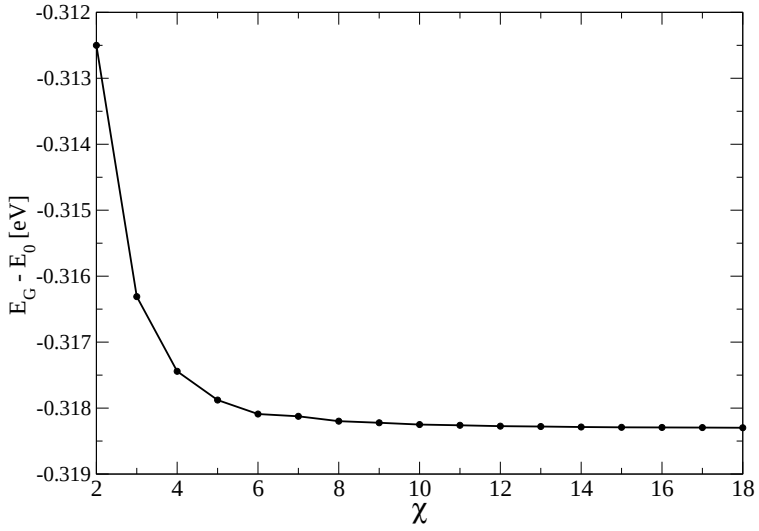

Figure 5.1: The ground-state energy for different χ obtained within the iTEBD method for $W = 2eV$, $W' \ll 1eV$. Here χ is the number of states that are kept. Note that $E_0 = \frac{U_4+U_9}{2}$ is the ground-state energy per site in the atomic limit.

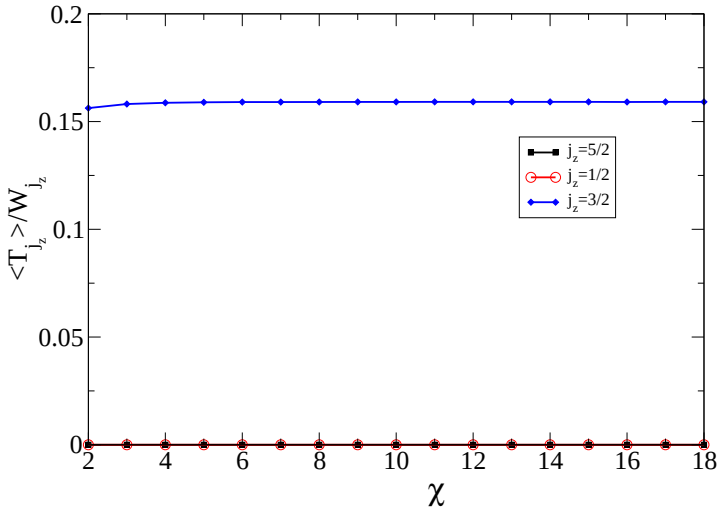

Figure 5.2: Indication of partial localization for $W = 2eV$ and $W' \ll 1eV$.

	$n_{-\frac{5}{2}}$	$n_{-\frac{3}{2}}$	$n_{-\frac{1}{2}}$	$n_{\frac{1}{2}}$	$n_{\frac{3}{2}}$	$n_{\frac{5}{2}}$
Site A	0.0000	0.0000	0.0000	1.0000	0.5000	1.0000
Site B	0.0000	0.0000	0.0000	1.0000	0.5000	1.0000

Table 5.1: Occupation number n_{j_z} when $\chi = 10$ for $W = 2eV$, $W' \ll 1eV$.

converge much faster than the ground-state energy does. In fact, even a simulation with $\chi = 2$ can well reproduce the results shown in table 5.1.

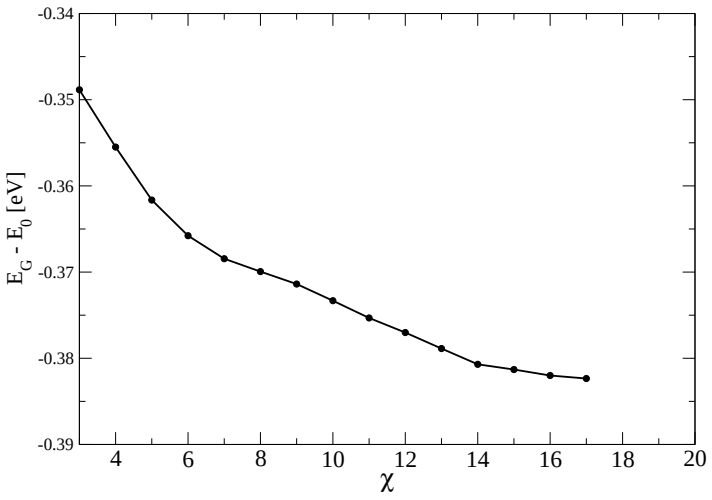

Figure 5.3: The ground-state energy obtained within the iTEBD method for $W \ll 1eV$ and $W' = 2eV$. Here $E_0 = \frac{\frac{U_4+U_9}{2}}{2}$ is the ground-state energy per site in the atomic limit.

Next, we turn to a discussion of the case with $W \ll 1eV$, $W' = 2eV$ where the ground-state obtained by the RISBMF method is in the FM $j_z = \frac{3}{2}$ localized phase (see appendix D). Fig. 5.3 presents the iTEBD ground-state energy $E_G(\chi)$ as a function of χ. In this case, with an increase in value of χ, $E_G(\chi)$ converges more slowly than it did in the above case. Thus, in order to yield the same required accuracy for the ground-state energy, one has to perform the simulations with larger values of χ. Furthermore,

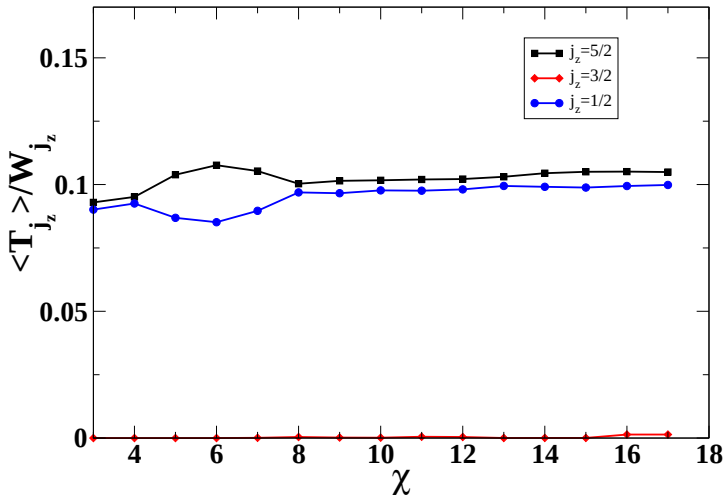

Figure 5.4: Indication of partial localization for $W \ll 1eV$ and $W' = 2eV$.

	$n_{-\frac{5}{2}}$	$n_{-\frac{3}{2}}$	$n_{-\frac{1}{2}}$	$n_{\frac{1}{2}}$	$n_{\frac{3}{2}}$	$n_{\frac{5}{2}}$
Site A	0.3588	0.6106	0.2019	0.6051	0.3894	0.2636
Site B	0.0196	0.0528	0.7563	0.0165	0.9472	0.7782

Table 5.2: Occupation number n_{j_z} when $\chi = 10$ for $W' = 2eV$, $W = 0eV$.

the required computational time is, in this case, often four times longer than that in the above case with the same χ. The occupations for different j_z-orbitals when $\chi = 10$ are shown in table 5.2. It is seen that the quantity $n_{\frac{3}{2}} + n_{-\frac{3}{2}} \approx 1$ as expected for localized orbitals. In addition, the ratio $\frac{T_{jz}}{W_{jz}}$ for the $|j_z| = \frac{3}{2}$ orbitals is normalized to zero whilst those for the $|j_z| = \frac{1}{2}$ and $|j_z| = \frac{5}{2}$ orbitals are still finite as shown in Fig. 5.4, meaning that electrons in the $|j_z| = \frac{3}{2}$ orbitals are localized. We find that the iTEBD and RISBMF methods are in good agreement with each other. However, the ground-state in the former is AFM while it is FM in the latter. That is due to the fact that in our slave-boson calculation, we assumed a fully translationally invariant phase, i.e, only PM and FM ones were considered. Thus, it is no surprise that it could not predict correctly the magnetic

order of the system when AF phase involves.

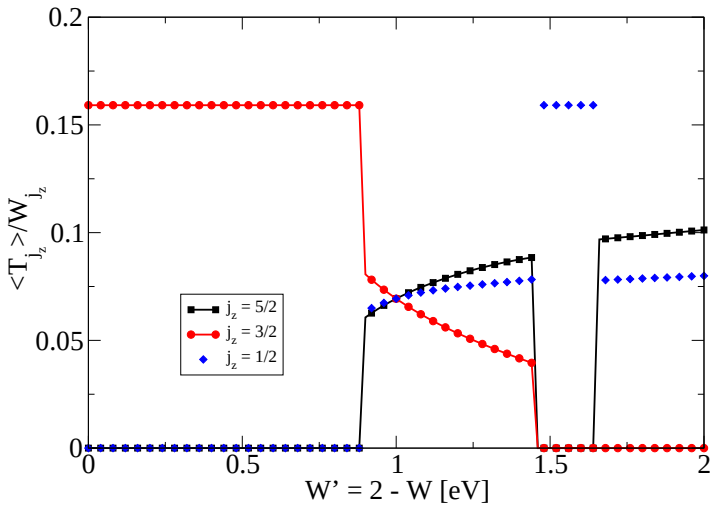

Figure 5.5: Ratios T_{j_z}/W_{j_z} along $W + W' = 2eV$ line within RISBMF method.

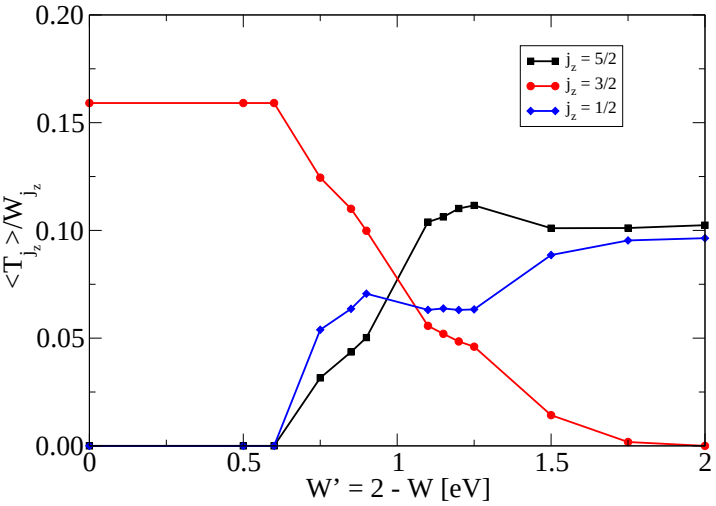

Figure 5.6: Ratios T_{j_z}/W_{j_z} along $W+W' = 2eV$ line within iTEBD method with $\chi = 10$.

Finally, we discuss results along the $W+W' = 2eV$ line of the phase diagram in $W-W'$

plane with $\chi = 10$. The ratios T_{j_z}/W_{j_z} for different orbitals along the $W + W' = 2eV$ line within the RISBMF and iTEBD methods are shown in Figs. 5.5 and 5.6, respectively. When $W' \lesssim 0.6eV$ or $W' \gtrsim 1.65eV$, the iTEBD and RISBMF methods are in good agreement with each other, i.e., they both yield ground-states in a partially localized phase. It is noticeable that the partially localized regions obtained within the RISBMF method are larger than those obtained within the iTEBD method. This is understandable since the RISBMF approach cannot describe with equal accuracy correlation effects for different phases. Thus, the relative error of correlation energy for a given phase differs from that of another. Therefore, the phase boundary is shifted towards the one in which electron correlations are better taken into account. Besides the regions where the RISBMF agrees with the iTEBD approach, we find an area, i.e., $1.45eV \lesssim W' \lesssim 1.65eV$, where the RISBMF approach provides an artificial ground-state. In this area, the RISBMF method predicts a localization of the $j_z = \frac{3}{2}, \frac{5}{2}$ orbitals whereas the iTEBD method shows that only the $j_z = \frac{3}{2}$ orbital is considerably localized.

5.4 Conclusions

In this chapter, we calculated the ground-state of the effective model (2.11) for a 1D lattice using the iTEBD method [30]. We only studied some particularly interesting points of the phase diagram to assess the validity of the RISBMF results obtained in chapter 4 and in appendix D. Results of the RISBMF and iTEBD methods for the $W + W' = 2eV$ case were shown in Figs. 5.5 and 5.6, respectively. Qualitatively, the RISBMF and iTEBD methods agree with each other. However, we found an area, i.e., $1.45eV \lesssim W' \lesssim 1.65eV$, where the RISBMF approach provides an artificial ground-state. This is understandable since the quality of mean-field methods is worse for lower dimensional systems.

Chapter 6

Summary

The localized/delocalized duality of $5f$ electrons plays an important role in understanding the complex physics of actinides. Band-structure calculations based on the *ad hoc* assumption that $5f$ electrons are simultaneously localized and delocalized explained the observed dHvA experiments very well [12, 13]. This *ad hoc* assumption also gives the correct equilibrium volume for δ-Pu [18]. Experimentally, the duality of $5f$ electrons is observed by inelastic neutron scattering experiments [10], or by soft X-ray angle-resolved photoelectron spectroscopy [11].

It is worth recalling that the origin of partial localization in the $3d$ and $5f$ systems is quite different [19]. In compounds with $3d$ electrons, the large crystalline electric field set up by the surrounding environment of transition metal ions plays a major role. On the other hand, in $5f$ systems, the Hund's rule correlations play the key role whilst the crystalline electric field is less important.

In this thesis we have studied the effect of intra-atomic correlations on anisotropies in hopping matrix elements of different $5f$ orbitals. For that purpose, we used the effective model defined by a microscopic Hamiltonian (2.11). The Hamiltonian includes on-site interactions that are responsible for Hund's rules and effective hopping terms that result from the hybridization of different $5f$ orbitals with the environment. The effective model was rederived in chapter 2. In that chapter some results for a two-site system were

discussed.

Two different approximations, namely, rotationally invariant slave-boson mean-field (RISBMF) [29] and infinite time-evolving block decimation (iTEBD) [30], have been used to investigate the ground-state properties of the Hamiltonian (2.11). Within the RISBMF method we considered the effective model on a lattice characterized by a orbital-dependent constant density of states and on an infinite linear chain. On the other hand, we only applied the iTEBD method for an infinite linear chain.

In chapter 3, we derived the RISBMF Eqs. (3.81)–(3.84) for the Hamiltonian (2.11) at arbitrary band-filling n_f. In order to mimic the situation in U-based heavy-fermion compounds we considered the regime with an intermediate f-electron count of $n_f = 2.5$ per site. We have managed to numerically solve the RISBMF equations for two different lattices. In chapter 4 we investigated a lattice characterized by an orbital-dependent constant density of states (4.1). In appendix D we studied a one-dimensional system whose orbital-dependent density of states is given by Eq. (D.1). Results are qualitatively similar for the two lattices. We thus focused mainly on the constant density of states case because the RISBMF equations can be simplified considerably. The simplification not only helped us to reduce numerical efforts significantly but also helped us to understand better the physics of the system. Results shown in appendix D, i.e., for a one-dimensional system, were used to compare with those obtained by the iTEBD method.

We have demonstrated that Hund's rule correlations enhance strongly anisotropies in hopping matrix elements. For a certain range of $5f$ bandwidth parameters this effect may result in a complete suppression of hopping processes for some of $5f$ orbitals, i.e., the system is in a partially localized phase. Within the RISBMF method, we calculated the ground-state properties and produced the phase diagram of the system (see Fig. 4.7 and Fig. 4.8)). The suppression of hopping processes in some of $5f$ orbitals due to Hund's rule correlations can be seen through orbital-dependent quasiparticle weights. In a mean-field theory, a quasiparticle weight of zero for an orbital means a complete suppression of hopping processes in this orbital. Thus, quasiparticle weights and occupation numbers were used to classify partially localized phases. In the calculated phase diagram we obtain

four partially localized phases that can be separated into two different sets. In the first set electrons in two orbitals, namely, $j_z = \frac{1}{2}$, $\frac{5}{2}$ or $j_z = \frac{3}{2}$, $\frac{5}{2}$ orbitals, are localized. In the second, electrons in one orbital, namely, $j_z = \frac{3}{2}$ or $j_z = \frac{5}{2}$, are localized. The difference between the two sets is not simply the number of localized orbitals but the mechanism for the partial localization. For the first set, the Hund's rule mechanism applies: only those $5f$ electrons that enable the remaining ones to form a Hund's rule state will delocalize. This mechanism requires to have at least two localized orbitals, therefore it is definitely not applicable to those phases with only one localized orbital. For the second set, a situation similar to a single-band Mott-Hubbard transition applies. The direct on-site Coulomb interaction between j_z and $-j_z$ electrons plays the key role for understanding the partial localization transition. The j_z orbital is localized if the ratio $\frac{U_{jz,-jz}}{W_{jz}}$ is above a critical value.

In order to assess the validity of the RISBMF results we have used the iTEBD method to calculate the ground-state properties of a 1D system. However, within the iTEBD method we did calculations only for the case where $W + W' = 2eV$. This case was chosen to enable us to analyze as many phases as possible. Note that the line $W + W' = 2eV$ in Fig. D.1 crosses four different phases in the phase diagram for a 1D lattice. Results of the RISBMF and iTEBD methods for the $W + W' = 2eV$ case were shown in Figs. 5.5 and 5.6, respectively. Qualitatively, the two approaches agree with each other. However, we found an area where the RISBMF yields an artificial ground-state. Note that the mean-field method is worst for a 1D system. Therefore one shoud not judge from it the quality of the RISBMF method for the more general case. Recently, the iTEBD method has been generalized to a 2D system [59]. Considering the fact that the z-projection of the total angular momentum is a conserved quantity, this may enable one to perform iTEBD simulations for a 2D lattice. This problem is left for a future study.

Appendix A

Mapping details

In this section we first define the two local basis sets to introduce slave bosons. Then we list all slave bosons for different M-particle Hilbert subspaces.

Fock states are the eigenstates of the local occupation numbers $f^\dagger_{j_z} f_{j_z}$. The convention $|\eta_{-\frac{5}{2}}\eta_{-\frac{3}{2}}\eta_{-\frac{1}{2}}\eta_{\frac{1}{2}}\eta_{\frac{3}{2}}\eta_{\frac{5}{2}}\rangle$ is used to represent an M-particle Fock state, where η_{j_z} is either 0 or 1 representing the occupation number of the j_z orbital; $M = \sum_{j_z} \eta_{j_z}$. For example, the 2-particle Fock state that has $j_z = \frac{1}{2}, \frac{5}{2}$ orbitals being occupied reads $|000101\rangle$. The convention of Fock states is mathematically convenient, e.g., for the symbolic representation of slave-bosons, but it is not useful for a discussion. In fact, an alternative way is to use the j_z quantum numbers (in ascending order) of occupied orbitals to denote Fock states, i.e., $|M; j_{z1}, .., j_{zM}\rangle$. The state $|000101\rangle$ in the above example now reads $|M = 2; \frac{1}{2}, \frac{5}{2}\rangle$. The alternative convention seems to be more appropriate. However, there is an inconvenience if we consider the Fock states of 4 or more particles, namely, the notations of Fock states are cumbersome and thus these corresponding slave bosons are cumbersome too. Therefore, we use the alternative convention for discussions throughout this thesis, except here for an introduction of slave bosons we use the convention $|\eta_{-\frac{5}{2}}\eta_{-\frac{3}{2}}\eta_{-\frac{1}{2}}\eta_{\frac{1}{2}}\eta_{\frac{3}{2}}\eta_{\frac{5}{2}}\rangle$.

Multiplet states $|\Gamma\rangle \equiv |M; J, J_z\rangle$ are eigenstates of the local interaction: $\hat{U}|\Gamma\rangle = E_\Gamma|\Gamma\rangle$, where M, $|\Gamma\rangle$, $\mathcal{J}_z$ are the number of particles, total angular momentum, z-component of total angular momentum of the state $|\Gamma\rangle$, respectively. In the following tables we list all the

multiplet states with their components in the Fock basis. For simplification the component presented here are not normalized. The energies E_Γ, in the forth column, are expressed in terms of the Coulomb parameters U_0, U_2 and U_4. The fifth column in the tables presents all the auxiliary bosons $\phi_{\Gamma n}$ which are considered within our approach for a given multiplet state. For convenience, we number the multiplet states $\phi_{\Gamma n}$, i.e., we identify each multiplet state $|M;\mathcal{J},\mathcal{J}_z\rangle$ to a number $\Gamma = 1,\cdots,64$. Each table corresponds to a charge sector $M = 0,\cdots,6$. Note that the choice of U_J was made in section 2.1. For convenience, we define $U_{\frac{9}{2}} = \frac{9U_2+33U_4}{14}$, $U_{\frac{3}{2}} = \frac{15U_2+6U_4}{7}$, and $U_{\frac{5}{2}} = \frac{4U_0+5U_2+9U_4}{6}$ being the eigenvalues of the local interaction $\hat{U}$ in the 3-particle subspace. In 4-particle subspace we define $\tilde{U}_J = U_J + \frac{U_0+5U_2+9U_4}{3}$ where $J = 0,2,4$. Tables of slave bosons for different charge sectors, i.e., $M = 0..6$, are in the next pages.

$M = 0$ (i.e., local vacuum)

$\mathcal{J}$	$\mathcal{J}_z$	$\|\Gamma\rangle$	E_Γ	$\phi_{\Gamma n}$	Γ
0	0	$\|000000\rangle$	0	$\phi_{1,\|000000\rangle}$	1

$M = 1$

$\mathcal{J}$	$\mathcal{J}_z$	$\|\Gamma\rangle$	E_Γ	$\phi_{\Gamma n}$	Γ
$\frac{5}{2}$	$\frac{5}{2}$	$\|000001\rangle$	0	$\phi_{2,\|000001\rangle}$	2
	$\frac{3}{2}$	$\|000010\rangle$		$\phi_{3,\|000010\rangle}$	3
	$\frac{1}{2}$	$\|000100\rangle$		$\phi_{4,\|000100\rangle}$	4
	$-\frac{1}{2}$	$\|001000\rangle$		$\phi_{5,\|001000\rangle}$	5
	$-\frac{3}{2}$	$\|010000\rangle$		$\phi_{6,\|010000\rangle}$	6
	$-\frac{5}{2}$	$\|100000\rangle$		$\phi_{7,\|100000\rangle}$	7

$M = 2$

$\mathcal{J}$	$\mathcal{J}_z$	$\|\Gamma\rangle$	E_Γ	$\phi_{\Gamma n}$	Γ
4	4	$\|000011\rangle$	U_4	$\phi_{8,\|000011\rangle}$	8
	3	$\|000101\rangle$		$\phi_{9,\|000101\rangle}$	9
	2	$\sqrt{5}\|000110\rangle + 3\|001001\rangle$		$\phi_{10,\|000110\rangle}$, $\phi_{10,\|001001\rangle}$	10
	1	$\sqrt{5}\|001010\rangle + \sqrt{2}\|010001\rangle$		$\phi_{11,\|001010\rangle}$, $\phi_{11,\|010001\rangle}$	11
	0	$2\|001100\rangle + 3\|010010\rangle + \|100001\rangle$		$\phi_{12,\|001100\rangle}$, $\phi_{12,\|010010\rangle}$, $\phi_{12,\|100001\rangle}$	12
	-1	$\sqrt{5}\|010100\rangle + \sqrt{2}\|100010\rangle$		$\phi_{13,\|010100\rangle}$, $\phi_{13,\|100010\rangle}$	13
	-2	$\sqrt{5}\|011000\rangle + 3\|100100\rangle$		$\phi_{14,\|011000\rangle}$, $\phi_{14,\|100100\rangle}$	14
	-3	$\|101000\rangle$		$\phi_{15,\|101000\rangle}$	15
	-4	$\|110000\rangle$		$\phi_{16,\|110000\rangle}$	16
2	2	$3\|000110\rangle - \sqrt{5}\|001001\rangle$	U_2	$\phi_{17,\|000110\rangle}$, $\phi_{17,\|001001\rangle}$	17
	1	$\sqrt{2}\|001010\rangle - \sqrt{5}\|010001\rangle$		$\phi_{18,\|001010\rangle}$, $\phi_{18,\|010001\rangle}$	18
	0	$4\|001100\rangle - \|010010\rangle - 5\|100001\rangle$		$\phi_{19,\|001100\rangle}$, $\phi_{19,\|010010\rangle}$, $\phi_{19,\|100001\rangle}$	19
	-1	$\sqrt{2}\|010100\rangle - \sqrt{5}\|100010\rangle$		$\phi_{20,\|010100\rangle}$, $\phi_{20,\|100010\rangle}$	20
	-2	$3\|011000\rangle - \sqrt{5}\|100100\rangle$		$\phi_{21,\|011000\rangle}$, $\phi_{21,\|100100\rangle}$	21
0	0	$\|001100\rangle - \|010010\rangle + \|100001\rangle$	U_0	$\phi_{22,\|001100\rangle}$, $\phi_{22,\|010010\rangle}$, $\phi_{22,\|100001\rangle}$	22

$M = 3$

$\mathcal{J}$	$\mathcal{J}_z$	$\lvert\Gamma\rangle$	E_Γ	$\phi_{\Gamma n}$	Γ
$\frac{9}{2}$	$\frac{9}{2}$	$\lvert 000111\rangle$	$\mathrm{U}_{\frac{9}{2}}$	$\phi_{23,\lvert 000111\rangle}$	23
	$\frac{7}{2}$	$\lvert 001011\rangle$		$\phi_{24,\lvert 001011\rangle}$	24
	$\frac{5}{2}$	$\lvert 010011\rangle + \lvert 001101\rangle$		$\phi_{25,\lvert 010011\rangle},\ \phi_{25,\lvert 001101\rangle}$	25
	$\frac{3}{2}$	$\lvert 001110\rangle + \sqrt{\frac{32}{5}}\lvert 010101\rangle + \lvert 100011\rangle$		$\phi_{26,\lvert 001110\rangle},\ \phi_{26,\lvert 010101\rangle},\ \phi_{26,\lvert 100011\rangle}$	26
	$\frac{1}{2}$	$\lvert 010110\rangle + \sqrt{\frac{4}{5}}\lvert 011001\rangle + \lvert 100101\rangle$		$\phi_{27,\lvert 010110\rangle},\ \phi_{27,\lvert 011001\rangle},\ \phi_{27,\lvert 100101\rangle}$	27
	$-\frac{1}{2}$	$\lvert 011010\rangle + \sqrt{\frac{4}{5}}\lvert 100110\rangle + \lvert 101001\rangle$		$\phi_{28,\lvert 010110\rangle},\ \phi_{28,\lvert 011001\rangle},\ \phi_{28,\lvert 100101\rangle}$	28
	$-\frac{3}{2}$	$\lvert 011100\rangle + \sqrt{\frac{32}{5}}\lvert 101010\rangle + \lvert 110001\rangle$		$\phi_{29,\lvert 011100\rangle},\ \phi_{29,\lvert 101010\rangle},\ \phi_{29,\lvert 110001\rangle}$	29
	$-\frac{5}{2}$	$\lvert 110010\rangle + \lvert 101100\rangle$		$\phi_{30,\lvert 110010\rangle},\ \phi_{30,\lvert 101100\rangle}$	30
	$-\frac{7}{2}$	$\lvert 110100\rangle$		$\phi_{31,\lvert 1101000\rangle}$	31
	$-\frac{9}{2}$	$\lvert 111000\rangle$		$\phi_{23,\lvert 111000\rangle}$	32
$\frac{3}{2}$	$\frac{3}{2}$	$\lvert 001110\rangle - \sqrt{\frac{5}{8}}\lvert 010101\rangle + \lvert 100011\rangle$	$\mathrm{U}_{\frac{3}{2}}$	$\phi_{33,\lvert 001110\rangle},\ \phi_{33,\lvert 010101\rangle},\ \phi_{33,\lvert 100011\rangle}$	33
	$\frac{1}{2}$	$\lvert 010110\rangle - \sqrt{5}\lvert 011001\rangle + \lvert 100101\rangle$		$\phi_{34,\lvert 010110\rangle},\ \phi_{34,\lvert 011001\rangle},\ \phi_{34,\lvert 100101\rangle}$	34
	$-\frac{1}{2}$	$\lvert 011010\rangle - \sqrt{5}\lvert 100110\rangle + \lvert 101001\rangle$		$\phi_{35,\lvert 010110\rangle},\ \phi_{35,\lvert 011001\rangle},\ \phi_{35,\lvert 100101\rangle}$	35
	$-\frac{3}{2}$	$\lvert 011100\rangle - \sqrt{\frac{5}{8}}\lvert 101010\rangle + \lvert 110001\rangle$		$\phi_{36,\lvert 011100\rangle},\ \phi_{36,\lvert 101010\rangle},\ \phi_{36,\lvert 110001\rangle}$	36
$\frac{5}{2}$	$\frac{5}{2}$	$\lvert 010011\rangle - \lvert 001101\rangle$	$\mathrm{U}_{\frac{5}{2}}$	$\phi_{37,\lvert 010011\rangle},\ \phi_{37,\lvert 001101\rangle}$	37
	$\frac{3}{2}$	$\lvert 001110\rangle - \lvert 100011\rangle$		$\phi_{38,\lvert 001110\rangle},\ \phi_{38,\lvert 100011\rangle}$	38
	$\frac{1}{2}$	$\lvert 010110\rangle - \lvert 100101\rangle$		$\phi_{39,\lvert 010110\rangle},\ \phi_{39,\lvert 100101\rangle}$	39
	$-\frac{1}{2}$	$\lvert 011010\rangle - \lvert 101001\rangle$		$\phi_{40,\lvert 011010\rangle},\ \phi_{40,\lvert 101001\rangle}$	40
	$-\frac{3}{2}$	$\lvert 011100\rangle - \lvert 110001\rangle$		$\phi_{41,\lvert 011100\rangle},\ \phi_{41,\lvert 110001\rangle}$	41
	$-\frac{5}{2}$	$\lvert 110010\rangle - \lvert 101100\rangle$		$\phi_{42,\lvert 110010\rangle},\ \phi_{42,\lvert 101100\rangle}$	42

$M = 4$

$\mathcal{J}$	$\mathcal{J}_z$	$\|\Gamma\rangle$	E_Γ	$\phi_{\Gamma n}$	Γ
4	4	$\|001111\rangle$	$\tilde{U}_4$	$\phi_{43,\|001111\rangle}$	43
	3	$\|010111\rangle$		$\phi_{44,\|010111\rangle}$	44
	2	$\sqrt{5}\|100111\rangle + 3\|011011\rangle$		$\phi_{45,\|100111\rangle}$, $\phi_{45,\|011011\rangle}$	45
	1	$\sqrt{5}\|101011\rangle + \sqrt{2}\|011101\rangle$		$\phi_{46,\|100111\rangle}$, $\phi_{46,\|011101\rangle}$	46
	0	$2\|110011\rangle + 3\|101101\rangle + \|011110\rangle$		$\phi_{47,\|110011\rangle}$, $\phi_{47,\|101101\rangle}$, $\phi_{47,\|011110\rangle}$	47
	-1	$\sqrt{5}\|110101\rangle + \sqrt{2}\|101110\rangle$		$\phi_{48,\|111001\rangle}$, $\phi_{48,\|101110\rangle}$	48
	-2	$\sqrt{5}\|111001\rangle + 3\|110110\rangle$		$\phi_{49,\|111001\rangle}$, $\phi_{49,\|110110\rangle}$	49
	-3	$\|111010\rangle$		$\phi_{50,\|111010\rangle}$	50
	-4	$\|111100\rangle$		$\phi_{51,\|111100\rangle}$	51
2	2	$3\|100111\rangle - \sqrt{5}\|011011\rangle$	$\tilde{U}_2$	$\phi_{52,\|100111\rangle}$, $\phi_{52,\|011011\rangle}$	52
	1	$\sqrt{2}\|101011\rangle - \sqrt{5}\|011101\rangle$		$\phi_{53,\|100111\rangle}$, $\phi_{53,\|011101\rangle}$	53
	0	$4\|110011\rangle - \|101101\rangle - 5\|011110\rangle$		$\phi_{54,\|110011\rangle}$, $\phi_{54,\|101101\rangle}$, $\phi_{54,\|011110\rangle}$	54
	-1	$\sqrt{2}\|110101\rangle - \sqrt{5}\|101110\rangle$		$\phi_{55,\|111001\rangle}$, $\phi_{55,\|101110\rangle}$	55
	-2	$3\|111001\rangle - \sqrt{5}\|110110\rangle$		$\phi_{56,\|111001\rangle}$, $\phi_{56,\|110110\rangle}$	56
0	0	$\|110011\rangle - \|101101\rangle + \|011110\rangle$	$\tilde{U}_0$	$\phi_{57,\|110011\rangle}$, $\phi_{57,\|101101\rangle}$, $\phi_{57,\|011110\rangle}$	57

$M = 5$

$\mathcal{J}$	$\mathcal{J}_z$	$\|\Gamma\rangle$	E_Γ	$\phi_{\Gamma n}$	Γ
$\frac{5}{2}$	$\frac{5}{2}$	$\|011111\rangle$	$\frac{2U_0+10U_2+18U_4}{3}$	$\phi_{58,\|011111\rangle}$	58
	$\frac{3}{2}$	$\|101111\rangle$		$\phi_{59,\|101111\rangle}$	59
	$\frac{1}{2}$	$\|110111\rangle$		$\phi_{60,\|110111\rangle}$	60
	$-\frac{1}{2}$	$\|111011\rangle$		$\phi_{61,\|111011\rangle}$	61
	$-\frac{3}{2}$	$\|111101\rangle$		$\phi_{62,\|111101\rangle}$	62
	$-\frac{5}{2}$	$\|111110\rangle$		$\phi_{63,\|111110\rangle}$	63

$M = 6$

$\mathcal{J}$	$\mathcal{J}_z$	$\|\Gamma\rangle$	E_Γ	$\phi_{\Gamma n}$	Γ
0	0	$\|111111\rangle$	$U_0 + 5U_2 + 9U_4$	$\phi_{64,\|111111\rangle}$	64

Appendix B

Mean-field equations for antiferromagnetic phases

In section 3.3 we obtained mean-field equations for paramagnetic and ferromagnetic solutions. Now we will derive mean-field equations for an antiferromagnetic (AF) phase. The equations are obtained in analogous way as developped by Hasegawa [26]: the original lattice is divided into 2 sublattices A and B. We label $a(b)$ to a site of sublattice A (B), respectively. The local $f-$electron operators in the sublattices are given by Eq. (3.58)

$$f_{aj_z} = R^{\dagger}_{j_z}[\Phi_A]\; d_{aj_z}, \tag{B.1}$$

$$f_{bj_z} = R^{\dagger}_{j_z}[\Phi_B]\; d_{bj_z}, \tag{B.2}$$

where Φ_A (Φ_B) represents the set of slave bosons introduced at site a (b) of the sublattice A (B), respectively. The operator $R^{\dagger}_{j_z}$ is given by Eq. (3.59). Following the standard slave boson mean-field approaches, we make the following approximations:
(i) The bosonic operators are replaced by their expectation values: $\phi^{\dagger}_{a,\Gamma n}, \phi_{a,\Gamma n} \longrightarrow \varphi_{A,\Gamma n}$, $\phi^{\dagger}_{b,\Gamma n}, \phi_{b,\Gamma n} \longrightarrow \varphi_{B,\Gamma n}$.
(ii) The constraints (3.63-3.64) are taken into account by introducing fourteen homogeneous Lagrange multipliers $\lambda_A,\ \lambda_B,\ \lambda_{Aj_z}$ and λ_{Bj_z}. The Hamiltonian (2.11) is written in terms of the auxiliary operators as follows

$$
\begin{aligned}
H^{MF} &= -\sum_{\langle a,b\rangle,\, j_z} t_{j_z} R_{j_z}[\Phi_A] R_{j_z}[\Phi_B] \left[d^\dagger_{aj_z} d_{bj_z} + H.c. \right] \\
&\quad + \sum_{a,\,\Gamma n} E_\Gamma \varphi^2_{A,\Gamma n} + \sum_{b,\,\Gamma n} E_\Gamma \varphi^2_{B,\Gamma n} \\
&\quad + \lambda_A \sum_a \left(\sum_{\Gamma n} \varphi^2_{A\Gamma n} - 1 \right) + \lambda_B \sum_b \left(\sum_{\Gamma n} \varphi^2_{B\Gamma n} - 1 \right) \\
&\quad + \sum_{aj_z} \lambda_{Aj_z} \left(n_{j_z}[\Phi_A] - d^\dagger_{aj_z} d_{aj_z} \right) + \sum_{bj_z} \lambda_{Bj_z} \left(n_{j_z}[\Phi_B] - d^\dagger_{bj_z} d_{bj_z} \right) \\
&\quad + \mu \sum_a \left(\sum_{j_z} n_{j_z}[\Phi_A] - n_f \right) + \mu \sum_b \left(\sum_{j_z} n_{j_z}[\Phi_B] - n_f \right). \qquad \text{(B.3)}
\end{aligned}
$$

Assuming a Néel ordered ground-state for the bipartite lattice, we make the following ansatz:

$$\lambda_A \equiv \lambda_B \equiv \lambda, \qquad \text{(B.4)}$$

$$\varphi_{A\Gamma n} \equiv \varphi_{B\bar{\Gamma}\bar{n}} \equiv \varphi_{\Gamma n}, \qquad \text{(B.5)}$$

$$\lambda_{A_j z} \equiv \lambda_{B\bar{j}_z} \equiv \lambda_{j_z}, \qquad \text{(B.6)}$$

where $\bar{j}_z \equiv -j_z$. $\bar{\Gamma}$ and $\bar{n}$ are counterparts of Γ and n obtained by replacing $j_z \mapsto \bar{j}_z \equiv -j_z$. By using the above ansatz one finds

$$n_{j_z}[\Phi_A] = n_{j_z}[\Phi] = \sum_{\Gamma n} \varphi^2_{\Gamma n} \langle n | f^\dagger_{j_z} f_{j_z} | n \rangle = n_{\bar{j}_z}[\Phi_B], \qquad \text{(B.7)}$$

$$\gamma_{j_z}[\Phi_A] = \gamma_{j_z}[\Phi] = \sum_{\Gamma\Gamma',nn'} \langle \Gamma | f^\dagger_{j_z} | \Gamma' \rangle \langle n | f^\dagger_{j_z} | n' \rangle \, \varphi_{\Gamma n} \varphi_{\Gamma' n'} = \gamma_{\bar{j}_z}[\Phi_B], \qquad \text{(B.8)}$$

$$\sum_{j_z} \lambda_{Aj_z} n_{j_z}[\Phi_A] = \sum_{j_z} \lambda_{j_z} n_{j_z}[\Phi] = \sum_{j_z} \lambda_{Bj_z} n_{j_z}[\Phi_B], \qquad \text{(B.9)}$$

$$\sum_{\Gamma n} \varphi^2_{A\Gamma n} = \sum_{\Gamma n} \varphi^2_{\Gamma n} = \sum_{\Gamma n} \varphi^2_{B\Gamma n}, \qquad \text{(B.10)}$$

The Hamiltonian (B.3) becomes:

$$
\begin{aligned}
H^{MF} &= -\sum_{\langle a,b\rangle,\, j_z} t_{j_z} Z[\Phi] \left[d^{\dagger}_{aj_z} d_{bj_z} + H.c. \right] \\
&\quad +\mu\mathcal{N}\left(\sum_{j_z} n_{j_z}[\Phi] - n_f \right) - \sum_{aj_z} \lambda_{j_z} d^{\dagger}_{aj_z} d_{aj_z} - \sum_{bj_z} \lambda_{\bar{j}_z} d^{\dagger}_{bj_z} d_{bj_z} \\
&\quad +\mathcal{N}\left[\sum_{\Gamma n} E_{\Gamma} \varphi^2_{\Gamma n} + \lambda \left(\sum_{\Gamma n} \varphi^2_{\Gamma n} - 1 \right) + \sum_{j_z} \lambda_{j_z} n_{j_z}[\Phi] \right]. \qquad \text{(B.11)}
\end{aligned}
$$

Here $\mathcal{N}$ is the total number of sites. The QP weight is

$$
\begin{aligned}
Z_{j_z}[\Phi] &\equiv R_{j_z}[\Phi_A] R_{j_z}[\Phi_B] = R_{j_z}[\Phi] R_{\bar{j}_z}[\Phi] \\
&= \frac{\gamma_{j_z}[\Phi]\gamma_{\bar{j}_z}[\Phi]}{\sqrt{n_{j_z}[\Phi]\left(1 - n_{j_z}[\Phi]\right)}\sqrt{n_{\bar{j}_z}[\Phi]\left(1 - n_{\bar{j}_z}[\Phi]\right)}}, \qquad \text{(B.12)}
\end{aligned}
$$

where γ_{j_z} and n_{j_z} are explicit functions of $\varphi_{\Gamma n}$ given by Eqs. (3.70-3.71). Invoking the momentum space representation

$$
d_{aj_z} \equiv \sqrt{2}/\sqrt{\mathcal{N}} \sum_{\mathbf{q}} e^{i\mathbf{q}\mathbf{r}_a} a_{\mathbf{q}j_z}, \qquad \text{(B.13)}
$$

$$
d_{bj_z} \equiv \sqrt{2}/\sqrt{\mathcal{N}} \sum_{\mathbf{q}} e^{i\mathbf{q}\mathbf{r}_b} b_{\mathbf{q}j_z} \qquad \text{(B.14)}
$$

the Hamiltonian (B.11) becomes

$$
\begin{aligned}
H^{MF} &= \sum_{\mathbf{q},j_z} \varepsilon_{\mathbf{q}j_z} Z_{j_z}[\Phi] \left[a^{\dagger}_{\mathbf{q}j_z} b_{\mathbf{q}j_z} + H.c. \right] \\
&\quad +\mu\mathcal{N}\left(\sum_{j_z} n_{j_z}[\Phi] - n_f \right) - \sum_{\mathbf{q},j_z} \lambda_{j_z} a^{\dagger}_{\mathbf{q}j_z} a_{\mathbf{q}j_z} - \sum_{\mathbf{q},j_z} \lambda_{\bar{j}_z} b^{\dagger}_{\mathbf{q}j_z} b_{\mathbf{q}j_z} \\
&\quad +\mathcal{N}\left[\sum_{\Gamma n} E_{\Gamma} \varphi^2_{\Gamma n} + \lambda \left(\sum_{\Gamma n} \varphi^2_{\Gamma n} - 1 \right) + \sum_{j_z} \lambda_{j_z} n_{j_z}[\Phi] \right], \qquad \text{(B.15)}
\end{aligned}
$$

where $\varepsilon_{\mathbf{q}j_z}$ is the energy associated to the hopping integral t_{j_z}. Mean-field parameters λ, λ_{j_z}, μ, and $\varphi_{\Gamma n}$ are determined self-consistently by minimizing the free energy

$$
\beta\mathcal{F} \equiv -\ln Tr[e^{-\beta H^{MF}}]. \qquad \text{(B.16)}
$$

Assuming that this minimum is obtained at a saddle point, we find

$$\sum_{\Gamma n} \varphi_{\Gamma n}^2 = 1, \tag{B.17}$$

$$n_{j_z}[\Phi] = \frac{1}{\mathcal{N}} \sum_{\mathbf{q}} \left[\langle a_{\mathbf{k}j_z}^\dagger a_{\mathbf{k}j_z} \rangle + \langle b_{\mathbf{k}\bar{j}_z}^\dagger b_{\mathbf{k}\bar{j}_z} \rangle \right], \tag{B.18}$$

$$\sum_{j_z} n_{j_z}[\Phi] = n_f, \tag{B.19}$$

$$\begin{aligned} 2(E_\Gamma + \lambda)\varphi_{\Gamma n} &= -\sum_{j_z} (\lambda_{j_z} + \mu) \frac{\partial n_{j_z}[\Phi]}{\partial \varphi_{\Gamma n}} \\ &\quad - \frac{1}{\mathcal{N}} \sum_{\mathbf{k}j_z} \frac{\partial Z_{j_z}[\Phi]}{\partial \varphi_{\Gamma n}} \varepsilon_{\mathbf{q}j_z} \langle a_{\mathbf{k}j_z}^\dagger b_{\mathbf{k}j_z} + H.C. \rangle, \end{aligned} \tag{B.20}$$

with

$$\tilde{\varepsilon}_{\mathbf{q}j_z} \equiv Z_{j_z} \varepsilon_{\mathbf{q}}, \tag{B.21}$$

$$E_{\mathbf{q}j_z}^{\pm} \equiv \lambda_{j_z}^+ \pm \sqrt{{\lambda_{j_z}^-}^2 + \tilde{\varepsilon}_{\mathbf{q}j_z}^2} = E_{\mathbf{q}\bar{j}_z}^{\pm}, \tag{B.22}$$

$$F_{\mathbf{q}j_z} \equiv \lambda_{j_z}^- + \sqrt{{\lambda_{j_z}^-}^2 + \tilde{\varepsilon}_{\mathbf{q}j_z}^2}, \tag{B.23}$$

$$u_{\mathbf{q}j_z} \equiv \frac{-\tilde{\varepsilon}_{\mathbf{q}j_z}}{\sqrt{F_{\mathbf{q}j_z}^2 + \tilde{\varepsilon}_{\mathbf{q}j_z}^2}}, \tag{B.24}$$

$$v_{\mathbf{q}j_z} \equiv \frac{F_{\mathbf{q}j_z}}{\sqrt{F_{\mathbf{q}j_z}^2 + \tilde{\varepsilon}_{\mathbf{q}j_z}^2}}, \tag{B.25}$$

$$\langle a_{\mathbf{k}j_z}^\dagger a_{\mathbf{k}j_z} \rangle = u_{\mathbf{q}j_z}^2 n_F\left(E_{\mathbf{q}j_z}^-\right) + v_{\mathbf{q}j_z}^2 n_F\left(E_{\mathbf{q}j_z}^+\right), \tag{B.26}$$

$$\langle b_{\mathbf{k}\bar{j}_z}^\dagger b_{\mathbf{k}\bar{j}_z} \rangle = v_{\mathbf{q}\bar{j}_z}^2 n_F\left(E_{\mathbf{q}\bar{j}_z}^-\right) + u_{\mathbf{q}\bar{j}_z}^2 n_F\left(E_{\mathbf{q}\bar{j}_z}^+\right) = \langle a_{\mathbf{k}j_z}^\dagger a_{\mathbf{k}j_z} \rangle, \tag{B.27}$$

$$\langle a_{\mathbf{k}j_z}^\dagger b_{\mathbf{k}j_z} + H.C. \rangle = 2u_{\mathbf{q}j_z} v_{\mathbf{q}j_z} \left[n_F\left(E_{\mathbf{q}j_z}^-\right) - n_F\left(E_{\mathbf{q}j_z}^+\right) \right]. \tag{B.28}$$

Here $\lambda_{j_z}^+ \equiv \frac{\lambda_{j_z} + \lambda_{\bar{j}_z}}{2}$, $\lambda_{j_z}^- \equiv \frac{\lambda_{j_z} - \lambda_{\bar{j}_z}}{2}$ and $n_F(\varepsilon) \equiv 1/\left(1 + e^{\beta\varepsilon}\right)$ is the Fermi distribution function. Eqs. (B.18) and (B.20) then become

$$n_{j_z}[\Phi] = \frac{2}{\mathcal{N}} \sum_{\mathbf{q}} \left[u_{\mathbf{q}j_z}^2 n_F\left(E_{\mathbf{q}j_z}^-\right) + v_{\mathbf{q}j_z}^2 n_F\left(E_{\mathbf{q}j_z}^+\right) \right], \tag{B.29}$$

$$\begin{aligned} 2(E_\Gamma + \lambda)\varphi_{\Gamma n} &= -\sum_{j_z} (\lambda_{j_z} + \mu) \frac{\partial n_{j_z}[\Phi]}{\partial \varphi_{\Gamma n}} - \frac{2}{\mathcal{N}} \sum_{j_z \mathbf{q}} \frac{\partial Z_{j_z}[\Phi]}{\partial \varphi_{\Gamma n}} \\ &\quad \times \varepsilon_{\mathbf{q}j_z} u_{\mathbf{q}j_z} v_{\mathbf{q}j_z} \left[n_F\left(E_{\mathbf{q}j_z}^-\right) - n_F\left(E_{\mathbf{q}j_z}^+\right) \right]. \end{aligned} \tag{B.30}$$

We introduce the orbital-dependent bare density of states

$$\rho_0^{j_z}(\omega) \equiv \frac{1}{\mathcal{N}} \sum_{\mathbf{k}} \delta\left(\omega - \varepsilon_{\mathbf{k}j_z}\right), \tag{B.31}$$

and assume that $\varepsilon_{\mathbf{q}+\mathbf{Q}j_z} = -\varepsilon_{\mathbf{q}j_z}$ with $\mathbf{Q}$ being the AF nesting wave-vector, Eqs. (B.29) and (B.30) can be rewritten as

$$n_{j_z}[\Phi] = \int d\omega\ \rho_0^{j_z}(\omega) \left[u_{j_z}^2(\omega) n_F\left(E_{j_z}^-(\omega)\right) + v_{j_z}^2(\omega) n_F\left(E_{j_z}^+(\omega)\right)\right], \tag{B.32}$$

$$\begin{aligned} 2(E_\Gamma + \lambda)\varphi_{\Gamma n} &= -\sum_{j_z} (\lambda_{j_z} + \mu) \frac{\partial n_{j_z}[\Phi]}{\partial \varphi_{\Gamma n}} - \sum_{j_z} \frac{\partial Z_{j_z}[\Phi]}{\partial \varphi_{\Gamma n}} \int d\omega\ \omega\ \rho_0^{j_z}(\omega) \\ &\quad \times u_{j_z}(\omega) v_{j_z}(\omega) \left[n_F\left(E_{j_z}^-(\omega)\right) - n_F\left(E_{j_z}^+(\omega)\right)\right]. \end{aligned} \tag{B.33}$$

Here

$$E_{j_z}^{\pm}(\omega) \equiv \lambda_{j_z}^+ \pm \sqrt{{\lambda_{j_z}^-}^2 + \omega^2 Z_{j_z}^2}, \tag{B.34}$$

$$F_{j_z}(\omega) \equiv \lambda_{j_z}^- + \sqrt{{\lambda_{j_z}^-}^2 + \omega^2 Z_{j_z}^2}, \tag{B.35}$$

$$u_{j_z}(\omega) = \frac{-\omega Z_{j_z}}{\sqrt{F_{j_z}^2(\omega) + \omega^2 Z_{j_z}^2}}, \tag{B.36}$$

$$v_{j_z}(\omega) = \frac{F_{j_z}(\omega)}{\sqrt{F_{j_z}^2(\omega) + \omega^2 Z_{j_z}^2}}. \tag{B.37}$$

Equations (B.17), (B.19), (B.32), and (B.33) are slave-boson mean-field equations for an AF phase. Given an analytical form for the bare density of states, Eqs. (B.32) and (B.33) can be further simplified.

Appendix C

Fully polarized ferromagnetic states

In this part we demonstrate that fully polarized ferromagnetic states characterized by the localization of $j_z = \frac{1}{2}, \frac{5}{2}$ orbitals and the delocalization of $j_z = \frac{3}{2}$ orbital are eigenstates of the Hamiltonian (2.11) when $W' = 0$.

We define a pseudo-vacuum $|\tilde{0}\rangle$ as follows:

$$|\tilde{0}\rangle \equiv \prod_a \left(f^\dagger_{a\frac{5}{2}} f^\dagger_{a\frac{1}{2}} \right) |0\rangle \ , \tag{C.1}$$

where $|0\rangle$ denotes the physical vacuum. It is easy to verify that the pseudo-vacuum is an eigenstate of the Hamiltonian with

$$H|\tilde{0}\rangle = \sum_a \hat{U}(a)|\tilde{0}\rangle = \mathcal{N}U_4|\tilde{0}\rangle \ , \tag{C.2}$$

where $\mathcal{N}$ is the number of lattice sites.

We prove that any of the 'pseudo one-body' states $f^\dagger_{\mathbf{k}\frac{3}{2}}|\tilde{0}\rangle$ is eigenstates of the Hamiltonian:

$$\begin{aligned} H f^\dagger_{\mathbf{k}\frac{3}{2}}|\tilde{0}\rangle &= \sum_{\mathbf{k}'} \epsilon_{\mathbf{k}'\frac{3}{2}} f^\dagger_{\mathbf{k}'\frac{3}{2}} f_{\mathbf{k}'\frac{3}{2}} f^\dagger_{\mathbf{k}\frac{3}{2}}|\tilde{0}\rangle + \sum_a \hat{U}(a) \sum_b \frac{e^{-i\mathbf{k}\mathbf{r}_b}}{\sqrt{\mathcal{N}}} f^\dagger_{b\frac{3}{2}}|\tilde{0}\rangle \\ &= \left(\epsilon_{\mathbf{k}\frac{3}{2}} + U_{\frac{9}{2}} - U_4 + \mathcal{N}U_4 \right) f^\dagger_{\mathbf{k}\frac{3}{2}}|\tilde{0}\rangle \ , \end{aligned} \tag{C.3}$$

where $U_{\frac{9}{2}} = \frac{9U_2+33U_4}{14}$ is the eigenergy of the local multiplets of total angular momentum $J = \frac{9}{2}$, in the charge sector $M = 3$.

Similarly, one proves that the 'pseudo two-body' state $f^\dagger_{\mathbf{k}\frac{3}{2}} f^\dagger_{\mathbf{k}'\frac{3}{2}} |\tilde{0}\rangle$ is also an eigenstate of the Hamiltonian with the eigenvalue $\epsilon_{\mathbf{k}\frac{3}{2}} + \epsilon_{\mathbf{k}'\frac{3}{2}} + 2(U_{\frac{9}{2}} - U_4) + \mathcal{N}U_4$. More generally, one can demonstrate that all states of the form $f^\dagger_{\mathbf{k}_1\frac{3}{2}} \cdots f^\dagger_{\mathbf{k}_p\frac{3}{2}} |\tilde{0}\rangle$ are eigenstates of the Hamiltonian (2.11) when $W' = 0$.

Appendix D

Numerical results for a one-dimensional system

In chapter 4, the effective model described by the microscopic Hamiltonian (2.11) was studied within the rotationally invariant slave boson mean-field (RISBMF) method [29]. For the sake of simplicity, the orbital-dependent density of states (DOS) was assumed to be constant as showed by Eq. (4.1). In this part, we consider a 1D lattice characterized by an orbital-dependent DOS as follows

$$\rho_{0j_z}(\omega) = \frac{2}{\pi W_{jz}} \frac{1}{\sqrt{1-\frac{4\omega^2}{W_{jz}^2}}}. \tag{D.1}$$

Here W_{j_z} is the bare bandwidth of the j_z-orbital. At temperature $T = 0$ the mean-field equations (3.81)–(3.84) read

$$\sum_{\Gamma n} \varphi_{\Gamma n}^2 = 1, \tag{D.2}$$

$$\lambda_{j_z} = -\frac{Cos\left(\pi n_{j_z}[\Phi]\right)}{2} W_{j_z} Z_{j_z}[\Phi] \ , \tag{D.3}$$

$$\sum_{j_z} n_{j_z}[\Phi] = n_f, \tag{D.4}$$

$$\left[E_\Gamma + \lambda + \mu \sum_{j_z} \langle n|f_{j_z}^\dagger f_{j_z}|n\rangle\right] \varphi_{\Gamma n} = \sum_{j_z} \frac{W_{j_z}}{4} \frac{\partial\left[\gamma_{j_z}^2[\Phi]\kappa_{jz}\left(n_{j_z[\Phi]}\right)\right]}{\partial \varphi_{\Gamma n}} \ , \tag{D.5}$$

where $\gamma_{j_z}[\Phi]$ and $\frac{\partial\gamma_{j_z}[\Phi]}{\partial\varphi_{\Gamma n}}$ are explicit functions of Φ, given by Eqs. (3.70) and (3.78), respectively and $\kappa_{jz}\left(n_{j_z[\Phi]}\right)$ is

$$\kappa_{jz}\left(n_{j_z[\Phi]}\right) = \frac{Sin\left(\pi n_{j_z}[\Phi]\right)}{\pi n_{j_z}[\Phi](1-n_{j_z}[\Phi])}. \tag{D.6}$$

The ground-state energy is given by

$$E[\Phi] = -\sum_{j_z}\frac{W_{j_z}}{2}\gamma_{j_z}^2\kappa_{jz}\left(n_{j_z[\Phi]}\right) + \sum_{\Gamma n}E_{\Gamma}\varphi_{\Gamma n}^2\ . \tag{D.7}$$

As we did in previous chapters, we consider $W \equiv W_{\frac{3}{2}}$ and $W' \equiv W_{\frac{1}{2}} = W_{\frac{5}{2}}$ as independent

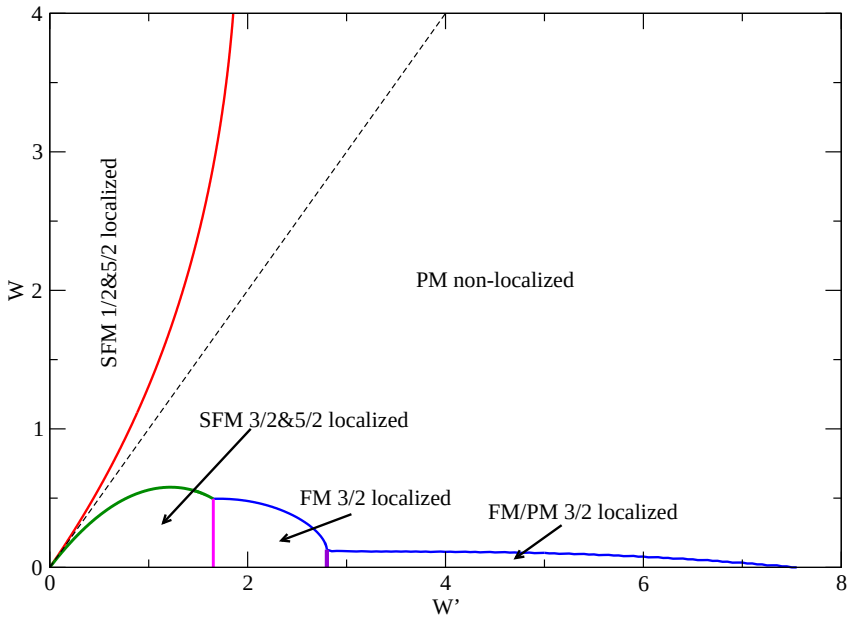

Figure D.1: Phase diagram for 1D lattice. The dotted line is a guide for the eye, corresponding to $W = W'$.

parameters. The Coulomb integrals U_J and the $5f$ band-filling n_f were chosen in chapter 4. We use the numerical method described in chapter 4 to solve the mean-field Eqs. (D.2)-(D.5). The calculated phase diagram is shown in Fig. D.1 that is qualitatively similar to

Fig. 4.8 for the case of constant DOS. The main difference is that, in the present case, the partial localization and magnetic transitions occur simultaneously and the regions for localized phases are roughly reduced by a factor of 2. In the region where $W > W'$ the magnetic order of the ground-state in partially localized phase is SFM, i.e., similar to that in the constant DOS case. However, for the region where $W < W'$ it is different. The ground-state for $W \ll W' \ll \triangle U_4$ is no longer degenerate as seen in the case of constant DOS, here the lowest energy solution is the SFM one. It is worth recalling that in the constant DOS case, PM $j_z = \frac{3}{2}$ localized solution is always unstable and the ground-state is in a FM one. But in the present problem for 1D lattice, it is not always the case. That is when $W << \Delta U$ and W' is large enough the energy of PM solution becomes smaller than that of FM one, although the energy difference is very small. The magnetic order of the ground-state of the system is depicted in Fig. D.1. Note that here we do not study $j_z = \frac{5}{2}$ localized phases which appear at rather large values of hopping integrals as seen in the constant DOS case.

Bibliography

[1] A. Sommerfeld, H. Bethe, Elektronentheorie der Metalle, Handbuch der Physik. Vol. 24-2. Springer Verlag, Heidelberg 1933.

[2] L. D. Landau, Theory of fermi-liquids, Zh. Eksp. Teor. Fiz. 30 (1956) 1058 [Sov. Phys. JETP 3 (1957) 920].

[3] L. D. Landau, On the theory of the fermi-liquid, Zh. Eksp. Teor. Fiz. 35 (1958) 97 [Sov. Phys. JETP 8 (1959) 70].

[4] N. F. Mott, Metal-insulator transitions, Proc R. Soc. London A62 (1949) 236.

[5] S. A. Carter, T. F. Rosenbaum, J. M. Honig, J. Spalek, New phase boundary in highly correlated, barely metallic V_2O_3, Phys. Rev. Lett. 67 (1991) 3440.

[6] J. Hubbard, Proc R. Soc. London A276 (1963) 238.

[7] P. Fulde, Electron correlations in molecules and solids, Berlin; Heidelberg; New York: Springe, 1995.

[8] P. Fulde, P. Thalmeier, G. Zwicknagl, Strongly correlated electrons, Solid State Physics 60 (2006) 1.

[9] K. T. Moore, G. van der Laan, Nature of the 5f states in actinide metals, Rev. Mod. Phys. 81 (2009) 235.

[10] N. Sato, N. Aso, K. Miyake, R. Shiina, P. Thalmeier, G. Varelogiannis, C. Geibel, F. Steglich, P. Fulde, T. Komatsubara, Strong coupling between local moments and superconducting 'heavy' electrons in UPd_2Al_3, Nature 410 (2001) 340.

[11] S.-I. Fujimori, Y. Saitoh, T. Okane, A. Fujimori, H. Yamagami, Y. Haga, E. Yamamoto, Y. Onuki, Itinerant to localized transition of f electrons in the antiferromagnetic superconductor UPd_2Al_3, Nature Phys. 3 (2007) 618.

[12] G. Zwicknagl, A. N. Yaresko, P. Fulde, Microscopic description of origin of heavy quasiparticles in UPt_3, Phys. Rev. B 65 (2002) 081103.

[13] G. Zwicknagl, A. Yaresko, P. Fulde, Fermi surface and heavy masses for UPd_2Al_3 , Phys. Rev. B 68 (2003) 052508.

[14] P. Fulde, B. Schmidt, P. Thalmeier, Theoretical-model for the semimetal Yb_4As_3, Europhys. Lett. 31 (1995) 323.

[15] P. Fulde, V. Zevin, G. Zwicknagl, Model for heavy-fermion behavior of $Nd_{1.8}Ce_{0.2}CuO_4$, Z. Phys. B 92 (1993) 133.

[16] J. Igarashi, K. Murayama, P. Fulde, Magnetic impurity coupled to a strongly correlated electron system in two dimensions, Phys. Rev. B 52 (1995) 15966.

[17] H. Kusunose, K. Miyake, Competition between Hund-rule coupling and Kondo effect, J. Phys. Soc. Jpn. 66 (1997) 1180.

[18] J. Wills, O. Eriksson, A. Delin, P. Andersson, J. Joyce, T. Durakiewicz, M. Butterfield, A. Arko, D. Moore, L. Morales, A novel electronic configuration of the 5f states in delta-plutonium as revealed by the photo-electron spectra, J. El. Spectr. Rel. Phenom. 135 (2004) 163.

[19] G. Zwicknagl, 5f electrons in actinides: Dual nature and photoemission spectra, Int. J.Mod. Phys. B 21 (2007) 2232.

[20] G. Zwicknagl, P. Fulde, The dual nature of 5f electrons and the origin of heavy fermions in U compounds, J. Phys.: Condens. Matter 15 (2003) S1911.

[21] D. V. Efremov, N. Hasselmann, E. Runge, P. Fulde, G. Zwicknagl, Dual nature of 5f electrons: Effect of intra-atomic correlations on hopping anisotropies, Phys. Rev. B 69 (2004) 115114.

[22] F. Pollmann, Partielle lokalisierung in systemen mit teilgefuellten d- und f-schalen, Master's thesis, Technische Universitaet Braunschweig (2004).

[23] E. Runge, P. Fulde, D. V. Efremov, N. Hasselmannd, G. Zwicknagl, Approximative treatment of 5f-systems with partial localization due to intra-atomic correlations, Phys. Rev. B 69 (2004) 155110.

[24] G. Kotliar, A. Ruckenstein, New functional integral approach to strongly correlated Fermi systems: The Gutzwiller approximation as a saddle point, Phys. Rev. Lett. 57 (1986) 1362.

[25] M. Lavagna, Functional-integral approach to strongly correlated Fermi systems: Quantum fluctuations beyond the Gutzwiller approximation, Phys. Rev. B 41 (1990) 142.

[26] H. Hasegawa, Slave-boson mean-field theory of spin- and orbital-ordered states in the degenerate Hubbard model, Found. Phys. 30 (2000) 2061.

[27] G. Zwicknagl, Strongly correlated 5f electrons: spectral functions and mean-field ground states, J. Phys. Soc. Jpn. Suppl. 75 (2006) 226.

[28] V. Anisimov, I. Nekrasov, D. Kondakov, T. Rice, M. Sigrist, Orbital-selective Mott-insulator transition in $Ca_{2-x}Sr_xRuO_4$, Eur. Phys. J. B 25 (2002) 191.

[29] F. Lechermann, A. Georges, G. Kotliar, O. Parcollet, Rotationally invariant slave-boson formalism and momentum dependence of the quasiparticle weight, Phys. Rev. B 76 (2007) 155102.

[30] G. Vidal, Classical Simulation of Infinite-Size Quantum Lattice Systems in One Spatial Dimension, Phys. Rev. Lett. 98 (2007) 070201.

[31] S. Östlund, S. Rommer, Thermodynamic limit of density matrix renormalization, Phys. Rev. Lett. 75 (1995) 3537.

[32] G. Zwicknagl, M. Reese, Dual nature of strongly correlated 5f electrons, J. Magn. Magn. Mat. 310 (2007) 201.

[33] F. Pollmann, G. Zwicknagl, Spectral functions for strongly correlated 5f electrons, Phys. Rev. B 73 (2006) 035121.

[34] S. E. Barnes, New method for the Anderson model, J. Phys. F 6 (1976) 1375.

[35] S. E. Barnes, New method for the Anderson model: II. The U = 0 limit, J. Phys. F 7 (1977) 2637.

[36] N. Read, D. Newns, A new functional integral formalism for the degenerate Anderson model, J. Phys. C 16 (1983) L1055.

[37] P. Coleman, New approach to the mixed-valence problem, Phys. Rev. B 29 (1984) 3035.

[38] T. Li, P. Wölfle, P. J. Hirschfeld, Spin-rotation-invariant slave-boson approach to the hubbard model, Phys. Rev. B 40 (1989) 6817.

[39] J. Rasul, T. Li, One-loop corrections to the Gutzwiller approach to strongly interacting fermions, with application to liquid 3He, J. Phys. C 21 (1988) 5119.

[40] C. J. Pethick, G. M. Carneiro, Specific heat of a normal fermi liquid. i. landau-theory approach, Phys. Rev. A 7 (1973) 304.

[41] R. Fresard, P. Wolfle, Unified slave boson representation of spin and charge degrees of freedom for strongly correlated fermi systems, Int. J. Mod. Phys. B 6 (1992) 685.

[42] J. Sofo, C. Balseiro, Slave-boson mean-field theory for the negative-U Hubbard model, Phys. Rev. B 45 (1992) 377.

[43] B. Bulka, S. Robaszkiewicz, Superconducting properties of the attractive Hubbard model: A slave-boson study, Phys. Rev. B 54 (1996) 13138.

[44] B. Bulka, M. Robaszewska, Superconductivity in Hubbard model with correlated hopping, Acta Phys. Polon. A 91 (1997) 363.

[45] M. Bak, R. Micnas, Superconducting properties of the attractive Hubbard model in the slave-boson approach, J. Phys.: Condens. Matter 10 (1998) 9029.

[46] H. Hasegawa, Slave-boson functional-integral approach to the Hubbard model with orbital degeneracy, J. Phys. Soc. Jpn. 66 (1997) 1391.

[47] R. Fresard, G. Kotliar, Interplay of Mott transition and ferromagnetism in the orbitally degenerate Hubbard model, Phys. Rev. B 56 (1997) 12909.

[48] H. Hasegawa, Slave-boson mean-field theory of the antiferromagnetic state in the doubly degenerate Hubbard model: The half-filled case, Phys. Rev. B 56 (1997) 1196.

[49] J. Hubbard, Proc R. Soc. London A285 (1965) 542.

[50] Z. Zou, P. Anderson, Neutral fermion, charge-e boson excitations in the resonating-valence-bond state and superconductivity in La_2CuO_4-based compounds, Phys. Rev. B 37 (1988) 627.

[51] C. Jayaprakash, H. R. Krishnamurthy, S. Sarker, Mean-field theory for the t-j model, Phys. Rev. B 40 (1989) 2610.

[52] J. J. Vicente Alvarez, C. A. Balseiro, H. A. Ceccatto, Spin- and charge-rotation invariant approach to the Hubbard model, Phys. Rev. B 54 (1996) 11207.

[53] M. Powell, A hybrid method for nonlinear algebraic equations, Gordon and Breach, 1970.

[54] K. G. Wilson, Renormalization group and critical phenomena. ii. phase-space cell analysis of critical behavior, Phys. Rev. B 4 (1971) 3184.

[55] S. R. White, Density matrix formulation for quantum renormalization groups, Phys. Rev. Lett. 69 (1992) 2863.

[56] S. R. White, Density-matrix algorithms for quantum renormalization groups, Phys. Rev. B 48 (1993) 10345.

[57] G. Vidal, Efficient classical simulation of slightly entangled quantum computations, Phys. Rev. Lett. 91 (2003) 147902.

[58] G. Vidal, Efficient simulation of one-dimensional quantum many-body systems, Phys. Rev. Lett. 93 (2004) 040502.

[59] J. Jordan, R. Orús, G. Vidal, F. Verstraete, J. I. Cirac, Classical simulation of infinite-size quantum lattice systems in two spatial dimensions, Phys. Rev. Lett. 101 (2008) 250602.

[60] A. Ekert, P. Knight, Entangled quantum-systems and the schmidt decomposition, Am. J. Phys. 63 (1995) 415.

[61] M. Suzuki, Fractal decomposition of exponential operators with applications to many-body theories and monte-carlo simulations, Phys. Lett. A 146 (1990) 319.

Acknowledgments

I owe my deepest gratitude to my supervisor, Prof. Peter Fulde, for giving me this unique opportunity to be here, and for his wise guidances and advises from the preliminary to the concluding level enabled me to develop an understanding of the topic. He did always encourage and help me step by step overcome various problems to accomplish my PhD thesis. I thank him for his patience and unconditional support.

I am grateful to Dr. Sebastien Burdin for his great help and useful discussions. I really enjoyed the time I worked with him on different subjects. It seems that he always has solutions for whatever difficulties I have.

I would like to thank Dr. Frank Pollmann since the iTEBD simulation for the effective model would not have been possible without his help. He shared not only his numerical coding program but also his tricks and experiences on the simulation. I am really indebted to him.

It is a pleasure to thank Prof. Gertrud Zwicknagl for her valuable and fruitful discussions, especially for the discussion on the one-localized-electron phase.

I wish to thank Prof. Nguyen Toan Thang, Prof. Nguyen Van Hieu, and Prof. Tran Minh Tien for that they critically read through and commented on the manuscript.

I acknowledge my friend Phan Van Nham for his help not only on the daily life in Dresden but also on my work.

I thank very much Aroon O'Brien who improved the English of the thesis considerably.

I acknowledge Frau Ngoc, Frau Duong, Frau Pacholik, and Frau Reinhardt for their orientation and great help on issues of the daily life in Dresden for which my German language was not good enough to deal with them.

I would like to thank the MPIPKS and the International Max-Planck Research School for the financial support of this work.

Finally, I am very greatful to my wife Quynh, who unconditionally supported me all the time in spite of my very frequent absences, being not only my wife and my daughter's mother, but also a great friend.

This work is dedicated to the memory of my mother who I love and miss so much.

Erklärung

Hiermit versichere ich, dass ich die vorliegende Arbeit ohne unzulässige Hilfe Dritter und ohne Benutzung anderer als der angegebenen Hilfsmittel angefertigt habe; die aus fremden Quellen direkt oder indirekt übernommenen Gedanken sind als solche kenntlich gemacht. Die Arbeit wurde bisher weder im Inland noch im Ausland in gleicher oder ähnlicher Form einer anderen Prüfungsbehrde vorgelegt.

Die Dissertation wurde in der Zeit von Mai 2007 bis Juli 2010 unter der Betreuung von Herrn Prof. Dr. Peter Fulde am Max-Planck Institut für Physik Complexer Systeme angefertigt. Es haben keine fru¨heren erfolglosen Promotionsverfahren stattgefunden. Ich erkenne die Promotionsordnung der Facultat¨ Mathematik und Naturwissenschafen an der Technishchen Universitat¨ Dresden vom 20. Maerz 2000 an.

Dresden, 07.07.2010

Duc-Anh LE